Nodal GABA facilitates axon spike transmission in the spinal cord.

Krishnapriya Hari[1,6], Ana M. Lucas-Osma[1,2,6], Krista Metz[1], Shihao Lin[1], Noah Pardell[1], David Roszko[1], Sophie Black[1], Anna Minarik[1], Rahul Singla[1], Marilee J. Stephens[1,3], Karim Fouad[1,2], Kelvin E. Jones[1,4], Monica A. Gorassini[1,3], Keith K. Fenrich[1,2,7], Yaqing Li[1,5,7] and David J. Bennett[1,2,7,8]

[1]Neuroscience and Mental Health Institute, University of Alberta, Edmonton, AB, T6G 2R3, Canada

[2]Faculty of Rehabilitation Medicine, University of Alberta, Edmonton, AB, T6G 2G4, Canada

[3]Department of Biomedical Engineering, Faculty of Medicine and Dentistry, T6G 2V2, University of Alberta, Edmonton, AB, Canada

[4]Faculty of Kinesiology, Sport and Recreation, University of Alberta, Edmonton, AB, T6G 2H9, Canada

[5]Present address: Department of Physiology, Emory University, Atlanta, GA, 30322, USA

[6]These authors contributed equally

[7]Senior author

[8]Lead Contact

*Correspondence: yaqing.li@emory.edu, bennettd@ualberta.ca,

SUMMARY

GABA is an inhibitory neurotransmitter that produces both postsynaptic and presynaptic inhibition. We describe here an opposing excitatory action of GABA that facilitates spike transmission at nodes of Ranvier in myelinated sensory axons in the spinal cord. This *nodal facilitation* results from axonal $GABA_A$ receptors that depolarize nodes toward threshold, enabling spike propagation past the many branch points that otherwise fail, as observed in spinal cords isolated from mice or rats. Activation of GABAergic neurons, either directly with optogenetics or indirectly with cutaneous stimulation, caused nodal facilitation that increased sensory transmission to motoneurons without postsynaptically exciting motoneurons. This increased transmission with optogenetic or cutaneous stimulation also occurred in awake mice and humans. Optogenetic inhibition of GABAergic neurons decreased sensory transmission, implying that axonal conduction relies on GABA. The concept of nodal facilitation likely generalizes to other large axons in the CNS, enabling recruitment of selective branches and functional pathways.

KEYWORDS

Axon, sodium channel, action potential, branch point failure, gamma-aminobutyric acid (GABA), nodes of Ranvier, nodal facilitation, $GABA_A$ receptor, presynaptic inhibition, $GABA_B$ receptor.

INTRODUCTION

While axons are viewed as the output of neurons, they also receive axoaxonic innervation from other neurons in the brain and spinal cord, allowing complex computations to occur at the axonal level (Debanne et al., 2011). This has been extensively studied for axon terminals, where for example axoaxonic contacts from GABAergic neurons produce presynaptic inhibition of transmitter release (Engelman and MacDermott, 2004; Hughes et al., 2005; Rudomin and Schmidt, 1999). Large myelinated axons in the spinal cord grey matter also receive synaptic inputs near their Na^+ channels (Na_V) at nodes of Ranvier, including GABAergic contacts (Walmsley et al., 1995) and related axonal $GABA_A$ receptors (Lucas-Osma et al., 2018), though their function is unclear. Here we report the counterintuitive finding that a population of GABAergic neurons that innervate terminals of sensory axons in the spinal cord (GAD2+ neurons; Betley et al. 2009; denoted here *$GABA_{axo}$ neurons*) also innervate nodes where they prevent failure of sodium spike transmission at branch points, and ultimately facilitate otherwise silent sensory pathways and reflexes. To this end we resolve and connect a number of long standing paradoxes of spinal cord physiology, as follows.

Like many large myelinated CNS axons, proprioceptive sensory afferents branch extensively, with their axons in the spinal dorsal columns giving off numerous collaterals that each in turn continue to branch en route to the motoneurons (Fig 1A)(Brown and Fyffe, 1978). Due to geometrical considerations, each branch point in axons poses a risk of spike failure (Debanne et al., 2011; Goldstein and Rall, 1974), though branch points are always near nodes (Na_V), which likely serves to minimize failure (Cho et al., 2017; Lucas-Osma et al., 2018). Nevertheless, indirect recordings suggest that sensory axon conduction failure is paradoxically common in the spinal cord, leading to a mismatch of anatomical and functional connections from axons to motoneurons (Burke and Glenn, 1996; Henneman, 1985; Luscher et al., 1983; Wall and McMahon, 1994). But how and why? Recently extrasynaptic α5 $GABA_A$ receptors have emerged as an unexpected candidate for modulating spike failure, since these receptors are consistently found adjacent to nodes on sensory axons (Lucas-Osma et al., 2018).

While GABA is the major inhibitory neurotransmitter in the adult spinal cord, it depolarizes many types of large axons, including sensory and cortical axons (Howell and Pugh, 2016; Price and Trussell, 2006; Trigo et al., 2008), making it paradoxically excitatory. This is caused by a high concentration of chloride in axons, leading to an outward chloride flow through activated $GABA_A$ receptors that depolarize axons (termed here V_{GABA}; also termed PAD) (Bardoni et al., 2013; Szabadics et al., 2006). It has long been known that GABA and associated V_{GABA} lowers the threshold for activation of spikes

with extracellular stimulation of sensory axons or other central axons (Dellal et al., 2012; Lomeli et al., 1998; Wall, 1958). Thus, it seems reasonable to propose that nodal $GABA_A$ receptors and related V_{GABA} may likewise help spike propagation by simply depolarizing the nodes closer to the spike threshold, preventing conduction failure (*nodal facilitation*), an idea we explore here. However, this idea seems to conflict with the longstanding view that $GABA_A$ receptors on sensory afferent terminals produce presynaptic inhibition of transmitter release from large proprioceptive sensory axon terminals contacting motoneurons in the monosynaptic reflex (MSR) pathway (Eccles et al., 1961a; Rudomin and Schmidt, 1999). Nevertheless, repeated efforts have unexpectedly failed to find many $GABA_A$ receptors or associated local depolarizations at these terminals (Alvarez et al., 1996; Betley et al., 2009; Fink et al., 2014; Lucas-Osma et al., 2018), throwing into doubt $GABA_A$-mediated terminal presynaptic inhibition, and forcing us to consider whether $GABA_B$ receptors instead mainly mediate terminal presynaptic, as in other axons (Howell and Pugh, 2016).

The final paradox is that a brief localized activation of sensory afferents from one muscle triggers a widespread and long-lasting GABA-mediated depolarization (V_{GABA} or PAD) of many other afferents of antagonist and contralateral muscles, defying any classical notion of reciprocal organization (Barron and Matthews, 1938; Lucas-Osma et al., 2018; Rudomin, 1999). This widespread excitation minimally involves a trisynaptic circuit where afferents contact intermediary excitatory neurons, which in turn contact $GABA_{axo}$ neurons that finally contact many other afferents to cause V_{GABA} (Betley et al., 2009; Hughes et al., 2005; Jankowska et al., 1981; Zimmerman et al., 2019). Cortical and locomotor activity further drive this circuit (Rossignol et al., 1998; Rudomin, 1999), begging the question of why sensory axons are so commonly depolarized. Here we examine whether this trisynaptic $GABA_{axo}$ circuit causes widespread nodal facilitation in sensory axons that increases reflexes, priming them for movement. Importantly, this sensory activation of $GABA_{axo}$ neurons has a uniquely long time-course that allows us to indirectly examine GABAergic priming in awake mice, rats and humans.

RESULTS

Nodal $GABA_A$ and terminal $GABA_B$ receptors.

To visualize how GABA regulates axons we examined the distribution of $GABA_A$ receptor subunit immunolabelling on nodes and terminals in large myelinated proprioceptive sensory axons, including extrasynaptic α5 subunits, α1 subunits that are mostly synaptic, and ubiquitous γ2 subunits (Figs 1 and S1)(Chua and Chebib, 2017). We labelled axons with neurobiotin injections in rats (Fig 1) or

fluorescent reporters in VGLUT1$^{Cre/+}$ mice (Fig S1), and reconstructed them in 3D. $GABA_A$ receptors containing α5, α1 and γ2 subunits were expressed on these axons (Figs 1D-E, G; S1), though preferentially near Na_V channels (< 6 μm away; Fig 1E, H, S1D). Specifically, $GABA_A$ receptors were on large myelinated 1st and 2nd order branches in the dorsal and ventral horn (Figs 1D-E, H; S1) near their nodes (identified by large Na_V clusters, paranodal Caspr, and an axonal taper; Figs 1C, J; S1), and on short unmyelinated terminal branches in the dorsal horn (3rd order; Figs 1B, G) near nodes on 2nd order branches. In contrast, $GABA_A$ receptors were mostly absent from the long unmyelinated terminal branches contacting motoneurons in the ventral horn (3rd order; Figs 1B, F, G; S1), which also generally lacked Na_V (Lucas-Osma et al., 2018). This left $GABA_A$ receptors on average far from the terminal boutons contacting motoneurons (~500 μm; Fig 1H) relative to the axon space constant (λ_S ~ 90 μm). Nodes were widely spaced, as were branch points (~50 μm separation, Fig 1I), but branch points were always near nodes (100%, within 7 μm; Na_V; Fig 1C-E, I) and associated $GABA_A$ receptors. While nodes sometimes occurred without branching (49%), the majority of nodes expressing $GABA_A$ receptors were at branch points (Fig 1J), implying an importance for branch point GABA. In contrast, $GABA_B$ receptors were found mostly on terminal branches in the ventral horn where boutons had dense receptor expression (within 10 μm; Figs 1F-H, S1F), and not usually on larger myelinated ventral or dorsal branches (not at nodes; Figs 1E, G, J; S1F).

Propagation failure in dorsal horn axons.

To directly record spike propagation failure in group I proprioceptive sensory axons, we made intracellular recordings from their large myelinated branches in the superficial dorsal horn of rat and mouse spinal cords (Figs 2 and 3). When we stimulated the dorsal root (DR) containing the axon, an all-or-nothing spike was recorded in many branches (Figs 2B, 3D) at the latency of the fastest afferent volley (EC) that arrived at the spinal cord (group I afferent; Fig 2B). However, in other axon branches this spike did not occur (~20%), but at the same latency there was a small all-or-nothing residual spike (*failure potential, FP*). This FP was indicative of a spike activating a distant node, but failing to propagate further to the recording site, leaving only its passively attenuated potential (Figs 2C-G, 3E-F), with smaller FPs reflecting more distal failure points in the spinal cord (failure never occurred in the DR itself, Fig 2F). These failing branches were otherwise indistinguishable from non-failing axon branches, exhibiting full spikes (> 60 mV) with current injection pulses (Fig 2Cii, G), and low conductances and resting potentials (~ -65 mV, Fig 2H), ruling out penetration injury. With high repetitive DR stimulation rates all branches (100%) eventually exhibited propagation failure and an

associated FP (at threshold interval for failure; Fig 2E-G), with again the FP implying that the spike is reliably initiated in the DR, but incompletely propagates within the spinal cord.

Axon spike failure was voltage dependent. In branches with failing spikes (FPs) depolarizations that brought the axon closer to threshold enabled full DR-evoked spikes (via current injection, Fig 2Ci; or spontaneous depolarization Fig 2D). Also, in branches without spike failure at rest (*secure spikes*, no FPs) a steady hyperpolarizing current induced spike failure, with more branches failing with increasing hyperpolarization (Fig S2 A-H). Of the two local nodes adjacent to the electrode, one failed first with hyperpolarization, leaving the attenuated spike from the other node (local FP, about 1 λ_S away, Fig S2 A and D), which eventually failed as well with further hyperpolarization, leaving a much smaller FP from more distal nodes (distal FP; Fig S2 A-D, pink FP). Spike failure in a node was always proceeded by a delay in the nodal spike (Figs S2 A-D; blue arrow).

Simulating spike propagation failure by applying a brief current pulse to mimic the current arriving from an upstream node (and FP) yielded similar results, with full spikes evoked at rest, but nearby nodal spikes delayed and then failing as the membrane was held progressively more hyperpolarized with a steady bias current (Fig S2 I, K-M). Large steady depolarizations could also inactivate these spikes (Fig S2 J,K,N; or DR-evoked spikes), though well outside of the physiological range (> -50 mV).

Nodal spike facilitation by GABA.

Since sensory axons are tonically depolarized by spontaneous GABA activity (tone)(Lucas-Osma et al., 2018), we wondered whether this tone influences spike propagation. Blocking either just extrasynaptic α5 $GABA_A$ receptors (with L655708) or other $GABA_A$ receptors (with gabazine) increased the incidence of spike failure (to ~45% and 65%, respectively; from 20%; Fig 2F) and sensitivity to hyperpolarization (Fig S2 E-H), without altering overall spike properties (Fig 2G), implying that spike propagation is highly dependent on GABA. Application of 5-HT to mimic natural brainstem derived 5-HT also increased failure (Fig 2F), likely via its indirect inhibition of tonic $GABA_A$ receptor activity (Lucas-Osma et al., 2019).

Nodal spike facilitation by $GABA_{axo}$ neuron activation.

To examine how GABA facilitates spike transmission, we next expressed light-sensitive channelrhodopsin-2 (ChR2) in $GABA_{axo}$ neurons in adult $GAD2^{CreER/+}$; $R26^{LSL\text{-}ChR2\text{-}EYFP}$ mice (termed GAD2//ChR2-EYFP mice, Fig 3). A brief light pulse (5 - 10 ms) produced a long-lasting depolarization

and spiking in these $GABA_{axo}$ neurons (Fig 3A), followed by an even longer lasting $GABA_A$-mediated depolarization (V_{GABA}) of proprioceptive axons at a monosynaptic latency (~1.5 ms after spike onset in $GABA_{axo}$ neurons, Methods; Fig 3A, B) that was blocked by gabazine (Fig 3B; V_{GABA}). In these mice, spikes in proprioceptive axons failed with a similar incidence as observed in rats (Figs 3C-H), but the light evoked V_{GABA} prevented this failure (Fig 3E-G), similar to direct depolarization (Fig 2). In branches with secure (non-failing) spikes light had little effect (Fig 3D), but blocking $GABA_A$ receptors again increased the incidence of spike failure (Fig 3H).

In GAD2//ChR2-EYFP or GAD2//ChR2-EYFP//tdTom mice the EYFP and tdTom reporters labelled GABAergic neurons (Fig 3L; VGAT+, GAD2+ and VGLUT1-) residing near the central canal and throughout much of the dorsal horn (Fig 3J-M). They densely innervated the dorsal horn with fine terminal boutons (Fig 3K, Mii), and less densely innervated both the ventral horn and dorsal columns (Fig 3Mi and iii), allowing GABAergic innervation of sensory axons along their entire length. They made both synaptic (VGAT+) and perisynaptic contacts all along proprioceptive sensory axons, both at nodes and sensory axon terminals on motoneurons (Figs 3L & 1E), confirming their identity as $GABA_{axo}$ neurons.

Computer simulations mimic branch point failure.

To prove that spike failure arises at the branch points where GABA can influence them, we generated a computer simulation of a fully reconstructed sensory axon arbour in the spinal cord (Walmsley et al., 1995). With simulated DR stimulation, spike failure mostly occurred distal to complex branch points (at nodes N2 and N3 in Fig S3A-B) that had associated increases in net conductance (shunting the nodal currents). Simulated nodal $GABA_A$ receptor activation rescued these failed spikes, with increasing $GABA_A$ activation (g_{GABA}) preventing more branch point failures (Fig S3C). In contrast, when we moved all these $GABA_A$ receptors to the terminals (away from the nodes) then their activation did not rescue failed spikes (Fig S3D). $GABA_A$ induced depolarizations (V_{GABA}) were attenuated sharply with distance ($\lambda_S \sim 90$ µm, Fig S3A); so only nodal, and not terminal, induced V_{GABA} was visible at our typical recording site near the dorsal columns (Figs 3 and S3 G-H).

Spike facilitation by sensory evoked $GABA_{axo}$ activity

We next examined whether natural activation of $GABA_{axo}$ neurons affects axon conduction. $GABA_{axo}$ neurons are indirectly activated by sensory activity via two variants of a classic trisynaptic circuit: one driven by cutaneous afferents (Fig S4 A) and the other by proprioceptive afferents (Fig S4 C). Both

these circuits cause fast synaptic and slower extrasynaptic $GABA_A$ receptor mediated depolarizations of proprioceptive axons (termed phasic V_{GABA} and tonic V_{GABA}, the latter especially cutaneous driven) that are blocked by $GABA_A$ antagonists (Lucas-Osma et al., 2018), and mimicked by optogenetic activation of $GABA_{axo}$ neurons (Fig 4B-D).

Like with direct $GABA_{axo}$ activation, spike propagation failure was prevented by sensory evoked phasic V_{GABA}, regardless of whether the failure was spontaneous (Figs 4E-F, H), 5-HT-induced (Fig 4H), or repetition-induced (Fig S4 D-H). This action was abolished by gabazine but not L655935, supporting a synaptic origin (Fig 4H). Slow extrasynaptic GABAergic depolarizations (tonic V_{GABA}; L655935-sensitive Lucas-Osma et al. 2018) further aided failed spikes (Fig 4G), especially as it built up with repeated DR stimulation (at 1 Hz; Fig S4 B). Cutaneous (Fig S4A-B), proprioceptive (Fig S4H) or mixed afferent (Fig 4 E-H) -evoked V_{GABA} all helped prevent spike failure.

In secure axon branches (not failing with a single DR stimulus), sensory-evoked V_{GABA} (Fig S5A; or optogenetic $GABA_{axo}$ activation, Fig 3D) sped up and narrowed the spike (Figs S5A-B, 3D) and lowered its threshold (Fig S5C-D; rheobase current), as predicted from computer simulations (Fig S3E). Importantly, the V_{GABA} depolarizations only slightly reduced the spike height (~1% or 1 mV; Figs S5A-B, 3D) indicating that nodal $GABA_A$ receptor conductances have minimal shunting action (Fig S5C-D).

$GABA_{axo}$ activity enables high frequency spike transmission.

Since sensory axons naturally fire at high rates (Prochazka and Gorassini, 1998) where they are vulnerable to spike failure (Fig 2E-F), we next examined the action of GABA on this failure. During rapid repetitive stimulation of a DR to evoke spikes in an axon there was an inevitable activation of V_{GABA} from low threshold proprioceptive axons (Fig S4 C-E). This V_{GABA} helped spikes fire at high physiological rates of up to 200-300 Hz (5 – 3 ms intervals) before spike inactivation and failure occurred because, in absence of V_{GABA}, isolated repetitive activation of the axon with intracellular current pulses (IC) led to failure at much lower rates (~100 Hz; longer spike intervals; Fig S4 D, G), even after just two stimuli (doublets; Fig S4 E, G). Additional V_{GABA} evoked by simultaneous stimulation of an adjacent DR (2xT) reduced failure from fast repeated IC stimuli (Fig S4 D, H), repeated DR stimuli (doublet, Fig S4 E-F, H) or hybrid IC-DR stimulation pairs (Fig S4 H).

Failure of axon conduction to motoneurons.

We next quantified the overall failure of spikes to conduct from the DR to the sensory axon terminals on motoneurons, by adapting a method developed by Wall and McMahon (1994), where failure was estimated by measuring whether failed axons were *not* refractory to subsequent stimulation from a microelectrode in the ventral horn (Fig S6 A-D). This method indicated that about 50 – 80% of sensory axons failed to conduct to their ventral terminals under resting conditions, especially in long axons, whereas evoking V_{GABA} with a prior DR stimulation decreased failure to < 30% (Fig S6E). Similar conclusions were reached by directly recording the extracellular afferent volley in the ventral horn produced by the spikes propagating from a DR stimulation to the motoneurons, which was consistently increased by evoking V_{GABA} (Fig S6 F-N).

Reflex priming mediated by $GABA_A$ receptors.

To examine the functional role of nodal GABA we recorded monosynaptic excitatory postsynaptic potentials (EPSPs) from motoneurons in response to proprioceptive sensory axon stimulation (of the DR; Fig 5A), the pathway that underlies the monosynaptic reflex. This EPSP was inhibited when sensory axon conduction was reduced by optogenetically silencing $GABA_{axo}$ neurons with light in mice expressing archaerhodopsin-3 (Arch3, induced in $GAD2^{CreER/+}$; $R26^{LSL\text{-}Arch3\text{-}GFP}$ mice; abbreviated GAD2//Arch3; Fig 5A-B, D), consistent with a tonic $GABA_A$ receptor tone facilitating spike transmission in axons. Likewise, the EPSP was reduced by blocking endogenous $GABA_A$ receptor tone with antagonists, despite markedly increasing motoneuron and polysynaptic reflex excitability (the latter minimized with APV, Fig 5C, D). $GABA_B$ antagonists slightly increased the EPSP, consistent with a tonic $GABA_B$ mediated presynaptic inhibition (Fig 5D).

Consistent with nodal facilitation by $GABA_A$ receptors, the monosynaptic EPSP was increased (*primed*) during, but not after, increasing sensory axon conduction by depolarizing them (V_{GABA}) with an optogenetic activation of $GABA_{axo}$ neurons in GAD2//ChR2 mice (10 ms *light conditioning stimulation*; Fig 5E-F). The EPSP was also increased by more naturally activating $GABA_{axo}$ neurons by a *sensory conditioning stimulation* (Fig S7A-B), including with conditioning stimulation of proprioceptive (Fig S7 E) and/or cutaneous (Fig S7 B, E) axons. The former indicates that proprioceptive activity primes subsequent proprioceptive reflex transmission (*self-priming*). $GABA_A$ receptor antagonists (gabazine), but not $GABA_B$ antagonists (CGP55845), blocked the EPSP priming with sensory (Fig S7E) or light (Fig 5F) conditioning.

The priming of the EPSP by conditioning arose from axonal $GABA_A$ receptors, rather than postsynaptic actions on the motoneurons, since it occurred with weak conditioning stimuli that produced only a transient background postsynaptic depolarization that terminated well before the EPSP testing (at 60 ms; Figs 5E, S7 B, G), followed by a slight hyperpolarization (Fig S7H, V_m) that if anything reduced the EPSP (shunting the synaptic current, Fig S7 H). Increasing the DR conditioning intensity produced large background motoneuron depolarizing conductances during the EPSP testing that led to some outright postsynaptic inhibition of the EPSP (shunting; Fig S7 D, G), masking the effect of nodal facilitation. Increasing the DR stimulus used to evoke the EPSP, also generally decreased the priming of the EPSP (Fig S7 F). This is likely because it reduced the headroom for increasing EPSPs by recruiting more proprioceptive axons, and increased self-priming prior to conditioning, the latter during repeated testing used to obtain EPSP averages.

Priming with repeated conditioning and self-priming.

Sensory conditioning was particularly effective when it was repeated to mimic natural firing, which increased V_{GABA} for minutes (tonic V_{GABA}; fast repetition, Fig 5G), and increased (primed) the EPSP for 1 – 3 min after a brief fast repetition (200 Hz, 0.5 s conditioning, Figs 5I, S7E, *Tonic*), and 1 min after slower repetition (0.1 Hz, 2 min conditioning, Fig S7 E, *After effect*), both long outlasting postsynaptic effects (< 1 s). This was blocked by L655708 or gabazine (α5 $GABA_A$ mediated; Fig S7E). ChR2 activation of $GABA_{axo}$ neurons lacked these long tonic V_{GABA}-mediated after effects on the EPSP priming (Fig 5E-F, Post), suggesting an additional source of GABA mediating these after effects.

Post activation depression masks reflex priming.

Importantly, when the DR conditioning stimulation (or light conditioning) was increased sufficiently V_{GABA} itself induced afferent spikes (Fig S5E; termed DRR spikes). Following these spikes, the EPSP was smaller than when these spikes were not present (n = 8/8 mice, not shown). This is because these DRR spikes themselves triggered EPSPs (not shows), leading to a post activation depression, as noted by Eccles (Eccles et al., 1961a).

Nodal facilitation increases the probability of unitary EPSPs.

We noticed large all-or-nothing EPSPs (unitary EPSPs) spontaneously fluctuating on and off during repeated EPSP testing, leading to discrete large changes in the total EPSP size (and time course; Fig 5J-K). We thought this might be due to spontaneous branch point failures, rather than quantal changes in transmitter release that produce much smaller fluctuations (Redman, 1990), as previously suggested

(Henneman et al., 1984). Indeed, when we increased the axon conduction by activating the $GABA_{axo}$ neurons (via a cutaneous conditioning train) the *probability* of unitary EPSPs occurring increased (Fig 5K-L), and this sometimes recruited further large unitary EPSPs (Fig 5K, units 2 and 3). In contrast, the *size* of the underlying unitary EPSP was not increased by this conditioning (Fig 5 J-L), ruling out increased transmitter release or postsynaptic actions contributing to the increased overall EPSP (Fig 5I, L).

Reflex priming in the awake mice with optogenetic conditioning.

To prove that $GABA_{axo}$ neurons increase sensory transmission to motoneurons in *awake* mice we activated these neurons directly with light applied through a window chronically implanted over the spinal cord of GAD2//ChR2 mice (Fig 6A), and assessed the monosynaptic reflex (MSR) recorded in tail muscles in response to nerve stimulation (counterpart of EPSPs of Fig 5). As expected, the MSR increased following a conditioning light pulse, during, and not after, the expected time of phasic V_{GABA} induced on sensory axons (Fig 6B, I). This light-induced *priming* occurred both at rest and when there was a background voluntary contraction (Bkg EMG), with the latter matched with and without light, again ruling out postsynaptic depolarization related differences in MSR (Fig 6C). Light alone caused a brief pause in ongoing EMG (at 30 - 40 ms post stimulation; Fig 6B), an expected postsynaptic inhibition (Discussion) that masked the priming at short latencies.

Reflex priming in humans and rats with sensory conditioning.

Finally, we evaluated whether sensory conditioning likewise increases the MSR in humans and awake rats. For this we recorded the MSR in humans in the leg extensor soleus muscle in response to tibial nerve stimulation (Fig 7A). Increasing $GABA_{axo}$ neuron activity with a brief cutaneous stimulation increased the MSR (Fig 7 Bi, D, 6 D-F) during a period consistent with nodal facilitation by V_{GABA} (30 – 200 ms post stimulation; in humans and rats, Fig 7 B ii, Fig 6 I). We again kept the conditioning stimulation small enough (Fig 6E-F) to not change the EMG or single motor unit (MU) firing (the latter in humans; Fig 7Biii), to rule out postsynaptic actions. Also, blocking $GABA_A$ receptor tone (in rats) decreased the MSR, at matched levels of background EMG (Fig 6G), suggesting a spontaneous promotion of the MSR by nodal GABA.

As previously reported (Hultborn et al., 1987), a brief vibration of the flexor TA muscle (to activate proprioceptive afferents and related V_{GABA}) reduced the soleus MSR in humans (for up to 200 ms; Fig 7Ci-ii). However, we noticed that this vibration alone inhibited the ongoing discharge of a single soleus

motor unit (MU; Fig. 7Ciii) while the MSR was inhibited, implying that this MSR inhibition was in part caused by postsynaptic inhibition, rather than presynaptic inhibition.

In both humans and rats, repeated cutaneous conditioning stimulation (trains) to induce a buildup in axon depolarization (tonic V_{GABA}) caused an associated buildup of the MSR that outlasted the conditioning and its postsynaptic actions by many seconds (after effect; Fig 7D, E; Fig 6 H), and this was inhibited by the extrasynaptic $GABA_A$ antagonist L655935 (for rats, n = 5/5; not shown). Importantly, in humans the probability of a single MU contributing to the MSR was increased by these cutaneous conditioning trains (Fig 7F i-ii), without increasing the estimated EPSP amplitude or rise time (computed using the PSF; see Methods; Fig 7F iii) or changing the MU firing prior to the MSR testing (Fig 7F iv, not depolarizing the motoneuron closer to threshold), consistent with an increased probability of unitary ESPSs, as in rats (Fig 5).

DISCUSSION

Following the pioneering studies of Eccles on inhibition of the monosynaptic connection from sensory axons to motoneurons (Eccles et al., 1961a), the concept of presynaptic inhibition of axon terminals has stood as a cornerstone of our modern understanding of mammalian brain and spinal cord function (Engelman and MacDermott, 2004). While presynaptic inhibition has surprisingly never been directly confirmed in these sensory axons, recordings from invertebrate sensory axons have shown that terminal $GABA_A$ mediated depolarizations sometimes lead to Na_V inactivation or conductance increases (shunts) that inhibit transmitter release (Cattaert and El Manira, 1999; Trigo et al., 2008). However, more direct recordings from the actual terminal boutons in the mammalian brain (e.g. Calyx of Held) show that such presynaptic receptors, including $GABA_A$ and glycine receptors, more often do the opposite, promoting transmitter release by, for example, depolarization-induced inactivation of K_V or facilitation of Ca_V channels (Howell and Pugh, 2016; Trigo et al., 2008; Zbili and Debanne, 2019). Our results take this one step further, unexpectedly showing that $GABA_A$ receptors cause little, if any, direct presynaptic inhibition of sensory transmission to motoneurons, simply because they are primarily located too far from the terminals to influence terminal depolarization (relative to short λ_S), as we have observed with direct terminal recordings (Lucas-Osma et al., 2018). Instead, $GABA_A$ receptors are near Na_V channels (nodes) and associated branch points, where they help prevent conduction failure by bringing nodes closer to the spike threshold, consistent with computer simulations.

We reached these conclusions by demonstrating four concepts: 1) Spike transmission fails in many central branches of large myelinated sensory axons, leaving large silent branches, depending on the branching structure and prior history of activity (frequency), the latter similar to failure in terminals of smaller axons (Kawaguchi and Sakaba, 2015). 2) Depolarizations from nodal $GABA_A$ receptors (synaptic and extrasynaptic) help prevent spike failure, without which failure can approach 50 - 80%. 3) $GABA_{axo}$ neurons innervate sensory axon nodes along the entire length of the axon, and prime sensory transmission to motoneurons. 4) Sensory driven circuits that produce widespread $GABA_{axo}$ activity cause priming of sensory transmission and reflexes, including in humans and awake rodents, suggesting substantial ongoing spike failure (prior to priming) that can be alleviated by repetitive afferent activity, similar to post-tetanic potentiation (Lloyd, 1949; Luscher et al., 1979b). These concepts of nodal facilitation may generalize to other large central axons (e.g. pyramidal cells) that are innervated by GABAergic neurons, branch extensively, and have depolarizing actions of GABA (Burke and Bender, 2019; Szabadics et al., 2006; Trigo et al., 2008; Zorrilla de San Martin et al., 2017), allowing selective recruitment of specific axon branches and functional pathways, especially for high frequency firing.

The pressing question that remains is how can nearly a century of data on sensory transmission and presynaptic inhibition be reconciled with GABA-mediated nodal facilitation and reflex priming (detailed in Table S1)? Sensory axon conduction failure has repeatedly been noted from indirect observations (Barron and Matthews, 1935; Gemes et al., 2013; Henneman et al., 1984; Howland et al., 1955; Li et al., 2020; Luscher et al., 1983). However, when GABAergic terminals were reported near nodes on myelinated branches, Wall and others started questioning whether GABA may regulate branch point failure (Wall, 1998; Wall and McMahon, 1994; Walmsley et al., 1995). Unfortunately, the prevailing idea that $GABA_A$ receptors should inhibit transmission led these investigators to only examine whether GABA could block spike transmission (Verdier et al., 2004; Wall and McMahon, 1994), rather than assist spikes. Thus this enquiry was largely dropped when computer simulations showed physiological GABA levels unlikely to block spikes (Walmsley et al., 1995), as we confirmed.

The evidence for $GABA_A$ receptor mediated terminal presynaptic inhibition of sensory transmission was from the outset circumspect, based mainly on the observation that a conditioning stimulation (on a flexor nerve) caused an inhibition of the MSR (evoked in extensor muscles) that was somewhat correlated to the time-course of V_{GABA} caused by this conditioning (in extensor afferents)(Eccles et al., 1961a; Eccles et al., 1962b). However, in retrospect this V_{GABA} is far too brief to account for the much longer (up to 1 s) inhibition caused by this conditioning (Curtis and Lacey, 1994; Eccles et al., 1962a;

Rudomin, 1999). Curtis and Lacey (1994) later concluded that much of this inhibition is blocked by $GABA_B$ antagonists and mediated by $GABA_B$ receptors (see also Fig 5D and Fink et al. 2014), which we have now confirmed by direct imaging of $GABA_B$ receptors in terminals of proprioceptive afferents. This fits with $GABA_B$ receptors being primarily responsible for presynaptic inhibition in many neurons (Howell and Pugh, 2016; Trigo et al., 2008), but does not rule out $GABA_A$-mediated presynaptic inhibition in other sensory axons that have dense terminal $GABA_A$ receptor expression (cutaneous afferents, Lucas-Osma et al., 2018).

In their pioneering work, Frank and Fortes (1957, 1959) suggested that the inhibition of the MSR by flexor nerve conditioning might be partly postsynaptic (rather than presynaptic), acting on remote dendrites of motoneurons. Subsequent anatomical studies confirmed that such postsynaptic inhibition is inevitable, since most $GABA_{axo}$ contacts on afferent terminals also contact motoneurons, in a triad (Hughes et al., 2005; Pierce and Mendell, 1993). Indeed, we find that $GABA_{axo}$ neuron activation produces an inhibition of motoneurons (Fig 6B) and associated MU firing (Fig 7C) that masks, and at times overwhelms, the facilitation of the MSR by nodal $GABA_A$ receptors (as with muscle vibration) (Hultborn et al., 1987). Previous arguments that isolated presynaptic inhibition with conditioning should be evident from reductions in the EPSP without changing its time course (McCrea et al., 1990) now seem untenable, especially as unitary EPSPs differ markedly in shape and conditioning alters the proportion of unitary EPSPs contributing to the EPSP (Fig 5K)(Henneman et al., 1984).

Early on Barron and Matthews (1938) and later others (Eccles et al., 1961b; Fink et al., 2014; Lucas-Osma et al., 2018)(Fig S5E) established that sensory-evoked V_{GABA} (or light-evoked) excites axons by directly inducing spiking, including spikes in the sensory axons mediating the MSR itself, raising a further contradiction with presynaptic inhibition. While these V_{GABA}-triggered spikes only sometimes fully propagate antidromically out the DRs (Beloozerova and Rossignol, 1999), they are more likely to conduct orthodromically (Lucas-Osma et al., 2018) where they activate the motoneurons (Bos et al., 2011; Duchen, 1986; Eccles et al., 1961a; Fink et al., 2014), making these axons and their motoneuron synapse refractory to subsequent testing (Eccles et al., 1961a). This contributes to a long lasting *post activation depression* of the MSR pathway that is $GABA_A$ mediated (sensitive to $GABA_A$ antagonists, like V_{GABA}) and is thus readily mistaken for $GABA_A$-mediated presynaptic inhibition (Eccles et al., 1963; Fink et al., 2014; Redman, 1998).

In summary, post activation depression, postsynaptic inhibition, and $GABA_B$-mediated presynaptic inhibition have historically been mistaken for $GABA_A$-mediated presynaptic inhibition, making nodal facilitation hard to demonstrate (Table S1). In humans and rats, our strongest evidence for nodal facilitation is that unitary EPSPs (and associated MU firing) become more probable during sustained V_{GABA} evoked with cutaneous stimulation (Fig 7). This increased probability occurs without increasing the unitary EPSP amplitude or the prior postsynaptic depolarization of the motoneurons, ruling out pre or postsynaptic facilitation, including ruling out previous arguments that MSR facilitation by cutaneous conditioning is due to a removal of presynaptic inhibition (Aimonetti et al., 2000; Rudomin et al., 1974).

Functionally, nodal facilitation by $GABA_A$ receptors acts like a global switching system that recruits entire silent sensory or motor circuits (altering receptive fields or reflexes). This works in concert to terminal pre- and postsynaptic inhibition (including $GABA_B$ and $GABA_A$ actions, depending on the axon type, Table S1), that locally fine tunes the reflex gains, to optimize the stability and compliance of movement (Bennett, 1993; Bennett et al., 1994). Branch point failure in sensory axons is under explicit cortical control, since it is decreased by spinal cord transection (Nelson et al., 1979), increased by 5-HT that is normally derived from the brainstem (Fig 2)(Lucas-Osma et al., 2019), and likely regulated by cortical drive that directly activates $GABA_{axo}$ neurons (Russ et al., 2013; Ueno et al., 2018). The diffuse nature of V_{GABA} (Lucas-Osma et al., 2018) implies that nodal facilitation acts over large regions of the spinal cord to ready sensory axons for action, reminiscent of the Jendrassik maneuver (Zehr and Stein, 1999), enabling quick sensory-driven responses to external disturbances, such as correcting stumbling during standing or walking. Overall, our results raise more functional questions than they answer, especially if axonal $GABA_A$ receptors (and V_{GABA}) also mediate nodal facilitation rather than presynaptic inhibition in other CNS axons.

ACKNOWLEDGEMENTS

We thank Leo Sanelli, Jennifer Duchcherer and Christopher K. Thompson for technical assistance, and Shawn Hochman, CJ Heckman, FJ Alvarez and Tia Bennett for discussions and editing the manuscript. VGLUT1^{Cre} mice were kindly donated by Dr. Francisco J. Alvarez. This research was supported by the Canadian Institutes of Health Research (MOP 14697 and PJT 165823 D.J.B.) and the US National Institutes of Health (NIH, R01NS47567; D.J.B. and K.F.).

AUTHOR CONTRIBUTIONS

K.H, and A.M.L-O. designed the study, carried out the animal experiments and analyzed data. K.M. and M.A.G. designed and performed the human experiments. N.P. and K.E.J. designed and performed the computer simulations. S.L., S.B., A.M., M.J.S. and R.S. assisted with animal electrophysiology. K.F. and A.M.L-O provided confocal microscopy. K.K.F, S.L., D.R. and K.H. developed the transgenic mice and performed the optogenetic experiments. Y.L. and D.J.B. conceived and designed the study, carried out experiments and analyzed data. D.J.B, K.H., and Y.L. wrote the paper, with editing from other authors.

DECLARATION OF INTERESTS

The authors declare no competing interests.

FIGURE LEGENDS

Figure 1. Nodal $GABA_A$ and terminal $GABA_B$ receptors in rats.

(A-B) Neurobiotin filled proprioceptive Ia axon in the sacrocaudal rat spinal cord (S4 and Ca1), reconstructed from fluorescent images (inset), with branching order indicated. Some ventral branches truncated in A, but typical arbour shown in B. Central canal: cc. Dorsal columns: dc. Dorsal and ventral horns: DH and VH.

(C) Node on axon branch in DH immunolabelled for sodium channels (Na_V), paranodal Caspr and myelin (MBP), with the paranodal taper indicated, and co-labelling within the axon rendered in 3D (bottom). 1st order branch in DH.

(D-F) α5 $GABA_A$, α1 $GABA_A$ and $GABA_B$ receptor immunolabelling (yellow) in 3D reconstructed axon branches in DH (also raw images in Di and ii, for α5 and α1), with nodes identified by Na_V and paranodal taper, GABA contacts by vesicular inhibitory amino acid transporter (VGAT, E) labelling, and terminals by vesicular glutamate transporter 1 (VGLUT1, F) or nearby NF200 (on motoneurons in VH). 1st to 2nd order branch points (bp) in DH.

(G) Receptor densities on axon branches of varying order. *Mean* ± *SD* plotted. Dashed lines: lower confidence interval, 1 SD below mean maximum density. * significantly more than ventral terminal (3rd order) receptor density, + ventral terminal receptor density significantly more than 1st and 2nd order branch densities, $P < 0.05$, $n = 10$ - 17 branches per condition.

(H) Distances between GABA receptor clusters and nodes (d_{RN}), branch points (d_{RB}) or terminals (d_{RT}). * significantly less than d_{RT}. + significantly less than d_{RN} and d_{RB}, $P < 0.05$, $n = 80$ - 110 clusters per condition.

(I) Distances between branch points (d_{BB}), nodes (Na_V clusters, d_{NN}), and nearest branch to node (d_{NB}). * significantly larger than d_{NB}, $P < 0.05$, $n = 60$ - 95 per condition.

(J) Proportion of nodes with GABA receptors (from H), with and without (hashed) nearby branch points.

Figure 2. Spike failure.

(A) Recording from ex vivo whole adult rat spinal cord.

(B-D) Intracellular recordings from proprioceptive axon branches in rat spinal cord dorsal horn (DH), with dorsal root (DR) stimulation (1.1x threshold T, 0.1 ms) evoking a spike in some branches (secure, B) and only a failed spike in others (failure potential, FPs; C, D), but depolarization restoring full spikes (black, C and D). Averages of 10 trials at 3 s intervals. Resting potential: thin line. EC: extracellular afferent volley. Axons from S4 sacral DR.

(E) Fast repeated DR stimulation induced failure in secure spikes (not failing on first stimulation, 1.1xT). Threshold (longest) interval for failure shown (with FP).

(F) Proportions of DH axon branches (or DR axons) failing to spike with DR stimulation under control resting conditions and with L655708 (0.3 μM), gabazine (50 μM; GBZ), 5-HT (10 μM) or fast repetition (doublet, E). * significantly more than control, χ-squared test, $P < 0.05$, n indicated in bars.

(G) Summary of spike and FP heights in secure and failing branches. Box plots: median, thin line; mean, thick line; interquartile range IQR, box; extreme data points within 1.5 x IQR of box, error bars. * significantly smaller than secure spike, $P < 0.05$, for spikes in F.

(H) Resting membrane potential and conductance for secure and failing branches, not significantly different, $P > 0.05$, for control axons in F.

Figure 3. Nodal facilitation by $GABA_{axo}$ neurons.

(A) Intracellular recording from $GABA_{axo}$ neuron in ex vivo spinal cord of GAD2//ChR2-EYFP mouse, with ChR2 activated with a light pulse (5 ms, λ = 447nm laser, 0.7 mW/mm^2, 1.5x light threshold, T) causing a long depolarization and asynchronous spiking; isolated in 50 μM gabazine (n = 5/5 similar). Average of 10 trials at 0.3 Hz, blue. V_{GABA} from B, grey. Resting at -61mV.

(B) Intracellular recording from proprioceptive axon branch (in DH, sacral S3) with light pulse (1.5xT) producing a long depolarization (V_{GABA}, n = 14). Average of 10 trials at 0.3 Hz. *significantly less with gabazine or omitting ChR2 (control mice), n = 12 each. Resting at -71 mV.

(C-G) DR stimulation at rest (1.1xT) evoked a secure spike in some axon branches (D) and not others (FPs, E, F; DH S3 axons). Light evoked V_{GABA} (λ, 1.5xT, 10 ms prior) rescued failed spikes (E, F) and sped up conduction in secure spikes (D). Box plots of FPs and spikes (G); * significant increase with light, n = 10; + significant reduction in light effect with 50 μM gabazine, n = 7.

(H) Incidence of branches with failed DR-evoked spikes. * significant change with gabazine, χ-squared test, $P < 0.05$, n indicated.

(J-M) $GABA_{axo}$ neurons imaged in S3 spinal cord of GAD2//ChR2-EYFP//tdTom (K, M; green/red, merge yellow) or GAD2//ChR2-EYFP (L, green, dorsal horn) mice. Innervation of 3D reconstructed neurobiotin filled sensory axons (gold in K and L, as in Fig 1) by $GABA_{axo}$ neurons (green; axon contacts labelled red in L) in dorsal horn. Nodes identified by Caspr and paranodal taper, sensory terminals by VGLUT1, $GABA_{axo}$ terminals by VGAT, and axonal $GABA_A$ receptors by the α5$GABA_A$ subunit. ChR2-EYFP is mainly expressed on plasma membranes (Boyden et al., 2005), whereas tdTom is cytoplasmic, and so tdTom rings EYFP labelling, especially evident on the soma and boutons (K, M).

Figure 4. Sensory driven nodal facilitation.

(A) Experimental setup to indirectly activate $GABA_{axo}$ neurons by DR stimulation (DR1), via a trisynaptic circuit detailed in Fig S5, in ex vivo spinal cords of rats or GAD2//ChR2-EYFP mice.

(B-C) Depolarization of a proprioceptive axon branch (B, intracellular in sacral S3 DH) or multiple axons in a DR (C, grease gap recording; sacral S3 DR; DR2) from stimulating the adjacent S4 DR (1.1xT, 0.1 ms pulse; DR1) or applying a light pulse to activate $GABA_{axo}$ neurons (5 ms, 447nm, 0.7 mW/mm^2, as in Fig 3B), both blocked by gabazine (50 µM; V_{GABA}), in GAD2//ChR2 mouse. Thin line resting potential.

(D) Summary box plots of peak phasic V_{GABA} evoked in axons by adjacent DR stimulation (DR1) or light, at rest (top, rats and mice, n = 14 each) and with hyperpolarization (-10 mV, bottom, same rats), and effects of applied gabazine (50 µM; n = 14 rats) or L655708 (0.3 µM; n = 8 rats). * significant difference from pre-drug (blue, lower plot), $P < 0.05$.

(E-G) DR axon branches (sacral S3 DH) exhibiting spike failure (FPs, magenta) following stimulating their DR (S3 DR, 1.1xT, 0.1 ms; DR2) in rats at rest. Spikes rescued by V_{GABA} evoked by prior conditioning of adjacent DR (S4 or contralateral S3 DR, at 3xT; DR1). Rescue occurs with fast synaptic depolarizations (phasic V_{GABA}; E-F) and tonic depolarizations (tonic V_{GABA}, G), both for local FPs (large, E) or distal FPs (small, F-G).

(H) FP or spike heights before and during DR evoked phasic V_{GABA} (n = 10) as in E-F, and actions of L655708 (n = 9, 0.3 µM), gabazine (n = 14, 50 µM) and 5-HT (n = 8, 10 µM) in rats. *, significant increase in spike with V_{GABA}, $P < 0.05$.

Figure 5. Priming of reflexes by GABA.

(A) Ex vivo recording from motoneurons while illuminating $GABA_{axo}$ neurons with collimated light λ.

(B-D) Composite monosynaptic EPSP in motoneurons (recorded in sacral S4 VR) evoked by a DR stimulation pulse alone (S4 DR, 0.1 ms, 1.1xT, magenta). Actions of optogenetic silencing $GABA_{axo}$ neurons with light (A-B, 532nm, 5 mW/mm^2, 80 ms, in GAD2//Arch3 mice, n = 7), blocking $GABA_A$ receptors (C, with bicuculline or gabazine, 50 µM, with and without NMDA antagonist APV, 50 µM; n = 23 and 13 in rats and mice combined), or blocking $GABA_B$ receptors (D, CGP55845, 0.3 µM, n = 10 rats and 10 mice). V_{GABA} shown for reference, recorded on S3 DR (C, top). Box plots of changes in EPSP and background postsynaptic activity (Bkg, over 10 ms prior to EPSP) with light or drugs, and with Arch3+ and Arch3- (n = 5) mice (D). * significant change Δ, $P < 0.05$. GAD2//Arch3 mice are VGAT+, not shown.

(E-F) Composite EPSP (evoked in S4 motoneurons, as in A-B) before, during and post V_{GABA} (recorded simultaneously on S3 DR) evoked by light activation of $GABA_{axo}$ neurons (10 ms, 1.1xT, 447nm, 0.5 mW/mm^2, 60 ms and 140 ms pre EPSP, ISI) in GAD2//ChR2 mice. Box plots of changes in EPSP and Bkg (10 ms prior) with light in ChR2+ mice without and with gabazine (50 μM, during V_{GABA}), and in ChR2- mice (60 ms ISI). * significant change, $P < 0.05$, $n = 7$ each.

(G) Tonic V_{GABA} (L655905 sensitive) recorded in sacral S4 proprioceptive axon in response to 0.5 s, 200 Hz DR stimulation train applied to the largely cutaneous Ca1 DR of caudal cord (3xT, DR2) in rat.

(H-I) Average EPSP in S4 motoneuron (intracellular recording, EPSP evoked by S4 DR stimulation at 3 s intervals used for average; DR1) before and during tonic V_{GABA} evoked by the brief DR train of G, at matched postsynaptic potentials (Bkg).

(J-K) Individual trials used to make EPSP averages in I (at 1 s intervals, H, thin lines), with large all or nothing unitary EPSPs (thick lines unitary averages; dotted single occurrence of Unit 3). Lowpass filtered at 3 kHz.

(L) Changes in unitary EPSP probability and size, and overall EPSP with tonic V_{GABA}. Box plots. * significant change, $P < 0.05$, $n = 18$.

Figure 6. Priming of reflexes in awake animals.

(A) Experimental setup to record tail muscle EMG and evoke monosynaptic reflexes (MSR) with tail nerve stimulation (1.1xT, 0.2 Hz), while activating $GABA_{axo}$ neurons (V_{GABA}) with light (λ = 447 nm, 10 ms pulse, 1.5xT, 5 mW/mm^2) in GAD2//ChR2 mice.

(B) Effect of light pulse λ on active background EMG (Active Bkg condition in Bi) and the MSR evoked 60 ms later, the latter expanded in Bii. MSR tested with (Bi and Bii, Active Bkg, 30% max) and without (Bii, Rest) background EMG. Thin lines in Bi: individual trial examples at 10 s intervals (0.1 Hz); thick lines: averages.

(C) Changes in MSR with light activation of $GABA_{axo}$ neurons at matched postsynaptic background (Bkg) (over 20 ms prior to MSR; lack of change in Bkg). Measured in active and resting (no Bkg) states, in ChR2+ and ChR2- mice (rest only), and during (60 ms ISI) and post V_{GABA} (200ms ISI at rest only). ISI: interstimulus interval. Box plots. * significant change, $P < 0.05$, $n = 5$ mice each.

(D-F) MSR recorded as in A-C, but in rat and with V_{GABA} instead activated with cutaneous conditioning (tip of tail, 0.2 ms, 2xT, 60 ms prior, 0.1 Hz repetition), at matched active Bkg EMG. * significant change, $P < 0.05$, $n = 8$ rats.

(G) Decrease in MSR with L655935 (1 mg/kg i.p.) at matched Bkg EMG. Box plot. * significant change, $P < 0.05$, $n = 5$ rats.

(H) Typical MSR amplitude before, during and after conditioning as in E, with after effect. Similar in *n* = 5/5 rats.

(I) Typical change in MSR with cutaneous conditioning as in E when the ISI is increased, compared to V_{GABA} (from Fig 4). Similar results in *n* = 5/5 rats.

Figure 7. Priming of reflexes in humans.

(A-B) MSR in soleus EMG evoked by a tibial nerve pulse (1.1xT, 0.2 Hz, A, Bi), and phasic priming of the MSR following a brief conditioning of the cutaneous branch of the deep peroneal nerve (cDP nerve) at varying intervals (ISIs, Bii, 1.0xT, perception threshold T, at rest), and lack of changes in background (Bkg) motor unit (MU) activity or EMG evoked by conditioning alone (Biii, peri-stimulus frequencygram, PSF; with weak contraction).

(C) Same as B, but with proprioceptive conditioning evoked by a brief tibial anterior (TA) muscle tendon vibration (A), which alone inhibited MU activity (postsynaptic inhibition, PSF Bkg, Ciii).

(D) Summary box plots of changes in MSR and postsynaptic (MU) activity with brief conditioning (cDP, *n* = 14 subjects; or TA vibration, n = 6; as in B-C) and long cutaneous conditioning trains (detailed in E, *n* = 14). * significant change with conditioning, $P < 0.05$.

(E) Tonic increase in MSR (tonic priming) after 0.5 s cutaneous conditioning train (cDP, 1.1xT, 200 Hz) at rest (Ei-ii), without prolonged changes in MU activity induced by conditioning alone (Eiii, PSF in weak contraction). MSR evoked by tibial stimulation every 5 s prior to and after train (Ei), with averages shown in 10 s bins (Eii). * significant change in MSR, $P < 0.05$, n = 5 subjects.

(F) Overlay of all MU firing (PSF) with repeated MSR testing (at 5 s intervals) during ongoing weak contraction, and effect of the 0.5 s cutaneous conditioning train (Fi). Summary box plots of increased probability of MU firing during MSR (Fii), without changing estimated EPSP size (Fiii, PSF thin line; thick line unitary EPSP shape from Fig 5J) or background MU firing (Bkg, Fiv). * significant change with conditioning, $P < 0.05$, *n* = 10 subjects.

METHODS

RESOURCES AVAILABILITY

Lead Contact

Requests for further information or reagents should be directed to and will be fulfilled by the Lead Contact, David J. Bennett (bennettd@ualberta.ca).

Materials Availability

This study did not generate new unique reagents.

Data and Code Availability

This study did not generate data sets. Computer code for axon simulations is available online at https://github.com/kelvinejones/noah-axon.git

EXPERIMENTAL MODELS AND SUBJECT DETAILS

Adult mice, rats and humans used.

Recordings were made from large proprioceptive group Ia sensory afferents, GABAergic neurons, motoneurons and muscles in adult mice (2.5 – 6 months old, both female and male equally; strains detailed below) and rats (3 - 8 months old, female only, Sprague-Dawley). All experimental procedures were approved by the University of Alberta Animal Care and Use Committee, Health Sciences division. Recordings were also made from the soleus muscle of neurologically intact adult humans (female and male equally), aged 21 to 58, with written informed consent prior to participation. Experiments were approved by the Health Research Ethics Board of the University of Alberta (Protocols 00023530 and 00076790) and conformed to the Declaration of Helsinki. No effects of sex were noted and data from both sexes were combined for analysis.

Mice used for optogenetics and imaging.

We evaluated GABAergic neurons in a strain of mice with Cre expressed under the endogenous *Gad2* promotor region. *Gad2* encodes the Glutamate decarboxylase 2 enzyme GAD2 (also called GAD65), which is unique to axoaxonic contacting GABAergic neurons that project to the ventral horn, whereas all GABAergic neurons express GAD1 (Betley et al., 2009). These GAD2+ neurons were activated or inhibit optogenetically using channelrhodopsin-2 (ChR2) (Pinol et al., 2012; Zhang et al., 2011) or archaerhodopsin-3 (Ach3) (Chow et al., 2010; Kralj et al., 2011), respectively. The following mouse strains were employed:

1) *Gad2*$^{tm1(cre/ERT2)Zjh}$ mice (abbreviated Gad2^{CreER} mice; The Jackson Laboratory, Stock # 010702; CreER^{T2} fusion protein expressed under control of the endogenous *Gad2* promotor) (Taniguchi et al., 2011),

2) B6;129S-*Gt(ROSA)26Sor*$^{tm32(CAG-COP4*H134R/EYFP)Hze}$ mice (abbreviated R26$^{LSL-ChR2-EYFP}$ mice; The Jackson Laboratory, Stock # 012569; ChR2-EYFP fusion protein expressed under the R26::CAG promotor in cells that co-express Cre because a loxP-flanked STOP cassette, LSL, prevents transcription of the downstream ChR2-EYFP gene) (Madisen et al., 2012),

3) B6.Cg-*Gt(ROSA)26Sor*$^{tm14(CAG-tdTomato)Hze}$ and B6.Cg-*Gt(ROSA)26Sor*$^{tm9(CAG-tdTomato)Hze}$ mice (abbreviated R26$^{LSL-tdTom}$ mice; The Jackson Laboratory, Stock # 007914 and #007909; tdTomato fluorescent protein expressed under the R26::CAG promotor in cells that co-express Cre) (Madisen et al., 2010),

4) B6;129S-*Gt(ROSA)26Sor*$^{tm35.1(CAG-aop3/GFP)Hze}$ mice (abbreviated R26$^{LSL-Arch3-GFP}$ mice; The Jackson Laboratory Stock # 012735; Arch3-GFP fusion protein expressed under the R26::CAG promotor in cells that co-express Cre) (Madisen et al., 2012), and

5) B6;129S-*Slc17a7*$^{tm1.1(cre)Hze}$ mice (abbreviated VGLUT1^{Cre} mice; The Jackson Laboratory, Stock # 023527; Cre protein expressed under control of the endogenous *Vglut1* promotor; kindly donated by Dr. Francisco J. Alvarez) (Harris et al., 2014).

Heterozygous GAD2^{CreER} mice (i.e., GAD2$^{CreER/+}$ mice) were crossed with homozygous reporter strains to generate GAD2$^{CreER/+}$; R26$^{LSL-ChR2-EYFP}$, GAD2$^{CreER/+}$; R26$^{LSL-tdTom}$ and GAD2$^{CreER/+}$; R26$^{LSL-Arch3-GFP}$ mice that we abbreviate: GAD2//ChR2, GAD2//tdTom and GAD2//Arch3 mice. Offspring without the GAD2^{CreER} mutation, but with the effectors ChR2, Arch3 or tdTom were used as controls. We also used mice bred by crossing homozygous VGLUT1^{Cre} mice with R26$^{lsl-tdTom}$ reporter mice to obtain mice with VGLUT1 labelled sensory axons (Todd et al., 2003).

CreER is an inducible form of Cre that requires tamoxifen to activate (Feil et al., 1997), which we applied in adult mice to prevent developmental issues of earlier induction of Cre. Specifically, mice were injected at 4 - 6 weeks old with two doses of tamoxifen separated by two days, and studied > 1 month later, long after washout of tamoxifen. Each injection was 0.2 mg/g wt (i.p.) of tamoxifen dissolved in a corn oil delivery vehicle (Sigma C8267). These tamoxifen-treated mice were denoted GAD2//ChR2+ and GAD2//Arch3+, and non treated mice were used as controls and denoted GAD2//ChR2- and GAD2//Arch2-.

For all mice, genotyping was performed according to the Jackson Laboratories protocols by PCR of ear biopsies using primers specific for the appropriate mutant and wild type alleles for each of the mouse lines (see Key Resources Table for primer details).

METHOD DETAILS

Ex vivo recording from axons and motoneurons in whole adult spinal cords.

Mice or rats were anaesthetized with urethane (for mice 0.11 g/100 g, with a maximum dose of 0.065 g; and for rats 0.18 g/100 g, with a maximum dose of 0.45 g), a laminectomy was performed, and then the entire sacrocaudal spinal cord was rapidly removed and immersed in oxygenated modified artificial cerebrospinal fluid (mACSF), as detailed previously (Harvey et al., 2006; Murray et al., 2010; Murray et al., 2011). This preparation is particularly useful as the small sacrocaudal spinal cord is the only portion of the adult spinal cord that survives whole ex vivo, allowing axon conduction to be assessed along large distances. Further, this segment of cord innervates the axial muscles of the tail that are readily assessable for reflex recording in awake animals, and has proven to be a useful model of motor function in normal and injured spinal cords (Li et al., 2004a; Murray et al., 2010). Spinal roots were removed, except the sacral S3, S4 and caudal Ca1 ventral and dorsal roots on both sides of the cord. After 1.5 hours in the dissection chamber (at 20° C), the cord was transferred to a recording chamber containing normal ACSF (nACSF) maintained at 23 - 32°C, with a flow rate > 3 ml/min. A one-hour period in nACSF was given to wash out the residual anaesthetic prior to recording, at which time the nACSF was recycled in a closed system. The cord was secured onto tissue paper at the bottom of a rubber (Silguard) chamber by insect pins in connective tissue and cut root fragments. The dorsal surface of the cord was usually oriented upwards when making intracellular recording from afferents in the dorsal horn, whereas the cord was oriented on its left side when making recordings from motoneurons

or afferent terminals in the ventral horn. The laser beam used for optogenetics was focused vertically downward on the GAD2 neurons, as detailed below.

Optogenetic regulation of $GABA_{axo}$ neurons.

The GAD2//ChR2 or GAD2//Arch3 mice were used to optogenetically excite or inhibit GAD2+ neurons (with 447 nm D442001FX and 532 nM LRS-0532-GFM-00200-01 lasers from Laserglow Technologies, Toronto), respectively, using methods previously described (Lin et al., 2019). Light was derived from the laser passed through a fibre optic cable (MFP_200/220/900-0.22_2m_FC-ZF1.25 and MFP_200/240/3000-0.22_2m_FC-FC, Doric Lenses, Quebec City) and then a half cylindrical prism the length of about two spinal segments (8 mm; 3.9 mm focal length, Thor Labs, Newton, USA,), which collimated the light into a narrow long beam (200 µm wide and 8 mm long). This narrow beam was focused longitudinally on the left side of the spinal cord roughly at the level of the dorsal horn, to target the epicentre of $GABA_{axo}$ neurons, which are entirely dorsally located (Fig 3). ChR2 rapidly depolarizes neurons (Zhang et al., 2011), and thus we used 5 – 10 ms light pulses to activate $GABA_{axo}$ neurons, as confirmed by direct recordings from these neuron (see below). Light was always kept at a minimal intensity, 1.1x T, where T is the threshold to evoke a light response in sensory axons, which made local heating from light unlikely. Arch3 is a proton pump that is activated by green light, leading to a hyperpolarization and slowly increased pH (over seconds), both of which inhibit the neurons (El-Gaby et al., 2016; Zhang et al., 2011). Thus, we used longer light pulses (~200 ms) to inhibit $GABA_{axo}$ neurons.

To directly confirm the presence of functional GAD2 expression in neurons ($GABA_{axo}$ neurons) we recorded from them with similar methods and intracellular electrodes used to record from motoneurons (see below). Electrodes were advanced into these cells through the dorsal horn (with the dorsal surface oriented upwards), and their identity established by a direct response to light activation of the ChR2 construct (5 – 10 ms light pulse, 447 nm, mW; in GAD2//ChR2 mice), without a synaptic delay (<1 ms) and continued light response after blocking synaptic transmission.

Dorsal and ventral root stimulation.

Dorsal and ventral roots (DR and VR) were mounted on silver-silver chloride wires above the nASCF of the recording chamber and covered with grease (a 3:1 mixture of petroleum jelly and mineral oil) for monopolar stimulation (Li et al., 2004a; Li et al., 2017; Lucas-Osma et al., 2018). This grease was surrounded by a more viscous synthetic high vacuum grease to prevent oil leaking into the bath flow.

Bipolar stimulation was also used at times to reduce the stimulus artifact during recording from ventral roots (detailed below). Roots were stimulated with a constant current stimulator (Isoflex, Israel) with short pulses (0.1 ms). Note that proprioceptive afferents are selectively activated by low intensity DR stimulation (1.1 – 1.5 x threshold, T) and cutaneous afferents are additionally activated by higher intensity DR stimulation (2 – 3xT). DRs were dissected to be as long as possible, and the distal end of this root was stimulated, so it was ~20 mm way from the spinal cord. In this way the DR stimulation site itself (at wire, and threshold for stimulation) could not be affected by axonal depolarizations in the spinal cord, since dorsal root potentials from spinal events (V_{GABA}) are only observed very close to the cord (within a few mm, see below), and drop exponentially in size with distance (Lucas-Osma et al., 2018).

Intracellular recording from sensory axon branches in the dorsal horn.

Electrode preparation and amplifier. Recording from fine afferent collaterals in the spinal cord without damaging them or disturbing their intracellular milieu required specialized ultra-sharp intracellular electrodes modified from those we developed for motoneuron recording (Harvey et al., 2006). That is, glass capillary tubes (1.5 mm and 0.86 mm outer and inner diameters, respectively; with filament; 603000 A-M Systems; Sequim, USA) were pulled with a Sutter P-87 puller (Flaming-Brown; Sutter Instrument, Novato, USA) set to make bee-stinger shaped electrodes with a short relatively wide final shaft (~1 mm) that tapered slowly from 30 to 3 µm over its length, and then abruptly tapered to a final tip over the final 20 µm length. The tip was subsequently bevelled to a 100 nm hypodermic-shaped point, as verified with electron microscope images (Harvey et al. 2006). This very small tip and wide shaft gave a combination of ease of penetrating axons in dense adult connective tissue, and good current-passing capabilities to both control the potential and fill the axons with neurobiotin. Prior to beveling, electrodes were filled through their tips with 2 M K-acetate mixed with varying proportions of 2 M KCl (to make intracellular Cl- concentrations ranging of 0, 100, 500, and 1000 mM) or 500 mM KCl in 0.1 Trizma buffer with 5 - 10% neurobiotin (Vector Labs, Birmingame, USA). They were then beveled from an initial resistance of 40 - 150 MΩ to 30 - 40 MΩ using a rotary beveller (Sutter BV-10). GABAergic chloride-mediated potentials (V_{GABA}) were the same with different concentrations of KCl, without passing large amounts of negative current, as we have previously detailed (Lucas-Osma et al., 2018), indicating that the ultra-sharp tips impeded passive fluid exchange between the electrode and intracellular milieu, with in particular electrode Cl^- not affecting the axon; thus, recordings were mostly made with electrodes with 1 M K-acetate and 1 M KCl, when not filling cells with neurobiotin.

Intracellular recording and current injection were performed with an Axoclamp2B amplifier (Axon Inst. and Molecular Devices, San Jose, USA). Recordings were low pass filtered at 10 kHz and sampled at 30 kHz (Clampex and Clampfit; Molecular Devices, San Jose, USA). Sometimes recordings were made in discontinuous-single-electrode voltage-clamp (gain 0.8 –2.5nA/mV; for Ca PICs) or discontinuous-current-clamp modes (switching rate 7 kHz), as indicated (the latter only when injecting current, for example during recording of input resistance or the voltage dependence of spikes).

Axon penetration. Electrodes were advanced into myelinated afferents with a stepper motor (Model 2662, Kopf, USA, 10 µm steps at maximal speed, 4 mm/s), usually at the boundary between the dorsal columns and dorsal horn gray matter. Extracellular tissue (especially myelin in the white matter) often impeded and blocked the electrode tip following a forward step, as determined by an increase in resistance to small current pulses passed from the tip of the electrode (20 ms, -0.3 nA, 1 Hz), and this was cleared with a brief high frequency current (from capacitance overcompensation buzz) and moving backwards slowly, the latter which helped prevent tissue dimpling. Prior to penetrating afferents, we recorded the extracellular (EC) afferent volley following dorsal root (DR) stimulation (0.1 ms pulses, 3xT, threshold, where T = ~3 uA, repeated at 1 Hz), to determine the minimum latency and threshold of afferents entering the spinal cord. The group Ia afferent volley occurs first with a latency of 0.5 - 1.0 ms, depending on the root length (which were kept as long as possible, 10 - 20 mm), corresponding to a conduction velocity of about 16 - 24 m/s, as previously described for in vitro conduction at 23 C (Li et al., 2004b; Lucas-Osma et al., 2018). When a forward step penetrated an axon, small slow movements were made to stabilize the recordings. Penetrations were usually in the myelinated portion of the axon between nodes, rather than at nodes, because the chance of penetrating a node is low since they only make up a small fraction of the total axon length (Fig 1). The spikes from the two nodes adjacent to the electrode were readily detected separately when testing for the spike threshold with current injection pulses (20 ms; rheobase test), because just at threshold the current sometimes evoked a spike from just one node and not the other, which usually halved the total spike height, consistent with the penetration being about halfway between the two nodes.

Proprioceptive afferent identification. Upon penetration, afferents were identified with direct orthodromic spikes evoked from DR stimulation. We focused on the lowest threshold (T) proprioceptive group Ia afferents, identified by their direct response to DR stimulation, very low threshold (< 1.5 x T), short latency (group Ia latency, coincident with onset of afferent volley), and antidromic response to ventral horn afferent terminal microstimulation (~ 10 µA stimulation via

tungsten microelectrode to activate Ia afferent terminals; tested in some afferents, detailed below)(Lucas-Osma et al., 2018). Clean axon penetrations without injury occurred abruptly with a sharp pop detected on speakers attached to the recorded signal, the membrane potential settling rapidly to near – 70 mV, and > 70 mV spikes readily evoked by DR stimulation or brief current injection pulses (1 – 3 nA, 20 ms, 1 Hz). Sensory axons also had a characteristic >100 ms long depolarization following stimulation of a dorsal root (V_{GABA}, also called primary afferent depolarization, PAD, at 4 - 5 ms latency, detailed below) and short spike afterhyperpolarization (AHP ~ 10 ms), which further distinguished them from other axons or neurons. Injured axons had higher resting potentials (> - 60 mV), poor spikes (< 60 mV) and low resistance (to current pulse; R_m < 10 MΩ) and were discarded.

Quantification of spike conduction failure in the dorsal horn: failure potentials (FPs). Sometimes healthy intracellular penetrations were made into a sensory axon branch (e.g. < -60 mV rest, large V_{GABA}), but dorsal root stimulation did not evoke a full spike, even though a full > 60 mV spike could be readily evoked by intracellular current injection. Instead, DR stimulation evoked a partial spike at the latency and threshold of group Ia afferents, indicating that this was a branch of a Ia afferent that failed to fully conduct spikes to the electrode, with only the passively attenuated spike from the last node to spike prior to conduction failure recorded at the electrode (failure potential, FP; also referred to as electronic residue by Luscher et al. 1994). The size of the FP reflected how far away the spike failure occurred, with spatial attenuation corresponding to a space constant of about 90 µm (see Results), and so FPs became exponentially smaller with distance from failure and undetectable when many mm away (nodes separated by about 50 µm). Occasionally axons were penetrated with undetectable DR evoked spikes or FPs, but otherwise they had characteristics of a Ia afferent (V_{GABA}, R_m similar). These were likely afferents with FPs too distal to detect, but were usually excluded from the main analysis to avoid ambiguity, though this underestimates the incidence of failure. However, some of these axons exhibited short latency, low threshold DR spikes when depolarized by a prior DR stimulation (V_{GABA}) of an adjacent DR, in which case they were unequivocally Ia afferents and included in the analysis (Fig 4F).

Both during extracellular and intracellular recording the group Ia afferent volley (small negative field) was observed as the first event after DR stimulation (the latter subthreshold to a spike), though this was usually small in relation to intracellular events and ignored. However, this was sometimes removed from the intracellular record by subtracting the extracellular potential recorded just outside the same axon to determine the actual transmembrane potential (Lucas-Osma et al., 2018). This was necessary to

see the very smallest FPs following DR stimulation in some afferents, as the negative volley from other nearby afferents obscured the FPs.

After quantifying the axons spikes and conduction failures (FPs) under resting conditions, we then examined the changes in spike conduction with changes in membrane potential induced by either directly injecting current into axons or inducing GABA-mediated changes in membrane potential by pharmacological methods, optogenetic methods (activating ChR2 on $GABA_{axo}$ neurons to induce V_{GABA}) or more naturally evoking V_{GABA} with a DR stimulation.

Neurobiotin filling of axons. Some of the proprioceptive afferents that we recorded intracellularly were subsequently filled with neurobiotin by passing a very large positive 2 - 4 nA current with 90% duty cycle (900 ms on, 100 ms off) for 10 - 20 min. The identity of group Ia proprioceptive afferents were then confirmed anatomically by their unique extensive innervation of motoneurons (Lucas-Osma et al., 2018). Prior to penetrating and filling axons with neurobiotin filled electrodes, a small negative holding current was maintained on the electrodes to avoid spilling neurobiotin outside axons.

Quantification of spike conduction failure in the ventral horn

Wall's method. To measure whether spikes fail during propagation to their fine terminals in the ventral horn we examined whether failed axon segments were relatively less refractory to activation after spike conduction failure, using a double pulse method adapted from Wall (Wall, 1998; Wall and McMahon, 1994). The essence of the method is that after DR activation all nodes that generate spikes become relatively refractory for a few ms, whereas nodes that fail to spike are not refractory to activation. Thus, a microelectrode placed near these failing nodes more readily activates them if they fail rather than generate spikes with DR stimulation and orthodromic conduction. For this we placed a tungston microelectrode (12 MΩ, #575400, A-M Systems, Sequim, USA) in the ventral horn near the axons terminals on motoneurons, to activate the branches/nodes of the axon projecting to the motoneuron that may have failed (VH stimulation).

Spikes from VH or DR stimulation were recorded intracellularly in a proprioceptive axon penetrated in the dorsal horn (near dorsal columns, as detailed above) directly above the VH stimulation site or in an adjacent segment, with two combinations of double axon stimulations. First, we applied two rapidly repeated VH stimuli (VH doublet; two 0.1 ms pulses) at a ~4 ms interval to make the axon relatively refractory to stimulation and determine both the threshold current to activate the first spike (T_{VH1}, with

VH1 stimulation) and the higher threshold current to overcome this the inactivation and generate a second spike (T_{VH2}, with VH2 stimulation). Second, we repeated this double spike activation, but with the first activation from a supra-threshold DR stimulation (at 1.5x DR threshold) and the second from a VH stimulation at the T_{VH2} intensity from B (DR-VH pair). In this case the VH stimulation readily activates the axon spike if the orthodromic DR evoked spike does not propagate to the ventral horn, leaving the silent portion of the axon non refractory. Accordingly, we also determined the threshold current to activate the VH after the DH in this arrangement (termed $T_{DR,VH}$), which was lower than T_{VH2}. For comparison to the spike inactivation with VH doublets, we adjusted the DR-VH pair timing slightly so that the pairs of spikes (or expected spikes, at vertical lines) are separated by the same interval (~ 4 ms) when they reach the recording site, to compensate for DR conduction delays. The putative spike failure with DR stimulation happens at a node somewhere between the recording site and the VH, because we only studied axons that securely conducted single DR pulses to the recording site, and thus failure was not directly visible.

We quantified the spike failure based on the following considerations: If the DR-evoked spike entirely fails to propagate to the VH, then the threshold for subsequently activating the ventral horn ($T_{DR,VH}$) should be the same as the threshold without any prior activation ($T_{VH1} = T_{DR,VH}$), whereas if it does not fail, then the threshold for activating the ventral horn should be the same as with a VH doublet ($T_{VH2} = T_{DR,VH}$). In between these two extreme scenarios, the DR evoked spike may only partially fail to propagate spikes to the ventral horn (by only some of its branches failing or conducting only partially to the VH); in this case $T_{DR,VH}$ should be between T_{VH1} and T_{VH2}, with the difference $T_{VH2} - T_{VH1}$ representing the range of possible thresholds between full failure and full conduction. Thus, overall the failure was quantified as: $Conduction\ failure = (T_{VH2} - T_{DR,VH}) / (T_{VH2} - T_{VH1}) \times 100\%$, which is 100% at full failure and 0% with no failure. This estimate is predicated on the assumption that the failed spikes are only relatively refractory to conduction and increased stimulation can overcome this failure, which is reasonable for the interspike intervals we used, and means that the computed % failure simply reflects the number of nodes that failed to spike, with more dorsal branch point failures giving more failed nodes. On the other hand, we used interspike intervals that were short enough for the DR stimulation not to evoke PAD that affected the subsequent spike threshold (~ 4 ms), in contrast to the longer intervals where PAD can help DR doublet firing (DR-DR in Fig S4, ~ 5 - 10 ms).

Extracellular recording from sensory axon terminals. To directly record conduction failure in proprioceptive afferent terminal branches in the VH we used our intracellular glass pipette electrode

(~30 MΩ) positioned just outside these axons (extracellular, EC), to avoid penetration injury in these fine axon branches. The DR was stimulated near threshold (1.1xT) to evoke the EC response in a few single axons near the electrode, and many trials were averaged to remove noise from these small signals (20 – 50 trials at 3 s intervals). The EC field was multiphasic as previously described for other axons (Dudel, 1965; Hubbard et al., 1969; Munson and Sypert, 1979a), with a small initial positive field resulting from passively conducted axial current from sodium spikes at distant nodes (closer to the DR; outward current at electrode), some of which fail to propagate spikes to the VH recording site, making this field a measure of conduction failure (Dudel, 1965; Hubbard et al., 1969). Following this, a larger negative field arises, resulting from spikes arising at nodes near the electrode (inward current), making this negative field a measure of secure conduction. A relatively large stimulus artifact is present prior to these fields, due to the small size of the EC fields themselves, and we truncated this.

We conducted three control experiments to confirm the relation of these EC fields to spike conduction. First, in the dorsal horn where we can readily intracellularly record from large proprioceptive axon branches, we compared intracellular (IC) recordings from axons to EC recordings just outside the same axon, to confirm that the DR evoked spike (IC) arrives at about the time of the negative EC field. Second, we locally applied TTX to the DR near the recording site (10 µl bolus of 100 µM TTX over DR) which eliminated the negative field and left only the initial positive field, confirming that the positive field is from distal nodes upstream of the TTX block, and generated by passive axial current conduction. This is important, since some investigators have argued on theoretical grounds that the positive field can instead result from the closed end electrical properties of axons at their terminals (Katz and Miledi, 1965), rather than spike failure, though others have refuted this (Dudel, 1965). Finally, we improved nodal spike conduction by reducing the divalent cations Mg^{++} and Ca^{++} in the bath medium, since divalent cations normally cause a guarding action on the sodium channel by one charge binding to the membrane and the other raising the local extracellular positive charge, and overall raising the local voltage drop across the channel and its spike threshold (Hess and Tsien, 1984). This decreased the failure-related initial positive field and increased the main EC negative field, indicating improved conduction, and again confirming the use of these fields as measures of conduction, similar to previous conclusions for the motor endplate (Hubbard et al., 1969) and mathematical consideration of axon cable properties (Stein, 1980).

To quantify the EC fields we estimated the overall conduction to the recording site as:

Conduction Index = nf / (nf + pf) x 100%, where pf and nf are the positive and negative EC field amplitudes. This conduction index approaches 100% for full conduction (pf ~=0) and 0% for no conduction (*nf* = 0). The absolute EC field potential amplitudes are highly variable between different recordings sites, and thus are difficult to quantify across animals and sites, whereas this ratio of field amplitudes (nf / (nf + pf)) eliminates the variability, and can effectively be viewed as a normalization of the negative field (nf) by the total field peak-to-peak size (nf + pf).

Intracellular recording from motoneurons.

The same intracellular glass electrode, stepper motor and amplifier used for recording sensory axons were used for intracellular recording from motoneurons, except that the electrodes were bevelled to a lower resistance (30 MΩ). The electrode was advanced into motoneurons with fast 2 µm steps and brief high frequency currents (capacitance overcompensation) guided by audio feedback from a speaker. After penetration, motoneuron identification was made with antidromic ventral root stimulation, and noting ventral horn location, input resistance and time constant (> 6 ms for motoneurons) (Murray et al., 2010). The monosynaptic excitatory postsynaptic potentials (EPSPs) and associated currents (EPSCs) were measured in motoneurons following stimulation of dorsal roots (at 1.1- 1.5 xT, 0.1 ms, 3 – 10 s trial intervals). These were identified as monosynaptic by their rapid onset (first component), lack of variability in latency (< 1 ms jitter), persistence at high rates (10 Hz) and appearance in isolation at the threshold for DR stimulation (< 1.1xT), unlike polysynaptic EPSPs which varying in latency, disappear at high rates, and mostly need stronger DR stimulation to activate.

Dorsal and ventral root grease gap recording.

In addition to recording directly from single proprioceptive axons and motoneurons, we employed a grease gap method to record the composite intracellular response of many sensory axons or motoneurons by recording from dorsal and ventral roots, respectively, as previously detailed for similar sucrose and grease gap methods, In this case, a high impedance seal on the axon reduces extracellular currents, allowing the recording to reflect intracellular potentials (Leppanen and Stys, 1997; Lucas-Osma et al., 2018; Luscher et al., 1979a; Stein, 1980). We mounted the freshly cut roots onto silver-silver chloride wires just above the bath, and covered them in grease over about a 2 mm length, as detailed above for monopolar recordings. Return and ground wires were in the bath and likewise made of silver-silver chloride. Specifically for sensory axons, we recorded from the central ends of dorsal roots cut within about 2 - 4 mm of their entry into the spinal cord, to give the compound potential from all afferents in the root (dorsal roots potential, DRP), which has previously been shown to correspond to

V_{GABA}, though it is attenuated compared to the intracellular recordings of V_{GABA} (Lucas-Osma et al., 2018). The signal attenuation has two reasons. First the voltage V_{GABA} is attenuated along the length of nerve in the bath, as detailed in the next paragraph. Second, the grease does not completely remove the extracellular fluid around the nerve, even though we deliberately allowed the nerve to dry for a few seconds before greasing, and this causes a conductance that shunts or short circuits the recorded signal, reducing it by about half (Hubbard et al., 1969; Leppanen and Stys, 1997). For optogenetic experiments we additionally added silicon carbide powder (9 % wt, Tech-Met, Markham) to the grease to make it opaque to light and minimize light induced artifactual current in the silver-silver chloride recording wire during optogenetic activation of ChR2 (detailed below). Likewise, we covered our bath ground and recording return wires with a plastic shield to prevent stray light artifacts. The dorsal root recordings were amplified (2,000 times), high-pass filtered at 0.1 Hz to remove drift, low-pass filtered at 10 kHz, and sampled at 30 kHz (Axoscope 8; Axon Instruments/Molecular Devices, Burlingame, CA).

These grease gap recordings of V_{GABA} on sensory afferents reflect only the response of largest diameter axons in the dorsal root, mainly group I proprioceptive afferents, because of the following considerations. First, the largest axons in peripheral nerves have a nodal spacing of about 1 mm (Arbuthnott et al., 1980; Rushton, 1951), and length constants λ_S are estimated to be similar, at about 1 – 2 times the nodal spacing (Blight, 1985), Further, in our recordings we were only able to get the grease to within about 2 mm of the spinal cord. Thus, the centrally generated signal (V_{GABA}) is attenuated exponentially with distance x along the axon length in the bath (2 mm). This is proportional to $\exp(-x / \lambda_S)$ (Stein, 1980), which is $1 / e^2 = 0.11$ for $x = 2\ \lambda_S$, as is approximately the case here. This makes a central V_{GABA} of about 4 mV appear as a ~0.4 mV potential on the root recording (DRP), as we previously reported (Lucas-Osma et al., 2018). Furthermore, the nodal spacing and λ_S decrease linearly with smaller axon diameters (Rushton, 1951; Stein, 1980), making the voltages recorded on the smaller afferents contribute to much less of the compound root potential (halving the diameter attenuates V_{GABA} instead by $1/e^4$ or 0.012, which is 99% attenuation). Finally, unmyelinated sensory axons attenuate voltages over a much shorter distance than myelinated axons, since that membrane resistance (Rm) drops markedly without myelin and λ_S is proportional to $\sqrt{Rm/Ri}$ (where Ri is axial resistance; Stein 1980). Thus, any centrally generated change in potential in these small axons is unlikely to contribute to the recorded signal 2 mm away.

The composite EPSPs in many motoneurons were likewise recorded from the central cut end of ventral roots mounted in grease (grease gap), which has also previously been shown to yield reliable estimates

of the EPSPs (though again attenuated by the distance from the motoneurons) (Fedirchuk et al., 1999). The monosynaptic EPSPs were again identified as monosynaptic by their rapid onset (first component, ~1 ms after afferent volley arrives in the ventral horn; see below), lack of variability in latency (< 1 ms jitter), persistence at high rates (10 Hz) and appearance in isolation at the threshold for DR stimulation (< 1.1xT), unlike polysynaptic reflexes which varying in latency, disappear at high rates, and mostly need stronger DR stimulation to activate.

Analysis of synaptic responses in sensory axons (V_{GABA}) and motoneurons (EPSPs).

When we recorded from sensory axons of an associated dorsal root (directly or via the dorsal roots) stimulation of an adjacent dorsal root (not containing the recorded axon; 0.1 ms, 1 – 3xT) evoked a characteristic large and long depolarization of the afferents, previously demonstrated to be mediated by GABAergic input onto the sensory axons (Lucas-Osma et al., 2018). Traditionally this depolarization is termed primary afferent depolarization (PAD), but here we term it V_{GABA}, to specifically refer to its GABAergic origin and not confuse it with other similar abbreviations (like that for post activation depression). V_{GABA} occurs at a minimal latency of 4 – 5 ms following the afferent volley, consistent with its trisynaptic origin (Jankowska et al., 1981; Lucas-Osma et al., 2018), making it readily distinguishable from earlier events on the axon. V_{GABA} has a fast synaptic component evoked by a single DR stimulation (rising within 30 ms and decaying exponentially over < 100 ms; termed phasic V_{GABA}) and a slower longer lasting extrasynaptic component (starting at about 30 ms and lasting many seconds) that is enhanced by repeated DR stimulation (tonic V_{GABA}, especially with cutaneous stimulation) (Lucas-Osma et al., 2018). We used this sensory activation of V_{GABA} or direct optogenetic activation of V_{GABA} to examine the action of GABA on sensory axon spike transmission to motoneurons, usually evoking phasic V_{GABA} about 10 – 60 ms prior to spikes or associated EPSPs on motoneurons (during phasic V_{GABA}), though we also examined longer lasting effects of tonic V_{GABA} evoked by repeated DR stimulation. Sometimes V_{GABA} is so large that it directly evokes spikes on the afferents, and these travel out the dorsal root, and thus they have been termed dorsal root reflexes (DRRs) (Barron and Matthews, 1938; Lucas-Osma et al., 2018). We usually minimized these DRRs by keeping the DR stimulus that evokes V_{GABA} low (1.1 - 3.0 xT), though there were inevitably some DRRs, as they even occur in vivo in cats and humans (Beloozerova and Rossignol, 1999; Eccles et al., 1961a; Shefner et al., 1992).

When we recorded from motoneurons (directly or via ventral roots) stimulation of proprioceptive afferents in a dorsal root (0.1 ms, 1.1-1.5xT) evoked a monosynaptic EPSP, and associated

monosynaptic reflex (MSR, spikes from EPSP). This EPSP is depressed by fast repetition (rate depended depression, RDD) (Boulenguez et al., 2010), and thus to study the EPSP we evoked it at long intervals (10 s, 0.1 Hz rate) where RDD was less. However, even with this slow repetition rate (0.1 Hz), at the start of testing the first EPSP was often not similar to the steady state EPSP after repeated testing. Thus, to avoid RDD we usually ran the 0.1 Hz EPSP testing continuously throughout the experiment, at least until a steady state response was reached (after 10 minutes). We then examined the action of activating (or inhibiting) $GABA_{axo}$ neurons on this steady state EPSP, by introducing light or sensory conditioning that activated these neurons at varying intervals (inter-stimulus intervals, ISIs) prior to each EPSP stimulation (control, GAD2//ChR2 mice and GAD2//Arch3 mice). We averaged the EPSP from ~10 trials (over 100 s) just before conditioning and then 10 trials during conditioning, and then computed the change in the peak size of the monosynaptic EPSP with conditioning from these averages. After conditioning was completed EPSP testing continued and any residual changes in the EPSP were computed from the 10 trials following conditioning (after-effect). Finally, EPSP testing continued over many minutes after which the original steady state EPSP was established. The background motoneuron potential, membrane resistance (Rm) and time constant just prior to the EPSP was also assessed before and after conditioning to examine whether there were any postsynaptic changes that might contribute to changes in the EPSP with conditioning. Along with the VR recordings, we simultaneously recorded V_{GABA} from DRs by similar averaging methods (10 trials of conditioning), to establish the relation of changes in EPSPs with associated sensory axon depolarization V_{GABA}.

Drugs and solutions

Two kinds of artificial cerebrospinal fluid (ACSF) were used in these experiments: a modified ACSF (mACSF) in the dissection chamber prior to recording and a normal ACSF (nACSF) in the recording chamber. The mACSF was composed of (in mM) 118 NaCl, 24 NaHCO3, 1.5 CaCl2, 3 KCl, 5 MgCl2, 1.4 NaH2PO4, 1.3 MgSO4, 25 D-glucose, and 1 kynurenic acid. Normal ACSF was composed of (in mM) 122 NaCl, 24 NaHCO3, 2.5 CaCl2, 3 KCl, 1 MgCl2, and 12 D-glucose. Both types of ACSF were saturated with 95% O2-5% CO2 and maintained at pH 7.4. The drugs sometimes added to the ACSF were APV (NMDA receptor antagonist), CNQX (AMPA antagonist), gabazine ($GABA_A$ antagonist), bicuculline ($GABA_A$, antagonist), L655708 (α5 $GABA_A$, antagonist), CGP55845 ($GABA_B$ antagonist; all from Tocris, USA), 5-HT, kynurenic acid (all from Sigma-Aldrich, USA), and TTX (TTX-citrate; Toronto Research Chemicals, Toronto). Drugs were first dissolved as a 10 - 50 mM stock in water or DMSO before final dilution in ACSF. DMSO was necessary for dissolving gabazine, L655708, bicuculline and CGP55845, but was kept at a minimum (final DMSO concentration in ACSF < 0.04%),

which by itself had no effect on reflexes or sensory axons in vehicle controls (not shown). L655708 was particularly difficult to dissolve and precipitated easily, especially after it had been exposed a few times to air; so immediately after purchase we dissolved the entire bottle and froze it at -40ºC in single use 5 - 20 µl aliquots, and upon use it was first diluted in 100 µl distilled water before dispersing it into ACSF.

Recording monosynaptic reflexes in awake mice and rats, and V_{GABA} activation.

Window implant over spinal cord. In GAD2//ChR2+ mice and control GAD2//ChR- mice a glass window was implanted over the exposed spinal cord to gain optical access to the sacrocaudal spinal cord, as described previously (Lin et al., 2019). Briefly, mice were given Meloxicam (1 mg/kg, s.c.) and then anesthetized using ketamine hydrochloride (100 mg/kg, i.p.) and xylazine (10 mg/kg, i.p.). Using aseptic technique, a dorsal midline incision was made over the L2 to L5 vertebrae. Approximately 0.1 ml of Xylocaine (1%) was applied to the surgical area and then rinsed. The animals were suspended from a spinal-fork stereotaxic apparatus (Harvard Apparatus) and the muscles between the spinous and transverse processes were resected to expose the L2 to L5 vertebrae. The tips of modified staples were inserted along the lateral edge of the pedicles and below the lateral processes of L2 and L5, and glued in place using cyanoacrylate. A layer of cyanoacrylate was applied to all of the exposed tissue surrounding the exposed vertebrae followed by a layer of dental cement to cover the cyanoacrylate and to form a rigid ring around the exposed vertebrae. A modified paperclip was implanted in the layer of dental cement to serve as a holding point for surgery. A laminectomy was performed at L3 and L4 to expose the spinal cord caudal to the transection site. Approximately 0.1 ml of Xylocaine (1%) was applied directly to the spinal cord for 2 – 3 s, and then rinsed. A line of Kwik-Sil (World-Precision Instruments) was applied to the dura mater surface along the midline of the spinal cord and a glass window was immediately placed over the exposed spinal cord. The window was glued in place along the outer edges using cyanoacrylate followed by a ring of dental cement. Small nuts were mounted onto this ring to later bolt on a backpack to apply the laser light (on the day of experimentation). Saline (1 ml, s.c.) and buprenorphine (0.03 mg/kg, s.c.) was administered post-operatively, and analgesia was maintained with buprenorphine (0.03 mg/kg, s.c.) every 12 hours for two days. Experimentation started 1 week after the window implant when the mouse was fully recovered.

Percutaneous EMG wire implant and fibre optic cable attachment. On the day of experimentation, the mouse was briefly sedated with isoflurane (1.5 %) and fine stainless steel wires (AS 613, Cooner Wire, Chatsworth, USA) were percutaneously implanted in the tail for recording EMG and stimulating the caudal tail trunk nerve, as previously detailed (wires de-insulated by 2 mm at their tip and inserted in

the core of 27 gauge needle that was removed after insertion). A pair of wires separated by 8 mm were inserted at base of the tail for recording EMG the tail muscles, and second pair of wires was inserted nearby for bipolar activation of the caudal trunk nerve to evoke reflexes. A fifth ground wire was implanted between the EMG and stimulation wires. Following this a backpack was bolted into the nuts imbedded in the dental cement ring around the window. This backpack held and aligned a light fibre optic cable that was focused on the centre of the S3 – S4 sacral spinal cord. The Cooner wires were secured to the skin with drops of cyanoacrylate and taped onto the backpack so that the mouse could not chew them. The isoflurane was removed, and the mouse quickly recovered from the anesthesia and was allowed to roam freely around an empty cage during recording, or was sometimes lightly restrained by hand or by a sling. The fibre optic cable was attached to a laser (447 nM, same above) and the Cooner wires attached to the same models of amplifiers and stimulators used for ex vivo monosynaptic testing detailed above.

MSR testing.

The monosynaptic reflex (MSR) was recorded in the tail EMG at ~6 ms latency after stimulating the caudal tail trunk nerve at a low intensity that just activated proprioceptive afferents (0.2 ms current pulses, 1.1 xT), usually near the threshold to activate motor axons and an associated M-wave (that arrived earlier). We studied the tail MSR reflex because our ex vivo recordings were made in the corresponding sacral spinal cord of adult mice and rats, which is the only portion of the spinal cord that survives whole ex vivo, due to its small diameter (Li et al., 2004a). This reflex was verified to be of monosynaptic latency because it was the first reflex to arrive, had little onset jitter, and had the same latency as the F wave (not shown; the F wave is evoked by a strong stimulation of all motor axons, at 5xT, which causes a direct motoneuron response on the same axons, while the monosynaptic EPSP is blocked by collision at this intensity) (Stalberg et al., 2019). The MSR also underwent rate dependent depression (RDD) with fast repeated stimulation and so was synaptic and not a direct muscle response (M-wave), which occurred earlier at sufficient intensity to recruit the motor axons (not shown).

Conditioning of the MSR by optogenetic activation of $GABA_{axo}$ neurons. As with in vitro EPSP testing, the MSR was tested repeatedly at long 5 – 10 s intervals until a steady state MSR was achieved. Then testing continued but with a conditioning light pulse applied just prior to the MSR stimulation (40 – 120 ms), to examine the effect of V_{GABA} evoked during this time frame on sensory transmission to motoneurons. Background EMG just prior to MSR testing was assessed to estimate the postsynaptic activity on the motoneurons. The changes in MSR and background EMG with light were quantified by

comparing the average response before and during the light application, computed from the mean rectified EMG at 6 – 11 ms after the nerve stimulation (MSR) and over 20 ms prior to the nerve stimulation (background just prior to the MSR, Bkg). Because awake mice spontaneously varied their EMG, we plotted the relation between the MSR and the background EMG, with as expected a positive linear relation between these two variables (Matthews, 1986), computed by fitting a regression line. In trials with conditioning light applied the same plot of EMG vs background EMG was made and a second regression line computed. The change in the MSR with conditioning at a fixed matched background EMG level was then computed for each mouse by measuring the difference between the regression line responses at a fixed background EMG. This ruled out changes in MSRs being due to postsynaptic changes. Two background levels were assessed: rest (0%) and 30% of maximum EMG, expressed as a percentage of the control pre-conditioning MSR. The change in background EMG with light was computed by comparing the EMG just prior to the light application (over 20 ms prior) to the EMG just prior to the MSR (over 20 ms prior, Bkg), and expressed as a percentage of the maximum EMG.

Cutaneous conditioning of the MSR in rats. A similar examination of how V_{GABA} affected the MSR was performed in rats with percutaneous tail EMG recording. However, in this case V_{GABA} was evoked by a cutaneous conditioning stimulation of the tip of the tail (0.2 ms pulses, 3xT, 40 – 120 ms prior to MSR testing) using an additional pair of fine Cooner wires implanted at the tip of the tail (separated by 8 mm). In rats the MSR latency is later than in mice due to the larger peripheral conduction time, ~12 ms (as again confirmed by a similar latency to the F wave). This MSR was thus quantified by averaging rectified EMG over a 12 – 20 ms window. Also, to confirm the $GABA_A$ receptor involvement in regulating the MSR, the antagonist L655708 was injected systemically (1 mg/kg i.p., dissolved in 50 µl DMSO and diluted in 900 µl saline). Again, the MSR was tested at matched background EMG levels before and after conditioning (or L655708 application) to rule out changes in postsynaptic inhibition.

Conditioning of the MSRs in humans

H-reflex as an estimate of the MSR. Participants were seated in a reclined, supine position on a padded table. The right leg was bent slightly to access the popliteal fossa and padded supports were added to facilitate complete relaxation of all leg muscles. A pair of Ag-AgCl electrodes (Kendall; Chicopee, MA, USA, 3.2 cm by 2.2 cm) was used to record surface EMG from the soleus muscle. The EMG signals were amplified by 1000 and band-pass filtered from 10 to 1000 Hz (Octopus, Bortec Technologies; Calgary, AB, Canada) and then digitized at a rate of 5000 Hz using Axoscope 10 hardware and software

(Digidata 1400 Series, Axon Instruments, Union City, CA) (Murray et al., 2010). The tibial nerve was stimulated with an Ag-AgCl electrode (Kendall; Chicopee, MA, USA, 2.2 cm by 2.2 cm) in the popliteal fossa using a constant current stimulator (1 ms rectangular pulse, Digitimer DS7A, Hertfordshire, UK) to evoke an H-reflex in the soleus muscle, an estimate of the MSR (Hultborn et al., 1987). Stimulation intensity was set to evoke a test (unconditioned) MSR below half maximum. MSRs recorded at rest were evoked every 5 seconds to minimize RDD (Hultborn et al., 1996a) and at least 20 test MSRs were evoked before conditioning to establish a steady baseline because the tibial nerve stimulation itself can presumably also activate spinal GABAergic networks, as in rats. All MSR were recorded at rest, except when the motor unit firing probabilities were measured (see below).

Conditioning of the MSR. To condition the soleus MSR by cutaneous stimulation, the cutaneous medial branch of the deep peroneal (cDP) nerve was stimulated on the dorsal surface of the ankle using a bipolar arrangement (Ag-AgCl electrodes, Kendall; Chicopee, MA, USA, 2.2 cm by 2.2 cm), set at 1.0xT, where T is the threshold for cutaneous sensation. A brief burst (3 pulses, 200 Hz for 10 ms) of cDP stimuli was applied before evoking a MSR at various inter-stimulus intervals (ISIs; interval between tibial and cDP nerve stimuli) within the window expected for phasic V_{GABA} evoked by cutaneous stimuli, presented in random order at 0, 30, 60, 80, 100, 150 and 200 ms ISIs. Seven conditioned MSR at each ISI were measured consecutively and the average of these MSR (peak-to-peak) was used as an estimate of the conditioned MSR. This was compared to the average MSR without conditioning, computed from the 7 trials just prior to conditioning.

The cDP nerve was also stimulated with a 500 ms long train at 200 Hz to condition the MSR, and examine the effect of tonic V_{GABA} evoked by such long trains, as in rats. Following the application of at least 20 test MSRs (every 5 s), a single cDP train was applied 700 ms before the next MSR and following this the MSR continued to be evoked for another 90 to 120 s (time frame of tonic V_{GABA}). We also conditioned the soleus MSR with tibialis anterior (TA; antagonist muscle, flexor) tendon vibration (brief burst of 3 cycles of vibration at 200Hz) to preferentially activate Ia afferents, as has been done previously (Hultborn et al., 1987).

Motor unit recording to examine postsynaptic actions of conditioning. Surface electrodes were used to record single motor units in the soleus muscle during low level contractions by placing electrodes on or near the tendon or laterally on the border of the muscle as detailed previously (Matthews, 1996). Alternatively, single motor unit activity from the soleus muscle was also recorded using a high density

surface EMG electrode (OT Bioelettronica, Torino, Italy, Semi-disposable adhesive matrix, 64 electrodes, 5x13, 8 mm inter-electrode distance) with 3 ground straps wrapped around the ankle, above and below the knee. Signals were amplified (150 times), filtered (10 to 900 Hz) and digitized (16 bit at 5120 Hz) using the Quattrocento Bioelectrical signal amplifier and OTBioLab+ v.1.2.3.0 software (OT Bioelettronica, Torino, Italy). The EMG signal was decomposed into single motor units using custom MatLab software as per (Negro et al., 2016). Intramuscular EMG was used to record MUs in one participant as detailed previously (Norton et al., 2008) to verify single motor unit identification from surface EMG.

To determine if there were any postsynaptic effects from the conditioning stimulation on the motoneurons activated during the MSR, we examined whether the cDP nerve stimulation produced any changes in the tonic firing rate of single motor units, which gives a more accurate estimate of membrane potential changes in motoneurons compared to compound EMG. Single motor units were activated in the soleus muscle by the participant holding a small voluntary contraction of around 5% of maximum. Both auditory and visual feedback were used to keep the firing rates of the units steady while the conditioning cutaneous was applied every 3 to 5 seconds. The instantaneous firing frequency profiles from many stimulation trials were superimposed and time-locked to the onset of the conditioning stimulation to produce a peri-stimulus frequencygram (PSF, dots in Fig 7Biii), as previously detailed (Norton et al., 2008; Turker and Powers, 2005). A mean firing profile resulting from the conditioning stimulation (PSF) was produced by averaging the frequency values in 20 ms bins across time post conditioning (thick lines in Fig 7Biii and Ciii). To quantify if the conditioning stimulation changed the mean firing rate of the tonically firing motor units, the % change in the mean PSF rate was computed at the time when the H reflex was tested (vertical line in Fig 7Bii-iii).

Unitary EPSP estimates from PSF. To more directly examine if the facilitation in MSR resulted from changes in transmission in Ia afferents after cutaneous afferent conditioning, we measured changes in the firing probability of single motor units (MUs) during the brief MSR time-course (typically 30 to 45 ms post tibial nerve stimulation) with and without cDP nerve conditioning. Soleus MSRs were as usual evoked by stimulating the tibial nerve, but while the participant held a small voluntary plantarflexion to activate tonic firing of a few single motor units. The size of the MSR was set to just above reflex threshold (and when the M-wave was < 5% of maximum) so that single motor units at the time of the MSR could be distinguished from the compound potential from many units that make up the MSR (Nielsen et al., 2019). For a given trial run, test MSRs were evoked every 3-5 s for the first 100 s and

then MSR testing continued for a further 100s, but with a cDP-conditioning train (50 ms, 200 Hz) applied 500 ms prior to each MSR testing stimulation. These repeated high frequency trains evoke a tonic V_{GABA} in rats that facilitates sensory conduction. A 500 ms ISI was used to ensure the firing rate of the motor unit returned to baseline before the MSR was evoked, and this would also be outside of the range of phasic V_{GABA}. Approximately 40-50 usable test and conditioned firing rate profiles were produced for a single session where the motor units had a steady discharge rate before the cDP nerve stimulation. Sessions were repeated 3-6 times to obtain a sufficient number of frequency points to construct the PSF (~ 200 trials).

Motor unit firing (MU) was again used to construct a PSF, as detailed above, but this time locked to the tibial nerve stimulation used to evoke the MSR, so that we could estimate the motoneuron behaviour prior to and during the MSR (to estimate the EPSP profile). When more than one MU was visible in the recordings firing from these units (usually 2 – 3) were combined into a single PSF. Overall this gave about of 100 – 600 MU MSR test sweeps to generate each PSF. Firing frequency values were averaged in consecutive 20 ms bins to produce a mean PSF profile over time after tibial nerve stimulation, for both unconditioned and conditioned MSR reflex trials. The mean background firing rate within the 100 ms window immediately preceding the tibial stimulation was compared between the test and conditioned MSR trials to determine if the conditioning cDP nerve stimulation produced a change in firing rate, and thus post-synaptic effect, just before the conditioned MSR was evoked. For each PSF generated with or without conditioning, the probability that a motor unit discharged during the MSR window (30 to 45 ms after the TN stimulation) was measured as the number of discharges during the time of the MSR window divided by the total number of tibial nerve test stimuli. As an estimate of EPSP size, the mean firing rate during the MSR window was also measured (this was computed with smaller PSF bins of 0.5 ms during the MSR).

Temperature, latency and V_{GABA} considerations.

Large proprioceptive group Ia sensory afferents conduct in the peripheral tail nerve with a velocity of about 33 m/s (33 mm/ms) in mice (Walsh et al., 2015). Motor axons are similar, though slightly slower (30 m/s) (Rasminsky et al., 1978). Thus, in the awake mouse stimulation of Ia afferents in the mouse tail evokes spikes that take ~ 2 ms to conduct to the motoneurons in the spinal cord ~70 mm away. Following ~1 ms synaptic and spike initiation delay in motoneurons, spikes in the motor axons take a further ~2 ms to reach the muscles, after which the EMG is generated with a further 1 ms synaptic and spike initiation delay at the motor endplate to produce EMG. All told this gives a monosynaptic reflex

latency of ~6 ms. The motor unit potentials within the EMG signal have a duration of about 3 – 5 ms, and thus we averaged rectified EMG over 6 – 11 ms to quantify the MSR. We have shown that similar considerations hold for the rat where tail nerve conduction velocities are similar, except the distance from the tail stimulation to the spinal cord is larger (150 mm), yielding a peripheral nerve conduction delay of ~10 ms and total MSR delay of ~12 ms (Bennett et al., 2004). In humans the MSR latency is dominated by the nerve conduction latency (50 – 60 m/s) over a large distance (~800 mm), yielding MSR latencies of ~30 ms.

In our ex vivo whole adult spinal cord preparation the bath temperature was varied between 23 and 32ºC. All data displayed is from 23 – 24ºC, though we confirmed the main results (facilitation of sensory axon transmission to motoneuron by V_{GABA}) at 32ºC. The Q10 for peripheral nerve conduction (ratio of conduction velocities with a 10 ºC temperature rise) is about 1.3 (Leandri et al., 2008), yielding a conduction in dorsal roots of about 20 m/s at 23 – 24 ºC, as we directly confirmed (not shown). Thus, when the DR is stimulated 20 mm from the cord the latency of spike arrival at the cord should be about 1 ms, which is consistent with the time of arrival of afferent volleys that were seen in the intracellular and extracellular recordings from sensory axons (e.g. Figs 2B and 4E).

When we found that V_{GABA} evoked in sensory axons can prevent failure of spikes to propagate in the cord after DR stimulation, we worried that V_{GABA} somehow influenced the initiation of the spike by the dorsal root stimulation at the silver wire. However, we ruled this out by stimulating dorsal roots as far away from the spinal cord as possible (20 mm), where V_{GABA} has no effect, due to the exponential attenuation of its dorsal root potential with distance (see above), and found that V_{GABA} still facilitated sensory axon spike transmission to motoneurons. The added advantage of these long roots is that there is a clean 1 ms separation between the stimulus artifact and the afferent volley arriving at the spinal cord, allowing us to quantify small FPs and afferent volleys that are otherwise obscured by the artifact.

We did not consistently use high temperature ex vivo baths (32ºC) because the VR and DR responses to activation of DRs or V_{GABA} neurons are irreversibly reduced by prolonged periods at these temperatures, suggesting that the increased metabolic load and insufficient oxygen penetration deep in the tissue damages the cord at these temperatures. Importantly, others have reported that in sensory axons V_{GABA}-evoked spikes (DRRs) are eliminated in a warm bath and argued that this means they are not present in vivo, and not able to evoked a motoneuron response (Fink et al., 2014), despite evidence to the contrary (Beloozerova and Rossignol, 1999; Eccles et al., 1961a). However, we find that V_{GABA}

itself is reduced in a warm bath by the above irreversible damage, and it is thus not big enough to evoke spikes in sensory axons; thus, this does not tell us whether these spikes should be present or not in vivo. Actually, in vivo we sometimes observed that with optogenetic activation of $GABA_{axo}$ neurons and associated V_{GABA} there was a direct excitation of the motoneurons (seen in the EMG) at the latency expected for V_{GABA} evoked spikes (not shown). However, this was also at the latency of the postsynaptic inhibition produced by this same optogenetic stimulation, which often masked the excitation (Fig 6). In retrospect, examining the $GABA_{axo}$ evoked motoneuron responses in Fink et al. (2014), or earlier sensory-evoked V_{GABA} (Stuart and Redman, 1992), there is a small excitation riding on the postsynaptic IPSPs from the activation of there $GABA_{axo}$ neurons. This is consistent with the V_{GABA} evoked spike activating the monosynaptic pathway, which inhibits subsequently tested monosynaptic responses by post activation depression (see Discussion).

The latency of a single synapse in our ex vivo preparation at 23 – 24ºC was estimated from the difference between the time arrival of the sensory afferent volley at the motoneurons (terminal potential seen in intracellular and extracellular recordings) and the onset of the monosynaptic EPSP in motoneurons. This was consistently 1 – 1.2 ms (Fig 5B and E). This is consistent with a Q10 of about 1.8 – 2.4 for synaptic transmission latency (Czeh and Dezso, 1982; Silver et al., 1996), and 0.4 ms monsynaptic latency at body temperature (Lev-Tov et al., 1983; Munson and Sypert, 1979b). Based on these considerations we confirm that the V_{GABA} evoked in sensory axons is monosynaptically produced by optogenetic activation of $GABA_{axo}$ neurons with light, since it follows ~1 ms after the first spike evoked in GABAaxo neurons by light (Fig 3A). This first spike in $GABA_{axo}$ neurons itself takes 1 – 2 ms to arise and so the overall latency from light activation to V_{GABA} production can be 2 - 3 ms (Fig 3 F), as seen for IPSCs at this temperature in other preparations (Takahashi, 1992). With DRs stimulation V_{GABA} arises with a minimally 4 – 5 ms latency, which is consistent with a trisynaptic activation of the sensory axon, after taking into account time for spikes to arise in the interneurons involved (Fig 4A, E).

Immunohistochemisty.

Tissue fixation and sectioning. After sensory axons in mouse and rat spinal cords were injected with neurobiotin the spinal cord was left in the recording chamber in oxygenated nACSF for an additional 4 – 6 hr to allow time for diffusion of the label throughout the axon. Then the spinal cord was immersed in 4% paraformaldehyde (PFA; in phosphate buffer) for 20-22 hours at 4°C, cryoprotected in 30% sucrose in phosphate buffer for 24-48 hours. Alternatively, afferents were labelled genetically in $VGLUT1^{Cre/+}$; $R26^{lsl\text{-}tdTom}$ mice, which were euthanized with Euthanyl (BimedaMTC; 700 mg/kg) and perfused

intracardially with 10 ml of saline for 3 – 4 min, followed by 40 ml of 4% paraformaldehyde (PFA; in 0.1 M phosphate buffer at room temperature), over 15 min. Then spinal cords of these mice were post-fixed in PFA for 1 hr at 4°C, and then cryoprotected in 30% sucrose in phosphate buffer (~48 hrs). Following cryoprotection all cords were embedded in OCT (Sakura Finetek, Torrance, CA, USA), frozen at -60C with 2-methylbutane, cut on a cryostat NX70 (Fisher Scientific) in sagittal or transverse 25 µm sections, and mounted on slides. Slides were frozen until further use.

Immunolabelling. The tissue sections on slides were first rinsed with phosphate buffered saline (PBS, 100 mM, 10 min) and then again with PBS containing 0.3% Triton X-100 (PBS-TX, 10 min rinses used for all PBS-TX rinses). For the sodium channel antibody, we additionally incubated slides three times for 10 min each with a solution of 0.2% sodium borohydride (NaBH4, Fisher, S678-10) in PB, followed by a PBS rinse (4x 5 min). Next, for all tissue, nonspecific binding was blocked with a 1 h incubation in PBS-TX with 10% normal goat serum (NGS; S-1000, Vector Laboratories, Burlingame, USA) or normal donkey serum (NDS; ab7475, Abcam, Cambridge, UK). Sections were then incubated for at least 20 hours at room temperature with a combination of the following primary antibodies in PBS-TX with 2% NGS or NDS: rabbit anti-α_5 $GABA_A$ receptor subunit (1:200; TA338505, OriGene Tech., Rockville, USA), rabbit anti-α1 $GABA_A$ receptor subunit (1:300; 06-868, Sigma-Aldrich, St. Louis, USA), chicken anti-γ2 $GABA_A$ receptor subunit (1:500; 224 006, Synaptic Systems, Goettingen, Germany), rabbit anti-$GABA_{B1}$ receptor subunit (1:500; 322 102, Synaptic Systems, Goettingen, Germany), mouse anti-Neurofilament 200 (NF200) (1:2000; N0142, Sigma-Aldrich, St. Louis, USA), guinea pig anti-VGLUT1 (1:1000; AB5905, Sigma-Aldrich, St. Louis, USA), rabbit anti-Caspr (1:500; ab34151, Abcam, Cambridge, UK), mouse anti-Caspr (1:500; K65/35, NeuroMab, Davis, USA), chicken anti-Myelin Basic Protein (MBP) (1:200; ab106583, Abcam, Cambridge, UK), chicken anti-VGAT (1:500; 131 006, Synaptic Systems, Goettingen, Germany), rabbit anti-VGAT (1:500; AB5062P, Sigma-Aldrich, St. Louis, USA), rabbit anti-EYFP (1:500; orb256069, Biorbyt, Riverside, UK), goat anti-RFP (1:500; orb334992, Biorbyt, Riverside, UK), rabbit anti-RFP (1:500; PM005, MBL International, Woburn, USA), rabbit anti-GFP (1:500, A11122, ThermoFisher Scientific, Waltham, USA), and mouse anti-Pan Sodium Channel (1:500; S8809, Sigma-Aldrich, St. Louis, USA). The latter is a pan-sodium antibody, labelling an intracellular peptide sequence common to all known vertebrate sodium channels. Genetically expressed EYFP, tdTom (RFP) and GFP were amplified with the above antibodies, rather than rely on the endogenous fluorescence. When anti-mouse antibodies were applied in mice tissue, the M.O.M (Mouse on Mouse) immunodetection kit was used (M.O.M; BMK-2201, Vector Laboratories, Burlingame, USA) prior to applying antibodies. This process included 1h

incubation with a mouse Ig blocking reagent. Primary and secondary antibody solutions were diluted in a specific M.O.M diluent.

The following day, tissue was rinsed with PBS-TX (3x 10 min) and incubated with fluorescent secondary antibodies. The secondary antibodies used included: goat anti-rabbit Alexa Fluor 555 (1:200; A32732, ThermoFisher Scientific, Waltham, USA), goat anti-rabbit Alexa Fluor 647 (1:500, ab150079, Abcam, Cambridge, UK), goat ant-rabbit Pacific orange (1:500; P31584, ThermoFisher Scientific, Waltham, USA), goat anti-mouse Alexa Fluor 647 (1:500; A21235, ThermoFisher Scientific, Waltham, USA), goat anti-mouse Alexa Fluor 488 (1:500; A11001, ThermoFisher Scientific, Waltham, USA), goat anti-mouse Alexa Fluor 555 (1:500; A28180, ThermoFisher Scientific, Waltham, USA), goat anti-guinea pig Alexa Fluor 647 (1:500; A21450, ThermoFisher Scientific, Waltham, USA), goat anti-chicken Alexa Fluor 405 (1:200; ab175674, Abcam, Cambridge, UK), goat anti-chicken Alexa Fluor 647 (1:500; A21449, ThermoFisher Scientific, Waltham, USA), donkey anti-goat Alexa Fluor 555 (1:500; ab150130, Abcam, Cambridge, UK), donkey anti-rabbit Alexa Fluor 488 (1:500; A21206, ThermoFisher Scientific, Waltham, USA), Streptavidin-conjugated Alexa Fluor 488 (1:200; 016-540-084, Jackson immunoResearch, West Grove, USA) or Streptavidin-conjugated Cyanine Cy5 (1:200; 016-170-084, Jackson immunoResearch, West Grove, USA) in PBS-TX with 2% NGS or NDS, applied on slides for 2 h at room temperature. The latter streptavidin antibodies were used to label neurobiotin filled afferents. After rinsing with PBS-TX (2 times x 10 min/each) and PBS (2 times x 10 min/each), the slides were covered with Fluoromount-G (00-4958-02, ThermoFisher Scientific, Waltham, USA) and coverslips (#1.5, 0.175 mm, 12-544-E; Fisher Scientific, Pittsburg, USA).

Standard negative controls in which the primary antibody was either 1) omitted or 2) blocked with its antigen (quenching) were used to confirm the selectivity of the antibody staining, and no specific staining was observed in these controls. Most antibodies had been previously tested with quenching for selectivity, as detailed in the manufacture's literature and other publications (Lucas-Osma et al., 2018), but we verified this for the GABA receptors with quenching. For antibody quenching, the peptides used to generate the antibodies, including anti-α5 $GABA_A$ receptor subunit (AAP34984, Aviva Systems Biology, San Diego, USA), anti-α1 $GABA_A$ receptor subunit (224-2P, Synaptic Systems, Goettingen, Germany) and anti-γ2 $GABA_A$ receptor subunit (224-1P, Synaptic Systems, Goettingen, Germany), were mixed with the antibodies at a 10:1 ratio and incubated for 20 h and 4°C. This mixture was then used instead of the antibody in the above staining procedure.

Confocal and epifluorescence microscopy

Image acquisition was performed by confocal (Leica TCS SP8 Confocal System) and epifluorescence (Leica DM 6000 B) microscopy for high magnification 3D reconstruction and low magnification imaging, respectively. All the confocal images were taken with a 63x (1.4 NA) oil immersion objective lens and 0.1 µm optical sections that were collected into a z-stack over 10–20 µm. Excitation and recording wavelengths were set to optimize the selectivity of imaging the fluorescent secondary antibodies. The same parameters of laser intensity, gain and pinhole size was used to take pictures for each animal, including the negative controls. Complete sagittal sections were imaged with an epifluorescence 10x objective lens using the Tilescan option in Leica Application Suite X software (Leica Microsystems CMS GmbH, Germany). Sequential low power images were used to reconstruct the afferent extent over the whole spinal cord, using CorelDraw (Ottawa, Canada), and to identify locations where confocal images were taken.

3D reconstruction of afferents and localization of GABA receptors.

The fluorescently labelled afferents (neurobiotin, tdTom), GABA receptors, VGLUT1, VGAT, NF200, Caspr, MBP and sodium channels were analyzed by 3D confocal reconstruction software in the Leica Application Suite X (Leica Microsystems CMS GmbH) (Lucas-Osma et al., 2018). To be very conservative in avoiding non-specific antibody staining, a threshold was set for each fluorescence signal at a minimal level where no background staining was observed in control tissue with the primary antibody omitted, less 10%. Signals above this threshold were rendered in 3D for each antibody. Any GABA receptor, Caspr or Nav expression within the volume of the neurobiotin filled axon (binary mask set by threshold) was labelled yellow, pink and white respectively (Fig 1), and the density within the afferents quantified using the same Leica software. Receptor densities were measured for all orders of branch sizes (1^{st}, 2^{nd}, 3^{rd} etc.; see below), for both branches dorsal to the central canal (dorsal) and ventral to the central canal (ventral). Nodes were identified with dense bands of Caspr or Na channel labelling (and lack of MBP). Branch points were also identified. We also examined raw image stacks of the neurobiotin afferents and receptors, to confirm that the automatically 3D reconstructed and identified receptors labelled within the afferent (yellow) corresponded to manually identified receptors colocalized with neurobiotin (Fig 1). This was repeated for a minimum of 10 examples for each condition, and in all cases the 3D identified and manually identified receptors and channels were identical. Many receptors and channels lay outside the afferent, and near the afferent these were difficult to manually identify without the 3D reconstruction software, making the 3D reconstruction the only practical method to fully quantify the receptors over the entire afferent. We also optimized the

reconstruction of the neurobiotin filled afferents following the methods of Fenrich (Fenrich et al., 2014), including brightening and widening the image edges slightly (1 voxel, 0.001 μm^3) when necessary to join broken segments of the afferent in the final afferent reconstruction, to account for the a priori knowledge that afferents are continuous and neurobiotin signals tend to be weaker at the membrane (image edges) and in fine processes.

GABA receptors usually occurred in the axons in distinct clusters. The distances between these receptor clusters and nodes or branch points was measured and average distances computed, from high power confocal images evenly sampled across the axon arbour (employing ~100 receptor clusters from ~10 images per labelled Ia afferent). The average distance between the receptor clusters and the nearest axon terminals on the motoneurons was also computed, but this was complicated by the very large distances often involved, forcing us to compute the distances from low power images and relate these to the high power images of receptors sampled relatively evenly along the axon arbour. For this distance calculation, to avoid sampling bias in the high power images, we only admitted images from branch segments (1st, 2nd and 3rd order, detailed below) that had a receptor density within one standard deviation of the mean density in branch types with the highest density (1st order ventral branches for $GABA_A$ receptors and 3rd order ventral terminal branches for $GABA_B$ receptors; i.e. images from branches with density above the dashed confidence interval lines in Fig 1G were included); this eliminated very large distances being included from branch segments with relatively insignificant receptor densities. We also confirmed these calculations by computing the weighted sum of all the receptor distances weighted by the sum of the receptor density for each branch type (and divided by the sum of all receptor densities), which further eliminated sampling bias. This gave similar average distance results to the above simpler analysis (not shown).

Sensory axon branch order terminology. The branches of proprioceptive axons were denoted as follows: dorsal column branches, 1st order branches that arose of the dorsal column and project toward the motoneurons, 2nd order branches that arose from the 1st order branches, and 3rd order branches that arose from the 2nd order branches. Higher order branches occasionally arose from the 3rd order branches, but these were collectively denoted 3rd order branches. First and second order branches were myelinated with large dense clusters of sodium channels at the nodes in the myelin gaps, which were characteristically widely spaced. As the second order branches thinned near the transition to 3rd order branches, they became unmyelinated, and at this point sodium channel clusters were smaller and more closely spaced (~6 μm apart, not shown). These thinned branches gave off 3rd order (and higher) unmyelinated terminal branches with chains of characteristic terminal boutons. The 1st order branches

gave off 2nd order branches along most of their length as they traversed the cord from the dorsal columns to the motoneurons, but we separately quantified 1st, 2nd and 3rd order branches in the dorsal and ventral horn.

Node identification. Nodes in myelinated axon segments nodes were identified either directly via direct Na channel clusters and paranodal Caspr, or indirectly by their characteristic paranodal taper. That is, in the paranodal region the neurobiotin filled portion of the axon tapered to a smaller diameter, likely because the Caspr and presumably other proteins displaced the cytoplasmic neurobiotin, which also made the intracellular neurobiotin label less dense (Fig 1C, black regions in taper). Regardless of the details, this taper made nodes readily identifiable. This taper forces the axial current densities to increase at the nodes, presumably assisting spike initiation, and consistent with previous reconstructions of myelinated proprioceptive afferents (Nicol and Walmsley, 1991).

Computer simulations

All computer models and simulations were implemented in NEURON ver7.5 (Hines and Carnevale, 2001). The geometry and myelination pattern of the model were extracted from a previous study that used serial-section electron microscopy to generate about 15,000 photomicrographs to reconstruct a large myelinated proprioceptive Ia afferent collateral in the cat (Nicol and Walmsley, 1991). This structure was used in a prior modeling study (Walmsley et al., 1995). Four classes of segment were defined in the model: myelinated internodes, nodes, unmyelinated bridges, and terminal boutons. Data from 18 of the 83 segments were missing from the original study. The missing data were estimated using mean values of the same segment class. The cable properties of the model were determined from diameter-dependent equations previously used for models of myelinated axons (McIntyre et al., 2002) and included explicit representation of myelinated segments using the double cable approach (Cohen et al., 2020; McIntyre et al., 2002; Stephanova and Bostock, 1995). Hodgkin-Huxley style models of voltage gated sodium (transient and persistent) and potassium channels were adopted from a previous study, at 37°C (McIntyre et al., 2002). All three voltage-gated conductances were colocalized to unmyelinated nodes throughout the modelled axon collateral. The density of sodium and potassium conductances was adjusted to match the size and shape of experimentally recorded action potentials. Current clamp stimulation was applied to the middle of the first myelinated segment (pulse width 0.1 ms, amplitude 2 nA; near dorsal root) to initiate propagating action potentials in the model. Voltage at multiple sites of interest along the collateral was measured to assess propagation of action and graded potentials through branch points. Transient chloride conductance (i.e. $GABA_A$ receptors) was modeled

using a double-exponential point process (Eq. 1); parameters were manually fit to experimental data. $GABA_A$ receptors were localized to nodes at branch points to match experimental data. The amplitude and time course of the modeled V_{GABA} (also termed PAD) was measured from the first myelinated internode segment, similar to the location of our intra-axonal recordings.

$$g(t) = g\_max * \beta * (e\text{^}((-t)/\tau\_decay) - e\text{^}((-t)/\tau\_rise)), \text{ where } \beta = 1/((e\text{^}((-\gamma)/\tau\_decay) - e\text{^}((-\gamma)/\tau\_rise))), \text{ and } \gamma = (\tau\_rise * \tau\_decay)/(\tau\_decay - \tau\_rise) * \log(\tau\_decay/\tau\_rise) \quad (Eq.\ 1)$$

The parameters at all synapses were the same: time constant of rise (τ_{rise}) = 6ms, time constant of decay (τ_{decay}) = 50ms, default maximum conductance (g_{max}) = 1.5nS (varied depending on simulation, see figure legends), and chloride reversal potential (E_{Cl^-}) = -25mV (i.e. 55 mV positive to the resting potential to match our experimental data) (Lucas-Osma et al., 2018).

QUANTIFICATION AND STATISTICAL ANALYSIS

Data were analyzed in Clampfit 8.0 (Axon Instruments, USA) and Sigmaplot (Systat Software, USA). A Student's *t*-test or ANOVA (as appropriate) was used to test for statistical differences between variables, with a significance level of $P < 0.05$. Power of tests was computed with $\alpha = 0.05$ to design experiments. A Kolmogorov-Smirnov test for normality was applied to the data set, with a $P < 0.05$ level set for significance. Most data sets were found to be normally distributed, as is required for a *t*-test. For those that were not normal a Wilcoxon Signed Rank Test was instead used with $P < 0.05$. Categorical data was instead analyzed using Chi-squared tests, with Yate's continuity correction used for 2 × 2 contingency tables and again significant difference set at $P < 0.05$. Data are plotted as bar graphs of mean ± standard deviation (SD, error bar representing variability) or as box plots representing the interquartile range and median and error bars extend to the most extreme data point within 1.5 times the interquartile range (mean also shown as thick lines in boxes).

SUPPLEMENTARY INFORMATION

Figure S1. Nodal and not terminal $GABA_A$ receptors in mice, related to Figure 1.

(A-C) In the sacrocaudal spinal cord of mice we examined the distribution of $GABA_A$ receptor subunits on nodes and terminals of sensory axons, including extrasynaptic α5 subunits, synaptic α1 subunits, and ubiquitous γ2 subunits (e.g. forming the common α1βγ2 or α5βγ2 receptors, though less common extrasynaptic α1βδ have been reported) (Chua and Chebib, 2017; Chuang and Reddy, 2018; Lagrange et al., 2018; Olsen and Sieghart, 2009). We genetically labelled primary sensory axons by their expression of the vesicular glutamate transporter VGLUT1 with a reporter in $VGLUT1^{Cre/+}$; $R26^{LSS\text{-}tdTom}$ mice (tdTom reporter displayed as green, for consistency with Fig 1). VGLUT1 is mainly only expressed in sensory axons (Todd et al., 2003), especially ventral proprioceptive afferents, as other afferents do not reach the ventral horn (Lucas-Osma et al., 2018). Axons are reconstructed in 3D as detailed in Fig 1. Branching order is indicated (1^{st}, 2^{nd} and 3^{rd}), where the dorsal column gives off many large myelinated 1st order branches at ~200 µm intervals, which give off smaller myelinated 2^{nd} order branches at ~50 µm intervals; finally, 2^{nd} order branches give off 3^{rd} order branches that are unmyelinated terminal branches with distinctive large terminal boutons. Typical axon branching patterns are shown in the deep dorsal horn (left), intermedial laminae and ventral horn (middle). Expanded images of nodes of Ranvier identified by paranodal Capsr immunolabelling are shown on 1^{st} order branches in the intermediate laminae (on right), along with raw confocal images prior to 3D reconstruction. Expanded terminal boutons from the ventral horn are also shown on the right. As in rats, nodes are often near branch points (where 2^{nd} order branch arises from 1^{st} order branches in this case, green arrow). We identified axonal GABA receptors as those colocalized with axonal neurobiotin (yellow, as in Fig 1), and the remaining GABA receptors are labelled red in the 3D reconstructions. The α5, α1 and γ2 $GABA_A$ receptors subunits were found on large axon branches (1^{st} and 2^{nd} order) in the dorsal, intermediate, and ventral cord, near nodes counterstained with Caspr immunolabelling (white, arrows), but not on ventral horn terminal boutons (3^{rd} order; examples at blue arrows; expanded on right). The presence of these 3 subunits is consistent with their mRNA previously reported in the dorsal root ganglion (Persohn et al., 1991). Also, the finding of α1 subunits on these axons is consistent with the recent observation that α1 is only on myelinated sensory axons, rather than unmyelinated C fibres (Paul et al., 2012). Similar results were obtained from n = 3 mice.

(D) Immunolabelling for γ2 $GABA_A$ receptor subunits on 3D reconstructed sensory axons, with same format and mice of A-C, but with nodes identified by Nav (sodium channels), rather than Caspr. Again, the node and GABA receptors are near a branch point (green arrow).

(E) Immunolabelling for VGLUT1 to confirm identity of ventral terminal boutons in tdTom labelled sensory axons, in same mice of A-C.

(F) Immunolabelling for $GABA_B$ receptors ($GABA_{B1}$ subunit) on 3D reconstructed sensory axons, with same format and mice of A-C. $GABA_B$ receptors were generally absent from nodes identified by Caspr, but present on ventral terminal boutons, as in rats (Fig 1).

Figures S2. Voltage dependence of nodal spike propagation failure, related to Figure 2.

(A-D) Intracellular recording from proprioceptive Ia afferent branches in the dorsal horn with secure spikes at rest, evoked by DR stimulation (1.1xT, 0.1 ms; sacral S4 DR; A, D). Spike failure was induced by increasing hyperpolarization (failure near rest in D, but not A), with a delay and then abrupt loss of height, reflecting failure of successively further away nodes (A, D). Estimated contributions from local nodes (B-C) computed by subtraction from traces in D. Note that due to attenuation of injected current with distance, larger hyperpolarizations were needed to stop spikes with more distal vulnerable nodes (secure spikes), as observed by smaller distal FPs (A vs D), and some axon spikes could not be stopped (not shown, but quantified in E, Spike only). Data collected in discontinuous current clamp (DCC) mode so electrode rectification during the injected hyperpolarizing current did not affect potential (DCC switching rate 7 kHz, low pass filtered at 3 kHz to remove switching artifact, which also removed stimulus artifact).

(E) Distribution of spiking in branches with full spikes only, one local nodal spike (local FP), or a distal nodal spike (distant FP) remaining after maximal hyperpolarization, and * significant change when blocking α5 $GABA_A$ receptors with L655708 (0.1 - 0.3 μM) using χ-squared test, $P < 0.05$; $n = 68$ control and $n = 47$ L655708 treated branches.

(F) Box plots of spike or FP heights and delays in branches indicated in E, measured just prior to spike failure (or at maximal hyperpolarization for secure spikes) and after failure (for local and distal FPs, as induced in A - D). Delay measured relative to peak of spike at rest. + FP significantly different than spike at rest, $P < 0.05$.

(G) Box plots of the hyperpolarization needed to induce failure, in branches from E. * significant change with L655708, $P < 0.05$.

(H) Incidence of failure at varying potentials (% of total spikes from E). * significant change with L655708, χ-squared test, $P < 0.05$.

(I) Simulated spike failure. Intracellular recording from proprioceptive Ia afferent branch in the dorsal horn (sacral S4 axon). A brief current injection pulse (0.5 ms) was applied to simulate the current arriving from distal nodes during normal axon spike conduction, and repeated at 1s intervals. During these pulses the membrane was held at varying potentials for 1 – 2 s with steady current injection, with numbers and colours denoting a given holding potential (in DCC mode). At the most hyperpolarized levels spikes failed to be evoked and only the passive response is seen, like a FP (blue, 1). As the potential was depolarized to near the axon's resting potential (-67 mV) partial spikes occurred (green, 2 and 3), likely from a single adjacent node activating, and then delayed broad spikes occurred, as both adjacent nodes were activated. At more depolarized levels the spikes arose more rapidly and increased in height to full secure spikes (4).

(J) In the same axon as I, at holding potentials well above those seen physiologically (near -50 mV, lower plots) spikes started to exhibit sodium channel inactivation and failure, with a decrease in spike height and delay (7 – 8) and eventually full failure (shown in K). Adjacent nodes started failing at slightly different times with different delays, broadening the spike and eventually separating into two distinct nodal spikes (*).

(K) Spike heights plotted as a function of holding potential, including those spikes illustrated in I and J, with spike number-labels indicated. Left grey line indicates passive leak current response, and shows deviation from passive response near rest. Shaded green region shows all or nothing failure or spikes near the resting potential. Middle grey line shows a region of secure spikes with relatively invariant spikes. Right grey line shows spike inactivation with large depolarizations and outright failure near - 50 mV. Note the split vertical axis. Similar voltage dependence of spike failure occurred for $n = 5/5$ axons tested. This demonstrates two modes of spike failure: 1) spikes that fail at rest or at hyperpolarized potentials and 2) spikes that fail with large depolarizations above rest. The latter is likely not physiological, since even the largest V_{GABA} that we have observed (5 – 10 mV; Fig 4D) will not depolarize axons to -50 mV, since axons rest near -70 mV, and V_{GABA} is only large at hyperpolarized levels (Fig 4D) and decreases steeply as the potential approaches the reversal potential for chloride (-15 mV) (Lucas-Osma et al., 2018).

(L) Schematic of recording arrangement and relation to adjacent nodes for data in M-N.

(M) Expansion of responses 1 (blue) and 2 (pink) from I, and difference (cyan) to show the first local nodal spike height at threshold, recorded at electrode. Active nodes from schematic in L shown with shaded boxes.

(N) Spikes near sodium inactivation from J (7 and 8), with differences indicating local nodal spikes (cyan and grey, nodes from L).

Figure S3. Computer simulation of branch point failure and rescue by GABA, related to Figures 3 and 4.

(A) Model of a 3D reconstructed proprioceptive afferent, drawn to scale, except myelinated branch lengths all shortened an order of magnitude. Double line segments are myelinated (white) and the rest unmyelinated. Adapted from anatomical studies of Walmsley et al. (1995). Nodes are indicated with a green dot, and ventrally projecting terminal boutons indicated with a yellow dot. To be conservative, sodium channels were placed at each node and bouton (g_{Na} = 1 S/cm^2), even though bouton immunolabelling for these channels was not common in our terminal bouton imaging (Fig 1), since disperse weak sodium channel labelling may have been missed. Removing these bouton sodium channels did not qualitatively change our computer simulation results (not shown). As in our axons of Fig 1, branch points were always at nodes. $GABA_A$ receptors of equal conductance (nS) were placed at each branch point (node), and total dorsal columns (dc) depolarization from phasically activating these receptors is shown in inset. Actual branch lengths (L) and space constants (λ_S) are indicated in gray boxes for each segment of the afferent, the latter computed from subthreshold current injections (100 ms) on the distal end of each branch segment and fitting an exponential decay (with space constant λ_S) to the passive depolarization along its length, and then repeating this with current injected in the proximal end to get a second λ_S, and finally averaging these two space constants. From left to right the gray boxes are for segments spanning from the dorsal columns (dc) to N0, N0 to N1, N1 to N5, N1 to N4, N4 to B2 and N5 to B1. Average space constant λ_S = 91 µm, similar to in other axons (Zorrilla de San Martin et al., 2017).

(B) Responses to simulated dorsal root (DR) stimulation (0.1 ms pulse, 2 nA, at black arrows) computed at various downstream branch points (nodes) and terminal boutons in the spinal cord, with resting potential indicated by thin dashed line (-82 mV). A sodium spike propagated to the branch point at node N1, but failed to invade into the downstream branches, leaving nodes N2 and N3 with only a passive depolarization from the N1 spike (failure potential, FP). Further downstream nodes and terminals experienced vary little depolarization during this failure (N5, B1 and B2). In this case the GABA conductance was set to zero (g_{GABA} = 0, control), simulating a lack of GABA tone. Note that only the nodes beyond the parent branch at node N1 failed due to the conductance increases in large daughter branches to nodes N2 and N3 that drew more current than node N1 could provide (shunting conductances). Node 3 is particularly complex with a large unmyelinated region (black) and a nearby branch contributing to its conductance and related failure, and Node 2 has two adjacent branches contributing to its conductance. Other branch points with relatively smaller conductance increases (N0, simpler branching) did not fail to conduct spikes. Generally speaking, if the upstream node of a parent branch cannot provide enough current to activate the nodes of its daughter branches then spikes fail, and this is especially likely with multiple sequential branch points, like in N1 – N2.

(C) As seen experimentally, nodal $GABA_A$ receptor activation to produce V_{GABA} prior to the DR stimulation (~ 10 ms prior; as in Fig 4F) rescued spikes from failing to propagate. That is, with GABA receptors placed just at branch points (i.e., at nodes) a weak phasic activation of these receptors (conductance g_{GABA} = 0.6 - 1.5 µS per node shown) rescued conduction down the branch to node N2, with full nodal spikes seen at the distal node N4 and the terminal bouton B2 (DR stimulation at peak of V_{GABA}, detailed in G – H, with black arrows indicating DR stimulation timing). A larger GABA receptor activation (2.4 nS) additionally rescued spike conduction down the branch to node N3, with full spike conduction to the distal node N5 and the terminal bouton B1. Note that increasing GABA conductance sped up the arrival of distal spikes (e.g. at N4 and B2), by up to 1 ms, suggesting substantial variation in sensory transmission times induced by GABA, as we see experimentally. Also note that this nodal GABA depolarized the nodes (N1 – N3) relative to rest (thin dashed line), thus assisting spike initiation. In contrast, nodal GABA did not depolarize the terminal boutons (B1 and B2), consistent with our recent direct recordings from terminals (Lucas-Osma, 2018). Sensitivity analysis revealed similar results with a wide range of sodium channel and GABA receptor conductances, though increasing sodium conductance sufficiently prevented failure all together (not shown, but like in Fig S6 K detailed below).

(D) When we removed all nodal GABA receptors and instead place them on terminal boutons (near B1 and B2, yellow, with equivalent total conductance, 2.4 µS condition), then activating them did not rescue the spikes propagation failure, since the associated depolarization of nodes is too attenuated at the failure point (N1-N3; no change from resting potential). The GABA receptors did depolarize the terminal boutons (B1 and B2, thick dashed lines) substantially relative to the resting potential (thin dashed lines), but this depolarization was sharply attenuated in more proximal nodes (N1-3).

(E) Reduction of spike height (shunt) and speeding of spike onset with increasing GABA conductance at a non-failing node (N1; model with nodal and not terminal bouton GABA conductances, C), consistent with actual recordings from axons in Fig 3D, S5A.

(F-H) V_{GABA} recorded at the dorsal columns (dc) during conditions in B-D, respectively. A phasic GABA induced depolarization (V_{GABA}) was generated by changing GABA conductances with a double exponential model, with a 6 ms rise and 50 ms decay time, and GABA receptor location varied as in C-D. DRs were stimulated at the peak of this V_{GABA} in C-D. Note that nodal (G) but not terminal (H) GABA receptors caused a visible depolarization at the dorsal columns (dc), due to less electrotonic attenuation in the former.

Figure S4. Circuits mediating V_{GABA} and their role in repetitive firing, related to Figure 4.

(A) Cutaneous driven dorsal trisynaptic circuit. A minimally trisynaptic circuit is classically known to depolarize afferents via $GABA_{axo}$ neurons. This circuit involves sensory afferents activating excitatory intermediary neurons (glutamatergic) that in turn activate $GABA_{axo}$ neurons that return to innervate sensory axons (Jankowska et al., 1981). Even though $GABA_{axo}$ neurons are small (Betley et al., 2009) this circuit influences afferents over large regions of the spinal cord (Lucas-Osma et al., 2018). Specifically, the activation of a small group of sensory axons in just one DR or nerve causes this trisynaptic circuit to produce a widespread activation of many axons across the spinal cord, even many segments away and across the midline (Lucas-Osma et al., 2018). This allowed us to activate V_{GABA} from adjacent roots without directly activating an axon in a particular root, as detailed in Fig 4 and the rest of this figure. One variant of this classic trisynaptic circuit specifically involves cutaneous stimulation activating dorsal intermediary neurons (Jankowska et al., 1981; Zimmerman et al., 2019) that activates $GABA_{axo}$ neurons that in turn innervate cutaneous afferents, which we term the cutaneous dorsal circuit. While this cutaneous dorsal circuit also synaptically innervates some proprioceptive afferents (Rudomin, 1999), its main action on proprioceptive afferents is to produce a pronounced extrasynaptic spillover of GABA that depolarizes these afferents tonically via α5 $GABA_A$ receptors (termed: tonic V_{GABA}, L655708 sensitive), especially with repetitive cutaneous nerve stimulation (1 - 200 Hz) that leads to minutes of depolarization (Lucas-Osma et al., 2018), and we see similar tonic V_{GABA} here (B, detailed next).

(B) Intracellular recording from a proprioceptive axon branch in rat dorsal horn (sacral S4 axon) and response to activation of a largely cutaneous DR (caudal Ca1 DR, innervating the tip of the tail, stimulation at intensity for cutaneous afferents, 3xT, 0.1 ms; denoted DR1) evoking a slowly rising tonic V_{GABA} when repeated at 1 Hz. The axon branch spontaneously exhibits spike propagation failure when its dorsal root is stimulated alone (also repeated at 1 Hz, 1.1xT, 0.1 ms; denoted DR2), with only a small failure potential (FP) visible. However, when combined with the repeated cutaneous stimulation of DR1 (60 ms prior to each DR2 stimulation) the slowly building V_{GABA} prevents spike failure, and this outlasts the cutaneous stimulation (after effect). Similar results obtained in n = 20/20 axons tested.

(C) Proprioceptive driven ventral trisynaptic circuit. A second variant of the classic trisynaptic circuit involves proprioceptive afferents activating more ventrally located excitatory intermediary neurons (glutamatergic) that then activate $GABA_{axo}$ neurons that innervate these same afferents, including ventral terminal regions of the afferents (Jankowska et al., 1981; Lucas-Osma et al., 2018). Thus, we term this the ventral circuit; this circuit is recurrent, with the same axons causing self-facilitation (homonymous V_{GABA}). This circuit produces a fast phasic axon depolarization (phasic V_{GABA}, fast synaptic Lucas-Osma et al., 2018; E and F detailed below and Fig 4C), as well as a slower tonic depolarization (tonic V_{GABA}, Fig 4C, likely from extrasynaptic GABA spillover).

(D) Intracellular recording from proprioceptive axon in rat dorsal horn (sacral S4 axon) with spikes securely evoked by fast repeated DR stimulation (top, 1.1xT, 0.1 ms, sacral S4 DR, denoted DR2; resting potential -68 mV), but spikes failing intermittently with repeated intracellular current injection (IC) at the same rate (bottom green), due to sodium channel inactivation. The reason that spike failure does not occur with the fast DR stimulation is that it is accompanied by a build up of tonic V_{GABA} (from self-activation) that helps prevent failure, because adding to the IC stimulation a simultaneous conditioning stimulation of other proprioceptive afferents in an adjacent DR (DR1 stim at 1.5xT, 0.1 ms, S3 DR) prevents spike failure (black trace, bottom), via the proprioceptive ventral circuit (C). This DR1 conditioning stimulation does not directly activate spikes in the axon, but it causes a fast depolarization (phasic V_{GABA}) that rapidly helps spikes (as early as 6 - 10 ms later), and a building tonic depolarization (tonic V_{GABA}) with repetition that further helps later spikes in the stimulation train (DR1 stimulation alone blue, middle trace). Similar results obtained in n = 7/7 axons. Likely similar tonic V_{GABA} and associated increased spike conduction helps explain post-tetanic potentiation of the monosynaptic EPSP, as previously suggested (Luscher et al., 1983).

(E) Repeated DR stimulation at higher rates eventually causes spike failure in proprioceptive axons (sodium spike relatively refractory), as shown in the top panel where a double stimulation (doublet, S4 DR, denoted DR2-DR2, 1.1xT, 0.1 ms, resting at -75 mV) exhibits failure on the second spike (with large FP indicated, magenta). However, additional V_{GABA} provided by stimulating an adjacent DR (DR1; 1.5xT, group I intensity, 0.1 ms) about 10 ms earlier helps prevent this spike failure (black trace; blue trace: V_{GABA} alone). When the same axon is stimulated slightly slower (with a longer doublet interval, second plot, DR-DR) failure does not occur, which we designate the failure interval threshold, which is quantified in G. The self-activated V_{GABA} caused by the first DR stimulation in this doublet helps prevent failure in second DR stimulation because replacing the first DR stimulation with an intracellular stimulation (IC, 2 nA) to activate the spike leads to failure of the second spike evoked by the DR stimulation at much longer intervals (lower trace, IC-DR).

(F) Another example of a failed doublet spike (DR2-DR2 stim, 1.1xT, 0.1 ms) that is rescued by V_{GABA} evoked by adjacent DR stimulation (DR1 1.5xT, 0.1 ms, resting at -78 mV), as in the top plots of E, except that in this case the failure is at a more distal node, since the FP is small.

(G) Failure interval threshold (minimum firing interval prior to failure, or maximal firing rate) with DR doublets (DR-DR), IC doublets (IC-IC) or IC-DR pair stimulation. Note the shorter intervals possible with the V_{GABA} evoked by the first stimulation (DR-DR). * significantly longer than minimum DR doublet interval (DR-DR), n = 18 each, $P < 0.05$.

(H) Quantification of the FP heights that were induced by a fast doublet (DR-DR or IC-IC; n = 14 each, at failure threshold interval) or IC and DR stimulation (IC-DR; n = 10), and the rescue of spikes by V_{GABA} evoked by adjacent DR stimulation. * significant increase in height with V_{GABA}, $P < 0.05$.

Figures S5. Other e*xcitatory actions of $GABA_A$ receptors on proprioceptive axons*, related to Figures 3 and 4.

(A) Intracellular recording from a sacral S3 proprioceptive Ia afferent branch in the dorsal horn with a secure spike evoked by S3 DR stimulation at rest (DR2, 1.1xT, 0.1 ms, - 60 mV rest, rat). Sensory-evoked V_{GABA} initiated by stimulating an adjacent DR (DR1; S4 DR; 2xT, 0.1 ms pulse, as in Fig 4) 10 ms prior to the DR2 stimulation only moderately influenced the spike. It sped up the spike latency and rise time, reduced the fall time and slightly reduced the spike height. Hyperpolarization induced spike failure (lower trace), as in Fig S2 A.

(B) Summary box plots of change in spike peak latency (advance) and height with prior sensory V_{GABA} activation as in A, * significant change, $P < 0.05$, $n = 20$ and 26, respectively.

(C) Intracellular recording from an S3 proprioceptive Ia afferent branch in the dorsal horn with a brief current injection pulse just subthreshold to initiating a pulse (near rheobase, bottom trace) at rest, only initiating a passive response with a small failed spike (middle trace). However, prior activation of V_{GABA} by stimulating an adjacent DR (DR1 as in A; S4 DR, 2xT, 0.1ms top trace) allowed the same current pulse to evoke a spike (above rheobase). The passive response to the current injection (double blue arrow; resistance R = V/I) was decreased during the V_{GABA}, corresponding to an increase in conductance, that contributed to a shunt (reduction) of the currents generating the spike, though this only caused about a 1% drop in spike height (1 mV; B). DCC recording mode, as in Fig S2.

(D) Summary box plots of rheobase (current threshold from C) before and during V_{GABA}, and change in shunt (conductance = 1/R) with V_{GABA}, as in C. * significant change with V_{GABA}, $P < 0.05$, $n = 37$ axon branches.

(E) By itself sensory evoked V_{GABA} sometimes initiated a spike on its rising phase, when the DR stimulation was large enough, demonstrating a direct excitatory action of $GABA_A$ receptors, as previously reported (Lucas-Osma et al., 2018). These spikes propagate antidromically toward the DR; and are thus termed dorsal root reflexes (DRR). Intracellular recording from rat sacral S3 proprioceptive afferent branch in the dorsal horn, similar to in Fig 4E (top trace), but V_{GABA} evoked by a larger DR1 stimulation (S4 DR stimulation 3.5xT, 0.1 ms) that itself evoked a spike (DRR). These V_{GABA} evoked spikes occur with a variable latency of 10 – 30 ms (Lucas-Osma et al., 2018) and thus make axons refractory for about 30 ms after the DR stimulation (Eccles et al., 1962a). These spikes can also evoke EPSPs in motoneurons via the monosynaptic pathway (Eccles et al., 1961a), and thus also produce a post activation depression of the EPSPs for many seconds. We thus kept the V_{GABA} low when examining the effects of V_{GABA} on EPSPs, to avoid these spikes and their subsequent inhibitory action (in Figs 5 – 7).

Figure S6. Overall spike conduction to motoneurons, related to Figures 4 and 2.

(A) *Experimental setup to indirectly measure sensory axon conduction failure following DR stimulation*, by examining whether failed axon segments are relatively less refractory to activation after failure, using a double pulse method adapted from Wall (Wall and McMahon, 1994). A tungsten microelectrode (12 MΩ) was placed in the ventral horn (VH) near the sensory axon terminals on motoneurons (S3 or S4 VH), to activate the branches/nodes of the axon projecting to the motoneuron that may have failed (VH stimulation). Spikes from VH or DR stimulation were recorded intracellularly in a proprioceptive axon penetrated in the dorsal columns.

(B) *VH threshold in refractory period*. Rapidly repeated VH stimulation (VH doublet; two 0.1 ms pulses) at an interval short enough to produce spike inactivation on the second stimulation (4 ms), with stimulus current adjusted to threshold for inactivation, T_{VH2}. This T_{VH2} (~15 uA) was always higher than the threshold VH stimulation for evoking a spike with the first stimulation, T_{VH1} (~10uA, not shown). Recorded in sacral S4 afferent resting at -72 mV, with doublets repeated at 3 s intervals to determine current thresholds.

(C) *VH threshold after DR stimulation*. Similar repeated activation of the axon in B, but with the first activation from a DR stimulation (at 1.5x DR threshold) and the second from VH stimulation at the T_{VH2} intensity from B. In this case the VH stimulation readily activated the axon spike, likely because the DR-evoked spike did not propagate to the VH, leaving the silent portion of the axon non refractory. Thus, this VH stimulation evoked spikes with a lower current than T_{VH2}, with the new threshold denoted $T_{DR,VH}$ (~ 12 μA, not shown). This DR – VH stimulation interval was deliberately set too short for the involvement of V_{GABA} (which rises in > 4 ms; Fig 4).

(D) *Computation of spike failure based on changes in VH stimulation thresholds*. If the DR-evoked spike entirely fails to propagate to the VH, then the threshold for subsequently activating the VH ($T_{DR,VH}$) should be the same as the threshold without any prior activation ($T_{VH1} = T_{DR,VH}$), whereas if it does not fail then the threshold for activating the VH should be the same as with a VH doublet ($T_{VH2} = T_{DR,VH}$). In between these two extreme scenarios, the DR evoked spike may only partially fail to propagate spikes to the VH; in this case $T_{DR,VH}$ should be between T_{VH1} and T_{VH2}, with the difference $T_{VH2} - T_{VH1}$ representing the range of possible thresholds between full failure and conduction. Overall the % conduction failure can be thus quantified as: $(T_{VH2} - T_{DR,VH})/(T_{VH2} - T_{VH1}) * 100\%$, which is 100% at full failure and 0% with no failure.

(E) *Average spike conduction failure to the VH in proprioceptive axons, and decrease following a DR conditioning stimulation that depolarized the axon* (V_{GABA}). Box plots of failure estimated as in B – D. Prior DR conditioning to produce V_{GABA} (via adjacent S4 or Ca1 DR stimulation at 3xT) reduced the failure estimated 20 ms later by the conduction testing (repeating DR – VH stimulations of B – D). DR conditioning itself lowered the thresholds for VH activation, as previously reported (not shown) (Wall, 1958). We studied two lengths of axons: long axons (intersegmental, *n* = 10) with the VH stimulation one segment away from the recording site, and short axons (segmental, *n* = 12) with the VH stimulation near the recording site, in the same segment. + significantly less failure with V_{GABA} and * significantly less failure with short compared to long axons, $P < 0.05$.

(F) *Experimental setup to directly record spike conduction failure in proprioceptive axon terminals in the ventral horn (VH) following DR stimulation.* Extracellular (EC) recordings from axon terminals in VH, with glass electrode positioned just outside these axons, and for comparison EC recording in the dorsal horn (DH).

(G) *EC field recorded in VH after DR stimulation* (S4 DR, 1.1xT), with a relatively large initial positive field (magenta arrows, pf) resulting from passively conducted axial current from sodium spikes at distant nodes (closer to the DR; outward current at electrode), some of which fail to propagate spikes to the VH recording site; thus, this field is a measure of conduction failure, as demonstrated in H – K. Following this, a negative field arises (blue arrow, nf), resulting from spikes arising at nodes near the electrode (inward current); thus, this field is a measure of secure conduction. Reducing conduction failure by depolarizing the axon (V_{GABA}) with a prior conditioning stimulation of an adjacent DR (Ca1, 2xT, 30 ms prior), decreased the positive field (pf) and increased the negative field (nf), consistent with increased conduction to the terminals, and in retrospect the same as Sypert et al. (1980) saw in cat (their Fig 4). Large stimulus artifacts prior to these fields are truncated.

(H) *Control recordings from proprioceptive axons in dorsal horn (DH) to confirm the relation of the EC negative field (nf) to spike conduction*. Intracellular (IC) recording from axon (sacral S4, resting at -64 mV) and EC recording just outside the same axon, showing the DR evoked spike (IC) arriving at about the time of the negative EC field (nf). There is likely little spike failure in this axon or nearby axons, due to the very small initial positive field (pf). EC fields are larger in DH compared to VH (G, 10x), and thus the artifact is relatively smaller.

(I) *Locally blocking nodes with TTX to confirm the relation of the positive EC field to spike failure*. EC recording from proprioceptive axon in the dorsal horn (S4), with an initial positive field (pf) followed by a negative field (nf), indicative of mixed failure and conduction. A local puff of TTX (10 μl of 100 μM) on the DR just adjacent to the recording site to transiently block DR conduction eliminated the negative field (nf) and broadened the positive field (pf), consistent with distal nodes upstream of the TTX block generating the positive field via passive axial current conduction, and closer nodes not spiking. Recordings were in the presence of synaptic blockade (with glutamate receptor blockers, kynurenic acid, CNQX and APV, at doses of 1000, 100 and 50 μM respectively), to prevent TTX spillover having an indirect action by blocking neuronal circuit activity, including $GABA_{axo}$ neuron activity. This synaptic blockade itself contributed to some spike failure, consistent with a block of $GABA_{axo}$ neuron activity, as there was a more prominent positive field (pf) compared to without blockade in H.

(J) *EC field recorded from terminals of proprioceptive axons in the ventral horn near motoneurons (S4), in the presence of an excitatory synaptic block* that largely eliminates most neuronal circuit behaviour (with kynurenic acid, CNQX and APV, as in I). In this synaptic block negative fields were generally absent (nf = 0), and only prominent positive fields (pf) occurred (as with TTX block), suggesting that conduction to the VH often completely failed when circuit behavior is blocked, which likely indirectly reduces $GABA_{axo}$ neuronal activity and its associated facilitation of nodal conduction.

(K) *Rescue of spike conduction to the ventral horn by increasing sodium channel excitability by reducing the divalent cations Mg++ and Ca ++ in the bath medium*. Same EC field recording as in J, but with divalent cations reduced (Mg^{++}, 0 mM; Ca^{++}, 0.1 mM). The positive field was largely eliminated (pf = 0) and replaced by a negative field (nf), consistent with elimination of conduction failure, and proving that the positive field is not a trivial property of axon terminals (Dudel, 1965; Katz and Miledi, 1965; Sypert et al., 1980).

(L) *Conduction index* computed from positive (pf) and negative (nf) field amplitudes: nf / (nf + pf) x 100%, which approaches 100% for full conduction (pf ~0; as in H) and 0% for no conduction (nf = 0; as in J).

(M – N) Summary of conduction index estimated from EC field potentials, shown with box plots. Without drugs present in the recording chamber, the axon conduction from the DR to the dorsal horn is about is 70% (M, *n* = 17), consistent with Fig 2, whereas conduction from the DR to the VH is only about 50% (N, *n* = 9), suggesting substantial failure at the many branch points in the axon projections from the dorsal horn to the motoneurons. Increasing $GABA_{axo}$ neuron activity with DR conditioning (30 – 60 ms prior) increased conduction (+GABA, in both the DH and VH, *n* = 5 and 9, as in G), whereas decreasing GABA and all circuit activity in a synaptic blockade decreased conduction (-GABA, in both DH and VH, *n* = 5 and 6, as in I – J). TTX (*n* = 4, M) or removal of divalent cations (Mg^{++} and Ca^{++}, -Divalent, *n* = 4, N) respectively reduced or increased conduction (as in I and K). * significant difference from control pre-drug or pre-conditioning, $P < 0.05$.

Figure S7. Sensory evoked priming of monosynaptic EPSPs by $GABA_A$ receptors, related to Fig 5.

(A) Whole spinal cord ex vivo preparation for intracellular recording of EPSPs from motoneurons while stimulating dorsal roots (DRs).

(B) Monosynaptic EPSP in an S4 motoneuron evoked by a proprioceptive group I stimulation of the S4 DR (1.1xT, denoted DR2, lower traces; resting potential -75 mV: black line), alone (pink) and 60 ms after (blue) a conditioning stimulation of cutaneous afferents in rat (stimulation of the largely cutaneous Ca1 DR, 2.5xT; denoted DR1). Averages of 10 trials each at 10 s intervals. V_{GABA} evoked by the same cutaneous conditioning stimulation in a proprioceptive S4 DR afferent is shown for reference (top, recorded separately, as in Fig 4B).

(C) Expanded time scale plot of EPSPs shown in B.

(D) Similar to B, but stronger conditioning stimulation (DR1, 3xT) evoking background postsynaptic activity (blue, Bkg) that lasted longer than 60 ms, and slightly inhibited the EPSP, likely from increased postsynaptic conductances shunting the EPSP (postsynaptic inhibition; light pink: overlay of EPSP alone) and masking nodal facilitation.

(E) Summary box plots of priming of EPSPs during phasic V_{GABA} evoked by either proprioceptive conditioning (S3 or contralateral S4 DR stimulation, 1.1xT, in rats and mice similar and combined, n = 6 and 5, blue) or cutaneous conditioning (Ca1 DR stimulation, 2-3xT, in rats, n = 42, pink), and action of $GABA_A$ and $GABA_B$ antagonists (gabazine 50 μM, L655708 0.3 μM and CGP55845 0.3 μM, grey, n = 5 – 9 each). EPSPs evoked in S3 and S4 motoneurons by DR2 (S3 or S4) stimulation at 1.1T, as in B. Priming measured 60 ms post conditioning during phasic V_{GABA} (phasic condition indicated) and when postsynaptic actions of conditioning (Bkg) were mostly *minimal* (as in B). After conditioning was completed EPSP testing continued and revealed a residual facilitation that lasted for a 10 - 100 s (After effect, green, n = 9 tested), due to a build up of tonic V_{GABA}, after which the EPSP returned to baseline (not shown), similar to post-tetanic potentiation (Luscher et al., 1983). Also, a brief high frequency cutaneous stimulation train (200 Hz, 0.5 s, 2.5xT) that led to a very long lasting depolarization of proprioceptive axons (Tonic V_{GABA}, example in Fig 5G) caused a facilitation of the monosynaptic EPSP that lasted for minutes (average shown, tonic cutaneous condition), and this was blocked by L655708 (in rats, n =5 each). * P < 0.05: significant change with conditioning. + P < 0.05: significant change with antagonist. Raw data points shown to indicate occasional inhibition of the MSR by conditioning, but overall facilitation.

(F) Summary box plots of change in EPSP induced by cutaneous DR (DR1) conditioning (and associated phasic V_{GABA}) 60 ms prior to evoking the EPSP, with varying EPSP stimulation intensity. When the DR that evoked the test EPSP (DR2) was stimulated at an intensity that produced less than half the maximal EPSP height (1.1xT, ~ 30% max EPSP, n =42, same data as in E) the facilitation of EPSP by conditioning was larger than when this DR2 stimulation was increased to produce a test EPSP near maximal (1.5xT, prior to conditioning, n =18). * P < 0.05: significant change with conditioning.

(G) Summary of cutaneous priming of EPSPs from F (evoked by DR2 at 1.1xT), but separated into trials without (as in B, n = 31) and with (as in D, n = 11) large background postsynaptic changes induced by conditioning that lasted up to and during the EPSP testing (at 60 ms post conditioning, Bkg). * P < 0.05: significant change with conditioning evoked V_{GABA}. + P < 0.05: significant reduction priming with increased background activity (Bkg).

(H) Remote postsynaptic inhibition from conditioning. Long lasting changes in intrinsic proprieties of motoneurons (S4 and S3) following a mixed proprioceptive and cutaneous conditioning DR stimulation (on S3 or contralateral S4 DR, 2.5xT, DR1) that only produced a transient postsynaptic depolarization that ended prior to EPSP testing (as in B), including a reduction in time constant (τ) and slight hyperpolarization of potential (V_m), both measured at the time of EPSP testing (measured at 60 ms post conditioning, but in trials without EPSP testing; rats, n = 15). At this time, there was little change in somatic membrane resistance (Rm) with conditioning, suggesting that conditioning induced postsynaptic activity at a remote location in distal dendrites of the motoneuron. When we voltage clamped the membrane potential during monosynaptic testing (DR2 at 1.1-1.5xT) to directly measure the synaptic current (EPSC), to minimize that inhibitory action of postsynaptic conductance increases, we found that the conditioning stimulation (DR1) produced a larger facilitation of the monosynaptic EPSC than the EPSP measured in current clamp in the same motoneurons. That is, conditioning induced mixed facilitation and inhibition of the EPSP, but mainly facilitation of the EPSC. These results are consistent with the priming of the EPSP being masked by postsynaptic inhibition from increases in remote dendritic postsynaptic conductances triggered by the conditioning stimulation. * P < 0.05: significant change with conditioning.

SUPPLEMENTARY TABLE

Table S1. Chronological list of evidence contradicting the classical concept of presynaptic inhibition of transmitter release from proprioceptive sensory axon terminals on motoneurons.

	Contradictions in classic view of terminal presynaptic inhibition mediated by terminal $GABA_A$ receptors and V_{GABA}	**Resolution of contradictions**
1938	*Primary afferent depolarization (V_{GABA}) directly evokes spikes in sensory axons, producing excitation rather than presynaptic inhibition.* Barron and Matthews (1938) discovered that sensory nerve conditioning evokes a long depolarization in many other sensory afferents (primary afferent depolarization, PAD), which we now know is $GABA_A$ mediated (Rudomin, 1999), and thus here we termed it V_{GABA} (rather than PAD) to dissociate it from depolarizations mediated by other transmitters. They and others noted that sometimes this V_{GABA} was large enough to directly induce axon spiking, even in vivo (Beloozerova and Rossignol, 1999), including spikes in the sensory axons mediating the MSR itself, raising a clear contradiction with the notion of GABA mediated presynaptic inhibition, that even now remains (Lucas-Osma et al., 2018). While these V_{GABA}-triggered spikes do not fully propagate antidromically out the DRs in many axons (they fail en route), they are actually initiated in most axons and more likely to conduct orthodromically (Lucas-Osma et al., 2018), making most axons and their motoneuron synapse refractory to subsequent testing (*post activation depression*). Indeed, numerous groups have shown that these spikes directly activate the MSR pathway (Bos et al., 2011; Duchen, 1986; Eccles et al., 1961a; Fink et al., 2014). Thus, these V_{GABA}-evoked spikes must inhibit afferent transmission in the MSR pathway by making axons refractory and producing post activation depression of their terminal synapse, even in humans where V_{GABA} evoked spikes appear in peripheral nerve recordings (Shefner et al., 1992). This indirect inhibition is $GABA_A$ mediated and thus readily mistaken for presynaptic inhibition (sensitive to $GABA_A$ antagonists)(Curtis, 1998; Redman, 1998). Even Eccles noted this issue, and showed that just the refractory period alone in the sensory axon inhibits the MSR (Eccles et al., 1961a).	*Post activation depression from V_{GABA} evoked spikes inhibits the MSR and masks priming of the MSR by nodal facilitation.* We find that priming of the MSR by conditioning evoked V_{GABA} is always reduced when it is associated with a large enough conditioning stimulation to evoke spikes in sensory afferents, which likely results from post activation depression of axon transmission. This likely explains why Fink et al. (2014) recently saw inhibition of the MSR by optogenetically activating $GABA_{axo}$ neurons, a topic we are currently pursuing. Crucially, when looking for MSR priming, avoiding these spikes and post activation depression requires using weak conditioning stimuli, unlike previous studies (Eccles et al., 1961a; Stuart and Redman, 1992).
1949	*Post-tetanic potentiation (PTP) of the MSR increases sensory nerve conduction, but its mechanisms have remained elusive.* Early on Lloyd (1949) concluded that increasing conduction along sensory axons (not just terminals) contributed to the minutes of facilitation of the MSR seen after a train of high frequency nerve stimulation (PTP). However, he supposed this might be due to hyperpolarization of the sensory axons, even though we now know that such bursts depolarize axons via tonic V_{GABA} (Lucas-Osma et al., 2018). The tonic V_{GABA} from these bursts must overwhelm the hyperpolarization driven by Na-K pump activity (Bostock and Grafe, 1985). Lloyd also concluded that PTP only occurred when the same nerve is used for the train (tetanus) as for testing the MSR.	*Repetitive nerve stimulation produces a tonic $GABA_A$ mediated depolarization (V_{GABA}) of axons that facilitates nodal conduction, and increases the MSR.* This V_{GABA} likely contributes to PTP, and is largest when the same nerve is tetanized, compared to other nerves, explaining why Lloyd may have missed the subtler facilitation from other nerves.
1958	*V_{GABA} is associated with a lowering of the threshold for activating spikes.* Early on Wall (1958) noted that a conditioning nerve stimulation that depolarized sensory axons (V_{GABA}) was associated with a lower threshold to extracellularly activate these axons. Subsequently this was assumed to be due to the action of terminal $GABA_A$ receptors and presynaptic inhibition, and spike threshold changes were used to estimate the size of V_{GABA} (Lomeli et al., 1998; Rudomin, 1999).	*V_{GABA} lowers the spike threshold via nodal $GABA_A$ receptors assisting the sodium spike.* This is not related to presynaptic inhibition, but can still be used to estimate V_{GABA} as Rudomin and others have done.
1957 - 1994	*V_{GABA} is not correlated with inhibition of the monosynaptic reflex (MSR)*. Shortly after Frank and Fortes discovered that the leg extensor muscle MSR is inhibited by a conditioning of a flexor nerve in cats (PBST; like Fig 6)(Frank, 1959; Frank and Fortes, 1957), Eccles proposed the concept of presynaptic inhibition mediated by this conditioning depolarizing of the proprioceptive sensory axon terminals in the MSR pathway (V_{GABA}), simply because the MSR and V_{GABA} are somewhat correlated in time (Eccles et al., 1961a). However, in retrospect V_{GABA} is far too brief to account for the much longer inhibition caused by this conditioning (Curtis and Lacey, 1994; Eccles et al., 1962a), and some flexor nerve conditioning (a single PBST pulse) inhibits the MSR (Fig 1 of Eccles, 1961a), even though it does not cause V_{GABA} in the extensor proprioceptors of the MSR at all (Eccles and Krnjevic, 1959).	*V_{GABA} is correlated with nodal spike facilitation and priming of the MSR.* V_{GABA} causes priming of the MSR, explaining this correlation. When V_{GABA} is large and evokes axonal spikes, these cause post activation depression (detailed above) that should also be correlated with V_{GABA}, but is not due to presynaptic inhibition. Also, barbiturates used by Eccles and others likely potentiated $GABA_A$ receptor currents.
1959 - 1993	*Postsynaptic inhibition inevitably accounts for part of the inhibition of the MSR by flexor nerve conditioning*. In his initial short report Frank (1959) correctly suggested that the early inhibition of the MSR by flexor nerve conditioning might be partly postsynaptic (rather than presynaptic), on motoneuron distal dendrites. Others dismissed postsynaptic inhibition because the decay times of the EPSP does not always change when the EPSP is reduced by conditioning, which they proposed indicated that there was no postsynaptic change in conductance in distal dendrites (McCrea et al., 1990; Rudomin, 1999). However, this method is likely not very sensitive (due to variability in unitary EPSP time course). Also, anatomically ~70% of	*Postsynaptic inhibition masks priming of the MSR by nodal facilitation.* We find evidence for long lasting postsynaptic inhibition on distal motoneuron dendrites during nerve conditioning stimulation (including postsynaptic reductions in Tau, Vm and unitary EPSP heights and single MU firing). Crucially, minimizing postsynaptic inhibition requires using a small

	$GABA_{axo}$ contacts on afferent terminals also contact motoneurons (in a triad), so postsynaptic inhibition is inevitable (Hughes et al., 2005; Pierce and Mendell, 1993).	conditioning stimulation when looking for MSR priming, unlike previous studies (Stuart and Redman, 1992).
1961 - 2014	*Self-priming during repeated MSR testing reduces the possibility of observing priming with subsequent conditioning stimuli, leaving only inhibitory actions of conditioning.* Eccles and others knew that the same proprioceptive nerve stimulation that activates the MSR also depolarizes these proprioceptive afferents (V_{GABA} self-activation) (Eccles et al., 1961a). Thus, just the act of repeatedly testing the MSR to find the average MSR prior to conditioning pre-activates V_{GABA} and produces self-priming of the MSR, reducing the headroom to observe changes in the MSR following a separate nerve conditioning stimulation that produces V_{GABA}. However, at the time it was not known that repeated nerve stimulation causes a tonic buildup of GABA and a tonic V_{GABA} that alters sensory transmission and MSR even at long repetition intervals of many seconds. Thus, Eccles and others used short test intervals (1 s) and strong maximal MSR test stimuli (Eccles et al., 1961a; Fink et al., 2014; Stuart and Redman, 1992), presumably assuming that there would be no interaction between test stimuli, which is not the case. In retrospect, these short test intervals and strong test stimuli must have preactivated tonic GABA, leaving little headroom to observe facilitation of the MSR (priming), and leaving mainly only inhibitory action possible.	*Self-priming masks priming of the MSR by a conditioning stimulation.* We find that to observe priming of the MSR by a conditioning stimuli that produces a V_{GABA} (light or sensory evoked) it is important to use long test intervals (5 - 10 s) and small MSR test intensities (1.1xT) to minimize self activation of a tonic V_{GABA} prior to conditioning. Typically, we average about 10 MSR test responses prior to conditioning and then a further 10 during conditioning. While experimentally troublesome, self priming during repetitive activation is actually one of the main functions of V_{GABA}, allowing sensory axons to faithfully transmit spikes to motoneurons at high frequencies that would otherwise produce sodium spike inactivation.
1980	*Sensory axon terminal potentials at motoneurons are consistent with spike failure.* Early efforts to examine how spikes propagated to sensory axon terminals employed extracellular recordings (EC) near the motoneurons, called terminal potentials (Sypert et al., 1980). However, unlike EC recordings from near conducting axons (Fig 2B), these terminal potentials lacked much of the obvious negative field associated with the action potential, and instead had a prominent positive field, followed by a smaller negative field (Fig S6; Sybert et al. 1980). This positive field has been shown in other axons to be indicative of spike propagation failure and result from the passive axonal current caused by the last non-failing node, similar to a FP, as demonstrated in motor axon recordings (Dudel, 1965; Hubbard et al., 1969). Indeed, we found that even dorsal horn recordings could exhibit this positive field if the nearby dorsal root conduction is blocked with a microinjection of TTX (Fig S6 I). Sypert et al. (1980) went on to show that with V_{GABA} evoked by nerve conditioning this positive terminal potential field was decreased, and incorrectly interpreted this as evidence for decreased spike conduction and thus supposed it was due to presynaptic inhibition.	*Positive terminal potential fields are decreased with V_{GABA}, indicative of decreased conduction failure, and in retrospect consistent with Sypert et al. (1980).* There is a small negative field that follows the positive field in terminal potential recordings, representing spikes that actually reach the terminals. We quantified negative field and found it to increase with V_{GABA}, consistent again with increased spikes conducting to motoneurons (Fig S6 G). Blocking activity in the spinal cord with glutamate antagonists, which would include blocking $GABA_{axo}$ circuit activity, decreased this negative field.
1988 - 1998	*$GABA_B$ receptors cause presynaptic inhibition and related RDD.* Decades, after Eccles popularized the notion of $GABA_A$ mediated presynaptic inhibition, Curtis (1998) later concluded that the late part of the inhibition of the MSR by flexor nerve conditioning is instead $GABA_B$ receptor mediated, since it is reduced by the $GABA_B$ antagonist CGP55845 (as Fink et al. 2014 also showed), as is RDD (Lev-Tov et al., 1988). RDD is a rate dependent depression in the MSR during repeated testing. We suggest RDD is partly mediated by a build up of GABA released by GABAergic neurons onto the terminals during this repeated MSR testing, though activity dependent homosynaptic depression likely also contributes (Hultborn et al., 1996b).	*$GABA_B$ mediated presynaptic inhibition masks priming of the MSR by nodal $GABA_A$ receptors. $GABA_B$ receptors* are located mostly on the terminals. They produce presynaptic inhibition (Fig 5) and contribute to RDD (Bennett and Hari, unpublished results), both of which are reduced by $GABA_B$ antagonists (CGP55845) or silencing $GABA_{axo}$ neurons.
1990 - 1998	*$GABA_A$ receptors have direct postsynaptic inhibitory effects on many spinal neurons, making the actions of $GABA_A$ antagonists difficult to attribute to presynaptic inhibition*. By the 1990s Redman and others tried to confirm the role of $GABA_A$ receptors in presynaptic inhibition by locally applying the $GABA_A$ antagonists bicuculline to the spinal cord, and indeed found this drug or other antagonists reduced the inhibition of the MSR by flexor nerve conditioning (Curtis, 1998; Curtis and Lacey, 1994; Eccles et al., 1963; Stuart and Redman, 1992). However, we now know that this is indirectly due to bicuculline causing a widespread disinhibition of the spinal cord (including loss of post activation depression, detailed above) that leads to a convulsive spinal cord with very long lasting polysynaptic reflexes evoked by the nerve conditioning or the MSR testing itself, making pre and postsynaptic actions hard to distinguish. Further, we know that $GABA_A$ receptors mediate dorsal root reflexes and associated post activation depression of the MSR (see above point), and thus bicuculline and picrotoxin likely reduce the inhibition of the MSR via reducing post activation depression (see above), rather than changing presynaptic inhibition.	*$GABA_A$ receptor antagonists reduce the MSR, by reducing nodal facilitation.* Postsynaptic $GABA_A$ receptors have potent inhibitory actions on many spinal neurons involved in polysynaptic reflexes. However, minimizing these polysynaptic reflexes (by using weak test stimuli and blocking NMDA receptors) reveals a direct inhibition of the MSR by $GABA_A$ antagonists, as does optogenetically silencing $GABA_{axo}$ neuron, consistent with $GABA_A$ receptors facilitating rather than inhibiting sensory transmission. This was actually our starting point, noticing decades ago that bicuculline did not increase the MSR (Fig 5C).
1990 - 1995	*V_{GABA} recorded in the dorsal roots cannot arise from terminal GABA receptors, due to spatial attenuation on the axon.* With advent of detailed anatomical and computer models of sensory axons (Graham and Redman, 1994; Segev, 1990; Walmsley et al., 1995) it became clear that signals like spikes or V_{GABA} are attenuated over short distances in axons, < 200 µm. This implies that V_{GABA} recorded on or near the DR is unlikely to bare any relation to terminal presynaptic inhibition, despite claims to the contrary (Eccles et al., 1963; Fink et al., 2014; Hultborn et al., 1987; Rudomin, 1999).	*The space constant λ_S of sensory axons is about 90 µm.* Thus, the V_{GABA} recorded in the dorsal root must arise from nearby nodal GABA receptors, and not bear any relation to GABA action at the terminals >1000 µm away.

1994 - 1999	*Shunting inhibition produced by axon terminal $GABA_A$ receptors is not adequate to produce presynaptic inhibition of the MSR*. Numerous invertebrate studies proposed that the conductance from $GABA_A$ receptors in terminals caused a reduction in spike height via its shunting action that contributed to presynaptic inhibition with nerve conditioning (Cattaert and El Manira, 1999). However, the effects of conditioning on spikes was small and terminals were not actually recorded from. Subsequently modelling considerations led to the conclusion that shunting inhibition is not adequate to produce presynaptic inhibition and calcium was somehow involved (Graham and Redman, 1994), possibly further implicating $GABA_B$ receptors, as we see. Considering our estimated space constant λ_S of ~90 µm, the small shunting inhibition of the spike height (1 mV) we observe is very unlikely to prevent the spike produced at a given node from activating a downstream neighbouring node, since nodes are ~50 µm apart, leading to only about a 50% reduction in spike height at the downstream node (to ~40 mV, unless of course the node is failing), which is well above that needed to initiate a full nodal spike. Thus, spike propagation is very unlikely to be blocked by shunting inhibition. Also, terminal boutons are mostly on unmyelinated axons without sodium channels (passive, 3rd order), and so a 1% reduction in the spike arising from the last/closest node on the 2nd order branch will have little effect on the terminal depolarization (1%), ruling out substantial shunting inhibition of transmitter release from the terminal.	*$GABA_A$ receptors only slightly decrease spikes by shunting conductances, and otherwise assist nodal spike conduction in proprioceptive axons.* In non-failing secure spikes in sensory axons $GABA_A$ receptors lower the threshold for spike activation (rheobase) and speed the spikes, the latter by decreasing the time constant of the axon (RC). They do decrease the spike, but only by about 1%, consistent with shunting being unlikely to inhibit spike transmission to motoneurons. However, this does not rule out densely expressed $GABA_A$ receptors causing shunting and presynaptic inhibition in cutaneous afferents (Lucas-Osma, 2018), as previously suggested (Verdier et al., 2004; Wall, 1998).
1994 - 1998	*Sodium spike inactivation from axon terminal $GABA_A$ receptor depolarization is not adequate to produce presynaptic inhibition.* Early poor quality recordings from sensory axons (resting near -50 mV from penetration injury) (Luscher et al., 1994) led to the prevailing view that spike failure with depolarization (V_{GABA}) was much more common than we now find with better recordings (resting near -70 mV, Fig S2 J). Further, Redman later questioned this view, and it seems unlikely for the MSR pathway (Redman, 1998; Stuart and Redman, 1992).	*Physiological V_{GABA} depolarizations do not block proprioceptive sensory axons spikes, and instead prevent them from failing in the MSR pathway.* However, this does not rule out densely expressed $GABA_A$ receptors causing spike inactivation in other axons (see previous point).
1995 - 1998	*Physiological $GABA_A$ receptor activation is unlikely to produce branch point failure in the sensory axons of the MSR pathway.* Over the years sensory axon conduction failure has been occasionally noted from indirect observations (Barron and Matthews, 1935; Henneman et al., 1984; Li et al., 2020; Wall, 1998), though it was only when GABAergic terminals were reported near nodes on myelinated branches (Walmsley et al., 1995) that Patrick Wall and others (Wall, 1998; Walmsley et al., 1995) started questioning whether this failure could be regulated. However, Wall thought GABA should inhibit rather than assist spikes by inactivating sodium channels, which is surprising, since Wall (1958) himself years earlier showed that V_{GABA} lowers the threshold for activating sensory axon terminals (via a microelectrode). However, Wall was misled by two issues. First, at the time poor quality recordings from sensory axons led to the misconception that spike failure with physiological depolarizations (V_{GABA}) was common, as mentioned in the previous point. To be fair, Wall was studying cutaneous, as well as proprioceptive, afferents, which are more densely innervated by GABA receptors (Lucas-Osma et al., 2018), making spike inactivation by V_{GABA} more likely (Wall, 1998). Second, by this time $GABA_A$ and associated V_{GABA} had been firmly entrenched as synonymous with presynaptic inhibition.	*$GABA_A$ receptors help prevent branch point failure and thus facilitate sensory transmission in the MSR.* Computer simulations by Walmsley and others (Graham and Redman, 1994; Walmsley et al., 1995) have led to the conclusion that physiological $GABA_A$ receptor conductances cannot stop spikes from propagating past a node. Instead we report here that they help prevent spike failure at branch points, including in our computer simulations.
1996 - 2018	*Little or no proprioceptive axon terminal $GABA_A$ receptors*. With the advent of good antibodies to label GABA receptor subtypes, repeated efforts to find immunolabelling for $GABA_A$ receptors on large proprioceptive afferents were attempted, but failed to find receptors (Alvarez et al., 1996; Betley et al., 2009; Fink et al., 2014; Lucas-Osma et al., 2018). $GABA_B$ receptor immunolabelling has surprisingly not previously been investigated in proprioceptive afferents, despite its presence on other afferents (Aβ) (Salio et al., 2017).	*$GABA_A$ receptors are mostly at nodes, whereas $GABA_B$ receptors are at terminals in large proprioceptive afferents*.
2005 - 2014	*When GAD2 expressing GABAergic neurons were identified that make axoaxonic connections onto terminals of proprioceptive sensory axons (Betley et al., 2009; Fink et al., 2014; Hughes et al., 2005) they were presumed to mainly produce presynaptic inhibition*. Thus, they were called $GABA_{pre}$ neurons (also called P-bouton neurons), unfortunately implying that their only role is presynaptic inhibition. We have instead referred to these neurons by the more generic termed $GABA_{axo}$, to indicate that they make axoaxonic connections, and do not necessarily produce presynaptic inhibition.	A key role of $GABA_{axo}$ neurons is to innervate proprioceptive afferent nodes via $GABA_A$ receptors and ventral terminals via $GABA_B$ receptors, producing nodal facilitation and presynaptic inhibition, respectively.
2018	*$GABA_{axo}$ neuron activation by sensory conditioning does not depolarize proprioceptive axon terminals*. With the development of improved electrodes, we have recently been able to make direct recordings from the fine terminals of proprioceptive afferents, and find that during sensory conditioning the terminal is not depolarized during the long V_{GABA} recorded on dorsal roots (Lucas-Osma et al., 2018).	*$GABA_{axo}$ neuron activation depolarizes nodes*. Dorsally located nodes produce the classic V_{GABA} (PAD) recorded in dorsal roots, and not terminal depolarization.

REFERENCES

Aimonetti, J.M., Vedel, J.P., Schmied, A., and Pagni, S. (2000). Mechanical cutaneous stimulation alters Ia presynaptic inhibition in human wrist extensor muscles: a single motor unit study. J Physiol *522 Pt 1*, 137-145.
Alvarez, F.J., Taylor-Blake, B., Fyffe, R.E., De Blas, A.L., and Light, A.R. (1996). Distribution of immunoreactivity for the beta 2 and beta 3 subunits of the GABAA receptor in the mammalian spinal cord. J Comp Neurol *365*, 392-412.
Arbuthnott, E.R., Boyd, I.A., and Kalu, K.U. (1980). Ultrastructural dimensions of myelinated peripheral nerve fibres in the cat and their relation to conduction velocity. J Physiol *308*, 125-157.
Bardoni, R., Takazawa, T., Tong, C.K., Choudhury, P., Scherrer, G., and Macdermott, A.B. (2013). Pre- and postsynaptic inhibitory control in the spinal cord dorsal horn. Ann N Y Acad Sci *1279*, 90-96.
Barron, D.H., and Matthews, B.H. (1935). Intermittent conduction in the spinal cord. J Physiol *85*, 73-103.
Barron, D.H., and Matthews, B.H. (1938). The interpretation of potential changes in the spinal cord. J Physiol *92*, 276-321.
Beloozerova, I., and Rossignol, S. (1999). Antidromic discharges in dorsal roots of decerebrate cats. I. Studies at rest and during fictive locomotion. Brain Res *846*, 87-105.
Bennett, D.J. (1993). Torques generated at the human elbow joint in response to constant position errors imposed during voluntary movements. Exp Brain Res *95*, 488-498.
Bennett, D.J., Gorassini, M., and Prochazka, A. (1994). Catching a ball: contributions of intrinsic muscle stiffness, reflexes, and higher order responses. Can J Physiol Pharmacol *72*, 525-534.
Bennett, D.J., Sanelli, L., Cooke, C.L., Harvey, P.J., and Gorassini, M.A. (2004). Spastic long-lasting reflexes in the awake rat after sacral spinal cord injury. J Neurophysiol *91*, 2247-2258.
Betley, J.N., Wright, C.V., Kawaguchi, Y., Erdelyi, F., Szabo, G., Jessell, T.M., and Kaltschmidt, J.A. (2009). Stringent specificity in the construction of a GABAergic presynaptic inhibitory circuit. Cell *139*, 161-174.
Blight, A.R. (1985). Computer simulation of action potentials and afterpotentials in mammalian myelinated axons: the case for a lower resistance myelin sheath. Neuroscience *15*, 13-31.
Bos, R., Brocard, F., and Vinay, L. (2011). Primary afferent terminals acting as excitatory interneurons contribute to spontaneous motor activities in the immature spinal cord. J Neurosci *31*, 10184-10188.
Bostock, H., and Grafe, P. (1985). Activity-dependent excitability changes in normal and demyelinated rat spinal root axons. J Physiol *365*, 239-257.
Boulenguez, P., Liabeuf, S., Bos, R., Bras, H., Jean-Xavier, C., Brocard, C., Stil, A., Darbon, P., Cattaert, D., Delpire, E.*, et al.* (2010). Down-regulation of the potassium-chloride cotransporter KCC2 contributes to spasticity after spinal cord injury. Nat Med *16*, 302-307.
Boyden, E.S., Zhang, F., Bamberg, E., Nagel, G., and Deisseroth, K. (2005). Millisecond-timescale, genetically targeted optical control of neural activity. Nat Neurosci *8*, 1263-1268.
Brown, A.G., and Fyffe, R.E. (1978). The morphology of group Ia afferent fibre collaterals in the spinal cord of the cat. J Physiol *274*, 111-127.
Burke, K.J., Jr., and Bender, K.J. (2019). Modulation of Ion Channels in the Axon: Mechanisms and Function. Front Cell Neurosci *13*, 221.
Burke, R.E., and Glenn, L.L. (1996). Horseradish peroxidase study of the spatial and electrotonic distribution of group Ia synapses on type-identified ankle extensor motoneurons in the cat. J Comp Neurol *372*, 465-485.
Cattaert, D., and El Manira, A. (1999). Shunting versus inactivation: analysis of presynaptic inhibitory mechanisms in primary afferents of the crayfish. J Neurosci *19*, 6079-6089.
Cho, I.H., Panzera, L.C., Chin, M., and Hoppa, M.B. (2017). Sodium Channel beta2 Subunits Prevent Action Potential Propagation Failures at Axonal Branch Points. J Neurosci *37*, 9519-9533.
Chow, B.Y., Han, X., Dobry, A.S., Qian, X., Chuong, A.S., Li, M., Henninger, M.A., Belfort, G.M., Lin, Y., Monahan, P.E.*, et al.* (2010). High-performance genetically targetable optical neural silencing by light-driven proton pumps. Nature *463*, 98-102.
Chua, H.C., and Chebib, M. (2017). GABAA Receptors and the Diversity in their Structure and Pharmacology. Adv Pharmacol *79*, 1-34.

Chuang, S.H., and Reddy, D.S. (2018). Genetic and Molecular Regulation of Extrasynaptic GABA-A Receptors in the Brain: Therapeutic Insights for Epilepsy. J Pharmacol Exp Ther *364*, 180-197.
Cohen, C.C.H., Popovic, M.A., Klooster, J., Weil, M.T., Mobius, W., Nave, K.A., and Kole, M.H.P. (2020). Saltatory Conduction along Myelinated Axons Involves a Periaxonal Nanocircuit. Cell *180*, 311-322 e315.
Curtis, D.R. (1998). Two types of inhibition in the spinal cord. . In Presynaptic Inhibition and Neuron Control, P. Rudmon, R. Romo, and L.M. Mendell, eds. (New York: Oxford University Press), pp. 150-161.
Curtis, D.R., and Lacey, G. (1994). GABA-B receptor-mediated spinal inhibition. Neuroreport *5*, 540-542.
Czeh, G., and Dezso, G.T. (1982). Separation of temperature sensitive and temperature insensitive components of the postsynaptic potentials in the frog motoneurons. Neuroscience *7*, 2105-2115.
Debanne, D., Campanac, E., Bialowas, A., Carlier, E., and Alcaraz, G. (2011). Axon physiology. Physiol Rev *91*, 555-602.
Dellal, S.S., Luo, R., and Otis, T.S. (2012). GABAA receptors increase excitability and conduction velocity of cerebellar parallel fiber axons. J Neurophysiol *107*, 2958-2970.
Duchen, M.R. (1986). Excitation of mouse motoneurones by GABA-mediated primary afferent depolarization. Brain Res *379*, 182-187.
Dudel, J. (1965). The Mechanism of Presynaptic Inhibition at the Crayfish Neuromuscular Junction. Pflugers Arch Gesamte Physiol Menschen Tiere *284*, 66-80.
Eccles, J.C., Eccles, R.M., and Magni, F. (1961a). Central inhibitory action attributable to presynaptic depolarization produced by muscle afferent volleys. J Physiol *159*, 147-166.
Eccles, J.C., Kozak, W., and Magni, F. (1961b). Dorsal root reflexes of muscle group I afferent fibres. J Physiol *159*, 128-146.
Eccles, J.C., and Krnjevic, K. (1959). Potential changes recorded inside primary afferent fibres within the spinal cord. J Physiol *149*, 250-273.
Eccles, J.C., Magni, F., and Willis, W.D. (1962a). Depolarization of central terminals of Group I afferent fibres from muscle. J Physiol *160*, 62-93.
Eccles, J.C., Schmidt, R., and Willis, W.D. (1963). Pharmacological Studies on Presynaptic Inhibition. J Physiol *168*, 500-530.
Eccles, J.C., Schmidt, R.F., and Willis, W.D. (1962b). Presynaptic inhibition of the spinal monosynaptic reflex pathway. J Physiol *161*, 282-297.
El-Gaby, M., Zhang, Y., Wolf, K., Schwiening, C.J., Paulsen, O., and Shipton, O.A. (2016). Archaerhodopsin Selectively and Reversibly Silences Synaptic Transmission through Altered pH. Cell Rep *16*, 2259-2268.
Engelman, H.S., and MacDermott, A.B. (2004). Presynaptic ionotropic receptors and control of transmitter release. Nat Rev Neurosci *5*, 135-145.
Fedirchuk, B., Wenner, P., Whelan, P.J., Ho, S., Tabak, J., and O'Donovan, M.J. (1999). Spontaneous network activity transiently depresses synaptic transmission in the embryonic chick spinal cord. J Neurosci *19*, 2102-2112.
Feil, R., Wagner, J., Metzger, D., and Chambon, P. (1997). Regulation of Cre recombinase activity by mutated estrogen receptor ligand-binding domains. Biochem Biophys Res Commun *237*, 752-757.
Fenrich, K.K., Zhao, E.Y., Wei, Y., Garg, A., and Rose, P.K. (2014). Isolating specific cell and tissue compartments from 3D images for quantitative regional distribution analysis using novel computer algorithms. J Neurosci Methods *226*, 42-56.
Fink, A.J., Croce, K.R., Huang, Z.J., Abbott, L.F., Jessell, T.M., and Azim, E. (2014). Presynaptic inhibition of spinal sensory feedback ensures smooth movement. Nature *509*, 43-48.
Frank, K. (1959). Basic mechanisms of synaptic transmission in the central nervous system. Inst Radio Eng Trans Med Electron *ME-6*, 85-88.
Frank, K., and Fortes, M.G.F. (1957). Presynaptic and postsynaptic inhibition of monosynaptic reflexes. . Fed Proc *16*, 39-40.
Gemes, G., Koopmeiners, A., Rigaud, M., Lirk, P., Sapunar, D., Bangaru, M.L., Vilceanu, D., Garrison, S.R., Ljubkovic, M., Mueller, S.J.*, et al.* (2013). Failure of action potential propagation in sensory neurons: mechanisms and loss of afferent filtering in C-type units after painful nerve injury. J Physiol *591*, 1111-1131.

Goldstein, S.S., and Rall, W. (1974). Changes of action potential shape and velocity for changing core conductor geometry. Biophys J *14*, 731-757.
Graham, B., and Redman, S. (1994). A simulation of action potentials in synaptic boutons during presynaptic inhibition. J Neurophysiol *71*, 538-549.
Harris, J.A., Hirokawa, K.E., Sorensen, S.A., Gu, H., Mills, M., Ng, L.L., Bohn, P., Mortrud, M., Ouellette, B., Kidney, J.*, et al.* (2014). Anatomical characterization of Cre driver mice for neural circuit mapping and manipulation. Front Neural Circuits *8*, 76.
Harvey, P.J., Li, Y., Li, X., and Bennett, D.J. (2006). Persistent sodium currents and repetitive firing in motoneurons of the sacrocaudal spinal cord of adult rats. J Neurophysiol *96*, 1141-1157.
Henneman, E. (1985). The size-principle: a deterministic output emerges from a set of probabilistic connections. J Exp Biol *115*, 105-112.
Henneman, E., Luscher, H.R., and Mathis, J. (1984). Simultaneously active and inactive synapses of single Ia fibres on cat spinal motoneurones. J Physiol *352*, 147-161.
Hess, P., and Tsien, R.W. (1984). Mechanism of ion permeation through calcium channels. Nature *309*, 453-456.
Hines, M.L., and Carnevale, N.T. (2001). NEURON: a tool for neuroscientists. Neuroscientist *7*, 123-135.
Howell, R.D., and Pugh, J.R. (2016). Biphasic modulation of parallel fibre synaptic transmission by co-activation of presynaptic GABAA and GABAB receptors in mice. J Physiol *594*, 3651-3666.
Howland, B., Lettvin, J.Y., McCulloch, W.S., Pitts, W., and Wall, P.D. (1955). Reflex inhibition by dorsal root interaction. J Neurophysiol *18*, 1-17.
Hubbard, J.I., Llinas, R., and Quastel, D.M.J. (1969). Electrophysiological Analysis of Synaptic Transmission (London: Edward Arnold Ltd).
Hughes, D.I., Mackie, M., Nagy, G.G., Riddell, J.S., Maxwell, D.J., Szabo, G., Erdelyi, F., Veress, G., Szucs, P., Antal, M.*, et al.* (2005). P boutons in lamina IX of the rodent spinal cord express high levels of glutamic acid decarboxylase-65 and originate from cells in deep medial dorsal horn. Proc Natl Acad Sci U S A *102*, 9038-9043.
Hultborn, H., Illert, M., Nielsen, J., Paul, A., Ballegaard, M., and Wiese, H. (1996a). On the mechanism of the post-activation depression of the H-reflex in human subjects. Exp Brain Res *108*, 450-462.
Hultborn, H., Illert, M., Nielsen, J., Paul, A., Ballegaard, M., and Wiese, H. (1996b). On the mechanism of the post-activation depression of the H-reflex in human subjects. Exp Brain Res *108*, 450-462.
Hultborn, H., Meunier, S., Morin, C., and Pierrot-Deseilligny, E. (1987). Assessing changes in presynaptic inhibition of I a fibres: a study in man and the cat. J Physiol *389*, 729-756.
Jankowska, E., McCrea, D., Rudomin, P., and Sykova, E. (1981). Observations on neuronal pathways subserving primary afferent depolarization. J Neurophysiol *46*, 506-516.
Katz, B., and Miledi, R. (1965). Propagation of Electric Activity in Motor Nerve Terminals. Proc R Soc Lond B Biol Sci *161*, 453-482.
Kawaguchi, S.Y., and Sakaba, T. (2015). Control of inhibitory synaptic outputs by low excitability of axon terminals revealed by direct recording. Neuron *85*, 1273-1288.
Kralj, J.M., Douglass, A.D., Hochbaum, D.R., Maclaurin, D., and Cohen, A.E. (2011). Optical recording of action potentials in mammalian neurons using a microbial rhodopsin. Nat Methods *9*, 90-95.
Lagrange, A.H., Hu, N., and Macdonald, R.L. (2018). GABA beyond the synapse: defining the subtype-specific pharmacodynamics of non-synaptic GABAA receptors. J Physiol *596*, 4475-4495.
Leandri, M., Leandri, S., and Lunardi, G. (2008). Effect of temperature on sensory and motor conduction of the rat tail nerves. Neurophysiol Clin *38*, 297-304.
Leppanen, L., and Stys, P.K. (1997). Ion transport and membrane potential in CNS myelinated axons I. Normoxic conditions. J Neurophysiol *78*, 2086-2094.
Lev-Tov, A., Fleshman, J.W., and Burke, R.E. (1983). Primary afferent depolarization and presynaptic inhibition of monosynaptic group Ia EPSPs during posttetanic potentiation. J Neurophysiol *50*, 413-427.
Lev-Tov, A., Meyers, D.E., and Burke, R.E. (1988). Activation of type B gamma-aminobutyric acid receptors in the intact mammalian spinal cord mimics the effects of reduced presynaptic Ca2+ influx. Proc Natl Acad Sci U S A *85*, 5330-5334.

Li, Y., Gorassini, M.A., and Bennett, D.J. (2004a). Role of persistent sodium and calcium currents in motoneuron firing and spasticity in chronic spinal rats. J Neurophysiol *91*, 767-783.
Li, Y., Hari, K., Lucas-Osma, A.M., Fenrich, K.K., Bennett, D.J., Hammar, I., and Jankowska, E. (2020). Branching points of primary afferent fibers are vital for the modulation of fiber excitability by epidural DC polarization and by GABA in the rat spinal cord. J Neurophysiol *124*, 49-62.
Li, Y., Harvey, P.J., Li, X., and Bennett, D.J. (2004b). Spastic long-lasting reflexes of the chronic spinal rat studied in vitro. J Neurophysiol *91*, 2236-2246.
Li, Y., Lucas-Osma, A.M., Black, S., Bandet, M.V., Stephens, M.J., Vavrek, R., Sanelli, L., Fenrich, K.K., Di Narzo, A.F., Dracheva, S.*, et al.* (2017). Pericytes impair capillary blood flow and motor function after chronic spinal cord injury. Nat Med *23*, 733-741.
Lin, S., Li, Y., Lucas-Osma, A.M., Hari, K., Stephens, M.J., Singla, R., Heckman, C.J., Zhang, Y., Fouad, K., Fenrich, K.K.*, et al.* (2019). Locomotor-related V3 interneurons initiate and coordinate muscles spasms after spinal cord injury. J Neurophysiol *121*, 1352-1367.
Lloyd, D.P. (1949). Post-tetanic potentiation of response in monosynaptic reflex pathways of the spinal cord. J Gen Physiol *33*, 147-170.
Lomeli, J., Quevedo, J., Linares, P., and Rudomin, P. (1998). Local control of information flow in segmental and ascending collaterals of single afferents. Nature *395*, 600-604.
Lucas-Osma, A.M., Li, Y., Lin, S., Black, S., Singla, R., Fouad, K., Fenrich, K.K., and Bennett, D.J. (2018). Extrasynaptic alpha5GABAA receptors on proprioceptive afferents produce a tonic depolarization that modulates sodium channel function in the rat spinal cord. J Neurophysiol *120*, 2953-2974.
Lucas-Osma, A.M., Li, Y., Murray, K., Lin, S., Black, S., Stephens, M.J., Ahn, A.H., Heckman, C.J., Fenrich, K.K., Fouad, K.*, et al.* (2019). 5-HT1D receptors inhibit the monosynaptic stretch reflex by modulating C-fiber activity. J Neurophysiol *121*, 1591-1608.
Luscher, C., Streit, J., Quadroni, R., and Luscher, H.R. (1994). Action potential propagation through embryonic dorsal root ganglion cells in culture. I. Influence of the cell morphology on propagation properties. J Neurophysiol *72*, 622-633.
Luscher, H.R., Ruenzel, P., Fetz, E., and Henneman, E. (1979a). Postsynatpic population potentials recorded from ventral roots perfused with isotonic sucrose: connections of groups Ia and II spindle afferent fibers with large populations of motoneurons. J Neurophysiol *42*, 1146-1164.
Luscher, H.R., Ruenzel, P., and Henneman, E. (1979b). How the size of motoneurones determines their susceptibility to discharge. Nature *282*, 859-861.
Luscher, H.R., Ruenzel, P., and Henneman, E. (1983). Composite EPSPs in motoneurons of different sizes before and during PTP: implications for transmission failure and its relief in Ia projections. J Neurophysiol *49*, 269-289.
Madisen, L., Mao, T., Koch, H., Zhuo, J.M., Berenyi, A., Fujisawa, S., Hsu, Y.W., Garcia, A.J., 3rd, Gu, X., Zanella, S.*, et al.* (2012). A toolbox of Cre-dependent optogenetic transgenic mice for light-induced activation and silencing. Nat Neurosci *15*, 793-802.
Madisen, L., Zwingman, T.A., Sunkin, S.M., Oh, S.W., Zariwala, H.A., Gu, H., Ng, L.L., Palmiter, R.D., Hawrylycz, M.J., Jones, A.R.*, et al.* (2010). A robust and high-throughput Cre reporting and characterization system for the whole mouse brain. Nat Neurosci *13*, 133-140.
Matthews, P.B. (1986). Observations on the automatic compensation of reflex gain on varying the pre-existing level of motor discharge in man. J Physiol *374*, 73-90.
Matthews, P.B. (1996). Relationship of firing intervals of human motor units to the trajectory of post-spike after-hyperpolarization and synaptic noise. J Physiol *492 (Pt 2)*, 597-628.
McCrea, D.A., Shefchyk, S.J., and Carlen, P.L. (1990). Large reductions in composite monosynaptic EPSP amplitude following conditioning stimulation are not accounted for by increased postsynaptic conductances in motoneurons. Neurosci Lett *109*, 117-122.
McIntyre, C.C., Richardson, A.G., and Grill, W.M. (2002). Modeling the excitability of mammalian nerve fibers: influence of afterpotentials on the recovery cycle. J Neurophysiol *87*, 995-1006.
Munson, J.B., and Sypert, G.W. (1979a). Properties of single central Ia afferent fibres projecting to motoneurones. J Physiol *296*, 315-327.

Munson, J.B., and Sypert, G.W. (1979b). Properties of single fibre excitatory post-synaptic potentials in triceps surae motoneurones. J Physiol *296*, 329-342.
Murray, K.C., Nakae, A., Stephens, M.J., Rank, M., D'Amico, J., Harvey, P.J., Li, X., Harris, R.L., Ballou, E.W., Anelli, R.*, et al.* (2010). Recovery of motoneuron and locomotor function after spinal cord injury depends on constitutive activity in 5-HT2C receptors. Nat Med *16*, 694-700.
Murray, K.C., Stephens, M.J., Rank, M., D'Amico, J., Gorassini, M.A., and Bennett, D.J. (2011). Polysynaptic excitatory postsynaptic potentials that trigger spasms after spinal cord injury in rats are inhibited by 5-HT1B and 5-HT1F receptors. J Neurophysiol *106*, 925-943.
Negro, F., Muceli, S., Castronovo, A.M., Holobar, A., and Farina, D. (2016). Multi-channel intramuscular and surface EMG decomposition by convolutive blind source separation. J Neural Eng *13*, 026027.
Nelson, S.G., Collatos, T.C., Niechaj, A., and Mendell, L.M. (1979). Immediate increase in Ia-motoneuron synaptic transmission caudal to spinal cord transection. J Neurophysiol *42*, 655-664.
Nicol, M.J., and Walmsley, B. (1991). A serial section electron microscope study of an identified Ia afferent collateral in the cat spinal cord. J Comp Neurol *314*, 257-277.
Nielsen, J.B., Morita, H., Wenzelburger, R., Deuschl, G., Gossard, J.P., and Hultborn, H. (2019). Recruitment gain of spinal motor neuron pools in cat and human. Exp Brain Res *237*, 2897-2909.
Norton, J.A., Bennett, D.J., Knash, M.E., Murray, K.C., and Gorassini, M.A. (2008). Changes in sensory-evoked synaptic activation of motoneurons after spinal cord injury in man. Brain *131*, 1478-1491.
Olsen, R.W., and Sieghart, W. (2009). GABA A receptors: subtypes provide diversity of function and pharmacology. Neuropharmacology *56*, 141-148.
Paul, J., Zeilhofer, H.U., and Fritschy, J.M. (2012). Selective distribution of GABA(A) receptor subtypes in mouse spinal dorsal horn neurons and primary afferents. J Comp Neurol *520*, 3895-3911.
Persohn, E., Malherbe, P., and Richards, J.G. (1991). In situ hybridization histochemistry reveals a diversity of GABAA receptor subunit mRNAs in neurons of the rat spinal cord and dorsal root ganglia. Neuroscience *42*, 497-507.
Pierce, J.P., and Mendell, L.M. (1993). Quantitative ultrastructure of Ia boutons in the ventral horn: scaling and positional relationships. J Neurosci *13*, 4748-4763.
Pinol, R.A., Bateman, R., and Mendelowitz, D. (2012). Optogenetic approaches to characterize the long-range synaptic pathways from the hypothalamus to brain stem autonomic nuclei. J Neurosci Methods *210*, 238-246.
Price, G.D., and Trussell, L.O. (2006). Estimate of the chloride concentration in a central glutamatergic terminal: a gramicidin perforated-patch study on the calyx of Held. J Neurosci *26*, 11432-11436.
Prochazka, A., and Gorassini, M. (1998). Ensemble firing of muscle afferents recorded during normal locomotion in cats. J Physiol *507 (Pt 1)*, 293-304.
Rasminsky, M., Kearney, R.E., Aguayo, A.J., and Bray, G.M. (1978). Conduction of nervous impulses in spinal roots and peripheral nerves of dystrophic mice. Brain Res *143*, 71-85.
Redman, S. (1990). Quantal analysis of synaptic potentials in neurons of the central nervous system. Physiol Rev *70*, 165-198.
Redman, S.J. (1998). The relative contributions of GABAA and GABAB receptors to presynaptic inhibition of group Ia EPSPs. In Presynaptic Inhibition and Neuron Control, P. Rudmon, R. Romo, and L.M. Mendell, eds. (New York: Oxford University Press), pp. 162-177.
Rossignol, S., Beloozerova, I., Gossard, J.P., and Dubuc, R. (1998). Presynaptc mechanisms during locomotion. In Presynaptic Inhibition and Neuron Control, P. Rudmon, R. Romo, and L.M. Mendell, eds. (New York: Oxford University Press), pp. 385-397.
Rudomin, P. (1999). Presynaptic selection of afferent inflow in the spinal cord. J Physiol Paris *93*, 329-347.
Rudomin, P., Nunez, R., Madrid, J., and Burke, R.E. (1974). Primary afferent hyperpolarization and presynaptic facilitation of Ia afferent terminals induced by large cutaneous fibers. J Neurophysiol *37*, 413-429.
Rudomin, P., and Schmidt, R.F. (1999). Presynaptic inhibition in the vertebrate spinal cord revisited. Exp Brain Res *129*, 1-37.
Rushton, W.A. (1951). A theory of the effects of fibre size in medullated nerve. J Physiol *115*, 101-122.

Russ, J.B., Verina, T., Comer, J.D., Comi, A.M., and Kaltschmidt, J.A. (2013). Corticospinal tract insult alters GABAergic circuitry in the mammalian spinal cord. Front Neural Circuits *7*, 150.
Salio, C., Merighi, A., and Bardoni, R. (2017). GABAB receptors-mediated tonic inhibition of glutamate release from Abeta fibers in rat laminae III/IV of the spinal cord dorsal horn. Mol Pain *13*, 1744806917710041.
Segev, I. (1990). Computer study of presynaptic inhibition controlling the spread of action potentials into axonal terminals. J Neurophysiol *63*, 987-998.
Shefner, J.M., Buchthal, F., and Krarup, C. (1992). Recurrent potentials in human peripheral sensory nerve: possible evidence of primary afferent depolarization of the spinal cord. Muscle Nerve *15*, 1354-1363.
Silver, R.A., Cull-Candy, S.G., and Takahashi, T. (1996). Non-NMDA glutamate receptor occupancy and open probability at a rat cerebellar synapse with single and multiple release sites. J Physiol *494 (Pt 1)*, 231-250.
Stalberg, E., van Dijk, H., Falck, B., Kimura, J., Neuwirth, C., Pitt, M., Podnar, S., Rubin, D.I., Rutkove, S., Sanders, D.B.*, et al.* (2019). Standards for quantification of EMG and neurography. Clin Neurophysiol *130*, 1688-1729.
Stein, R.B. (1980). Nerve and Muscle : Membranes, Cells, and Systems (Boston, MA: Springer US).
Stephanova, D.I., and Bostock, H. (1995). A distributed-parameter model of the myelinated human motor nerve fibre: temporal and spatial distributions of action potentials and ionic currents. Biol Cybern *73*, 275-280.
Stuart, G.J., and Redman, S.J. (1992). The role of GABAA and GABAB receptors in presynaptic inhibition of Ia EPSPs in cat spinal motoneurones. J Physiol *447*, 675-692.
Sypert, G.W., Munson, J.B., and Fleshman, J.W. (1980). Effect of presynaptic inhibition on axonal potentials, terminal potentials, focal synaptic potentials, and EPSPs in cat spinal cord. J Neurophysiol *44*, 792-803.
Szabadics, J., Varga, C., Molnar, G., Olah, S., Barzo, P., and Tamas, G. (2006). Excitatory effect of GABAergic axo-axonic cells in cortical microcircuits. Science *311*, 233-235.
Takahashi, T. (1992). The minimal inhibitory synaptic currents evoked in neonatal rat motoneurones. J Physiol *450*, 593-611.
Taniguchi, H., He, M., Wu, P., Kim, S., Paik, R., Sugino, K., Kvitsiani, D., Fu, Y., Lu, J., Lin, Y.*, et al.* (2011). A resource of Cre driver lines for genetic targeting of GABAergic neurons in cerebral cortex. Neuron *71*, 995-1013.
Todd, A.J., Hughes, D.I., Polgar, E., Nagy, G.G., Mackie, M., Ottersen, O.P., and Maxwell, D.J. (2003). The expression of vesicular glutamate transporters VGLUT1 and VGLUT2 in neurochemically defined axonal populations in the rat spinal cord with emphasis on the dorsal horn. Eur J Neurosci *17*, 13-27.
Trigo, F.F., Marty, A., and Stell, B.M. (2008). Axonal GABAA receptors. Eur J Neurosci *28*, 841-848.
Turker, K.S., and Powers, R.K. (2005). Black box revisited: a technique for estimating postsynaptic potentials in neurons. Trends Neurosci *28*, 379-386.
Ueno, M., Nakamura, Y., Li, J., Gu, Z., Niehaus, J., Maezawa, M., Crone, S.A., Goulding, M., Baccei, M.L., and Yoshida, Y. (2018). Corticospinal Circuits from the Sensory and Motor Cortices Differentially Regulate Skilled Movements through Distinct Spinal Interneurons. Cell Rep *23*, 1286-1300 e1287.
Verdier, D., Lund, J.P., and Kolta, A. (2004). Synaptic inputs to trigeminal primary afferent neurons cause firing and modulate intrinsic oscillatory activity. J Neurophysiol *92*, 2444-2455.
Wall, P.D. (1958). Excitability changes in afferent fibre terminations and their relation to slow potentials. J Physiol *142*, i3-21.
Wall, P.D. (1998). Some unanswered questions about the mechanims and function of presynaptic inhibition. In Presynaptic Inhibition and Neuron Control, P. Rudmon, R. Romo, and L.M. Mendell, eds. (New York: Oxford University Press), pp. 228-241.
Wall, P.D., and McMahon, S.B. (1994). Long range afferents in rat spinal cord. III. Failure of impulse transmission in axons and relief of the failure after rhizotomy of dorsal roots. Philos Trans R Soc Lond B Biol Sci *343*, 211-223.
Walmsley, B., Graham, B., and Nicol, M.J. (1995). Serial E-M and simulation study of presynaptic inhibition along a group Ia collateral in the spinal cord. J Neurophysiol *74*, 616-623.
Walsh, M.E., Sloane, L.B., Fischer, K.E., Austad, S.N., Richardson, A., and Van Remmen, H. (2015). Use of Nerve Conduction Velocity to Assess Peripheral Nerve Health in Aging Mice. J Gerontol A Biol Sci Med Sci *70*, 1312-1319.
Zbili, M., and Debanne, D. (2019). Past and Future of Analog-Digital Modulation of Synaptic Transmission. Front Cell Neurosci *13*, 160.

Zehr, E.P., and Stein, R.B. (1999). Interaction of the Jendrassik maneuver with segmental presynaptic inhibition. Exp Brain Res *124*, 474-480.

Zhang, F., Vierock, J., Yizhar, O., Fenno, L.E., Tsunoda, S., Kianianmomeni, A., Prigge, M., Berndt, A., Cushman, J., Polle, J.*, et al.* (2011). The microbial opsin family of optogenetic tools. Cell *147*, 1446-1457.

Zimmerman, A.L., Kovatsis, E.M., Pozsgai, R.Y., Tasnim, A., Zhang, Q., and Ginty, D.D. (2019). Distinct Modes of Presynaptic Inhibition of Cutaneous Afferents and Their Functions in Behavior. Neuron *102*, 420-434 e428.

Zorrilla de San Martin, J., Trigo, F.F., and Kawaguchi, S.Y. (2017). Axonal GABAA receptors depolarize presynaptic terminals and facilitate transmitter release in cerebellar Purkinje cells. J Physiol *595*, 7477-7493.

Figure 1

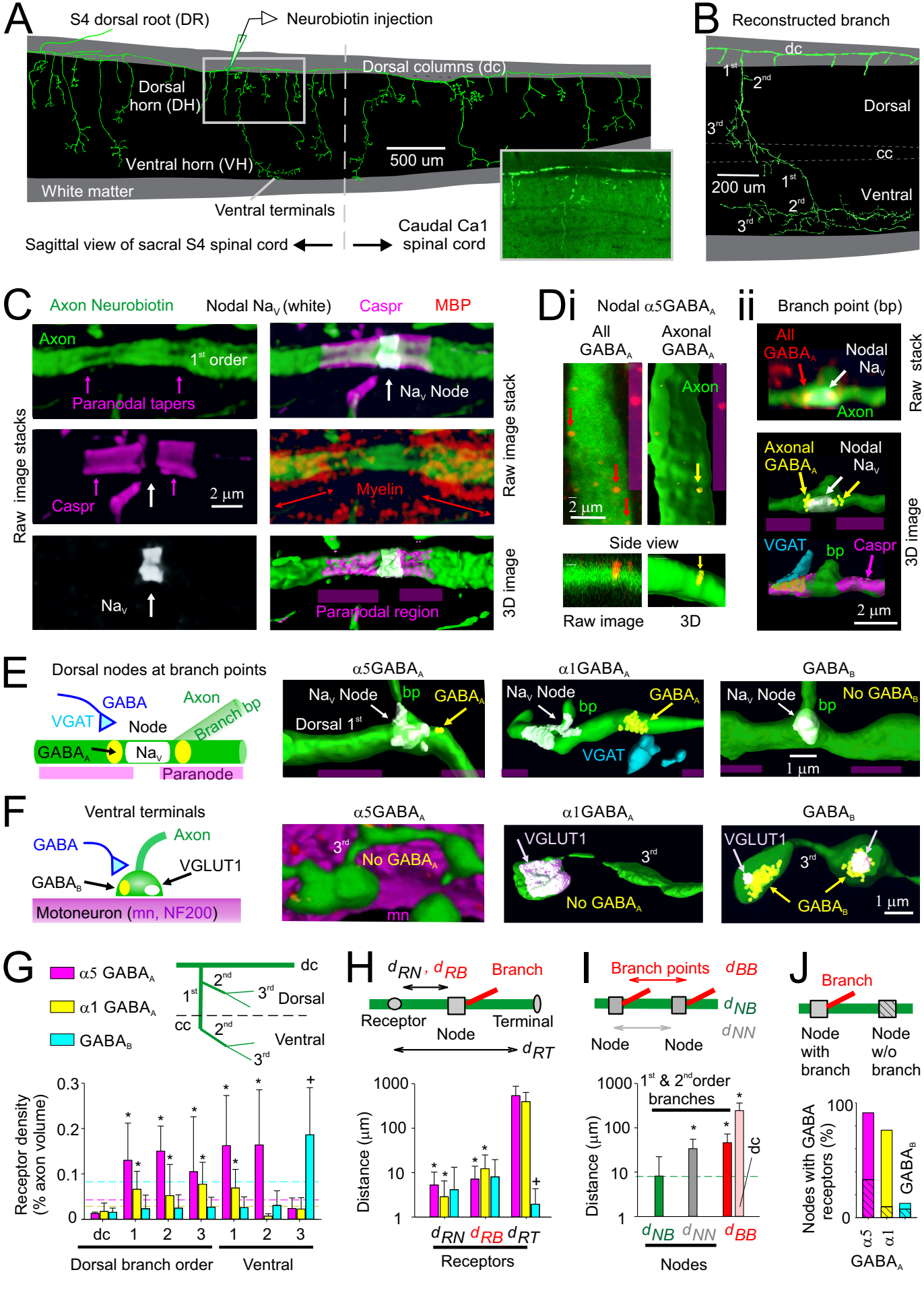

Figure 2

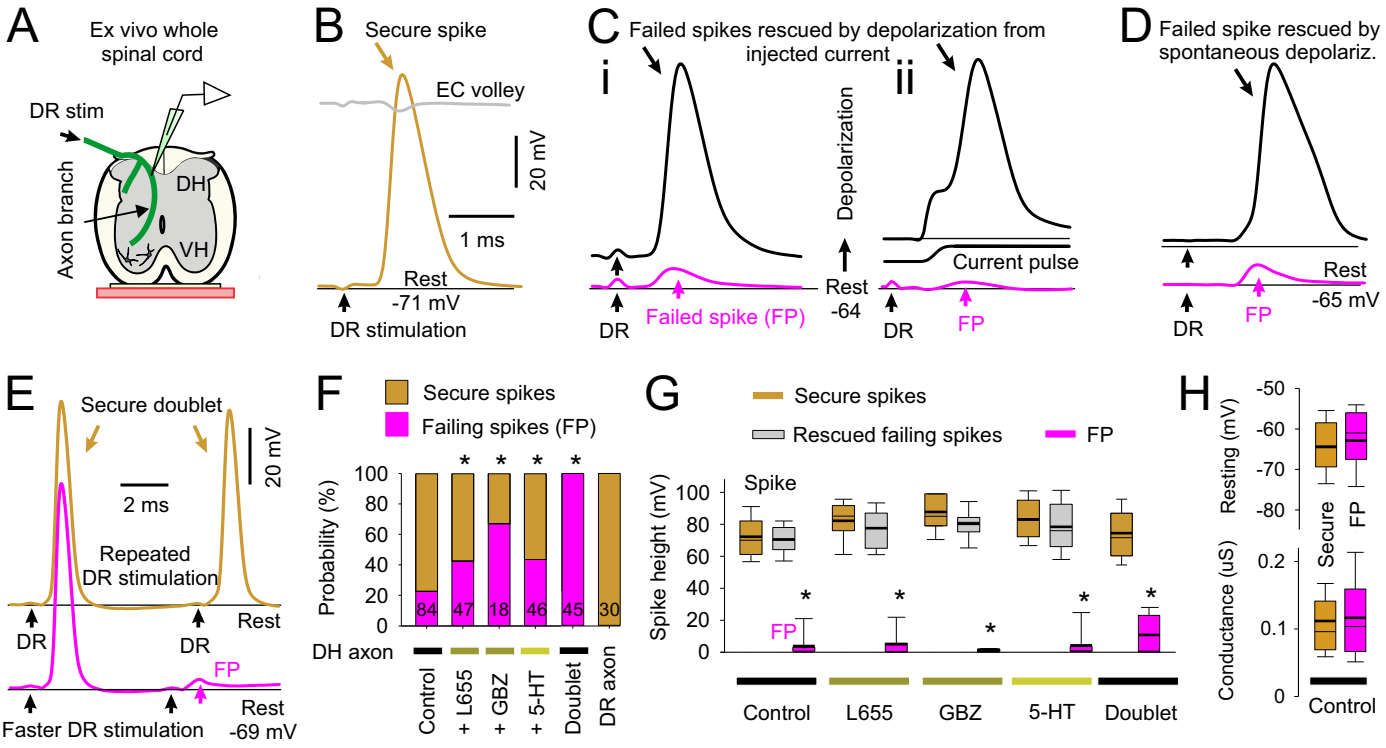

Figure 3

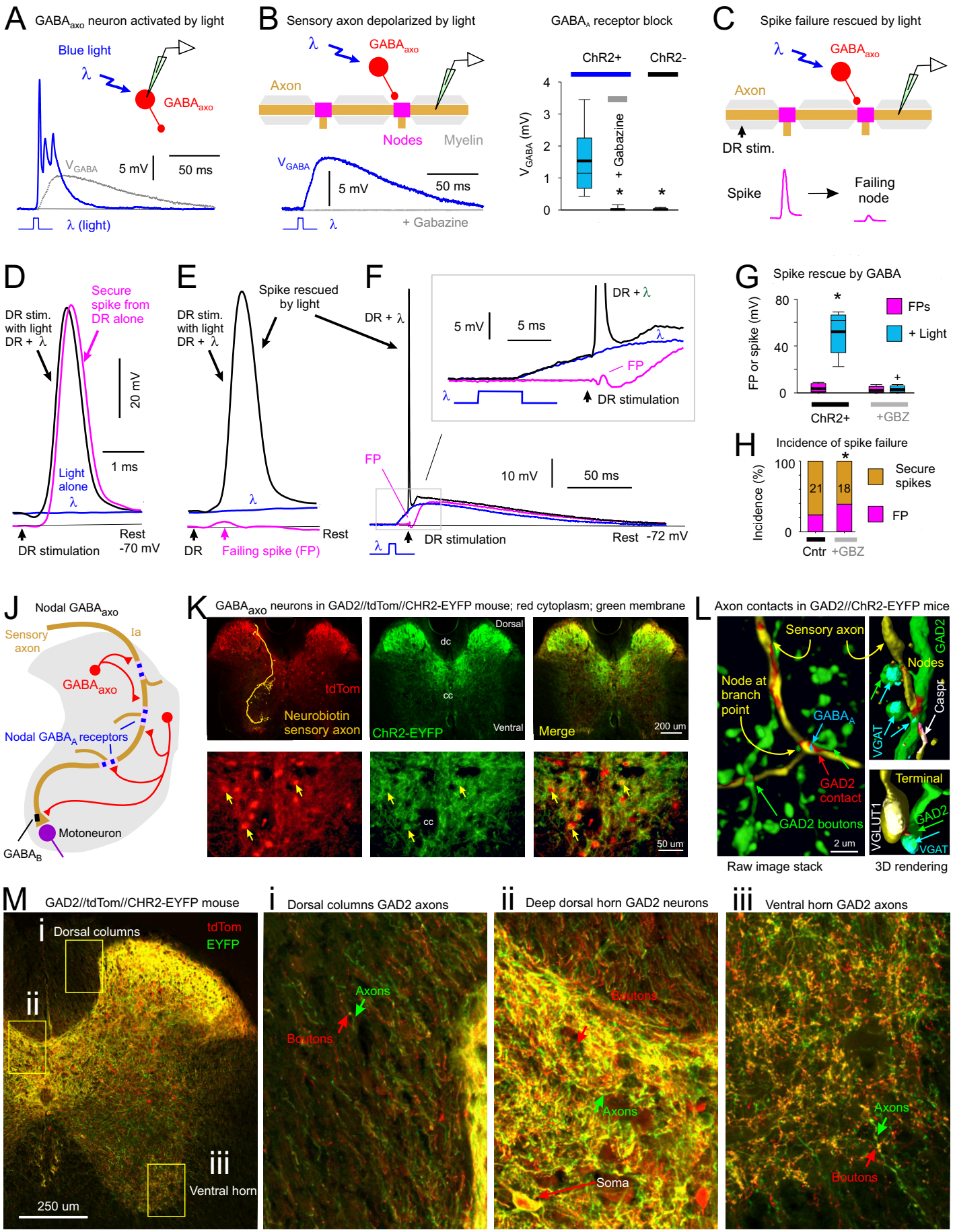

Figure 4

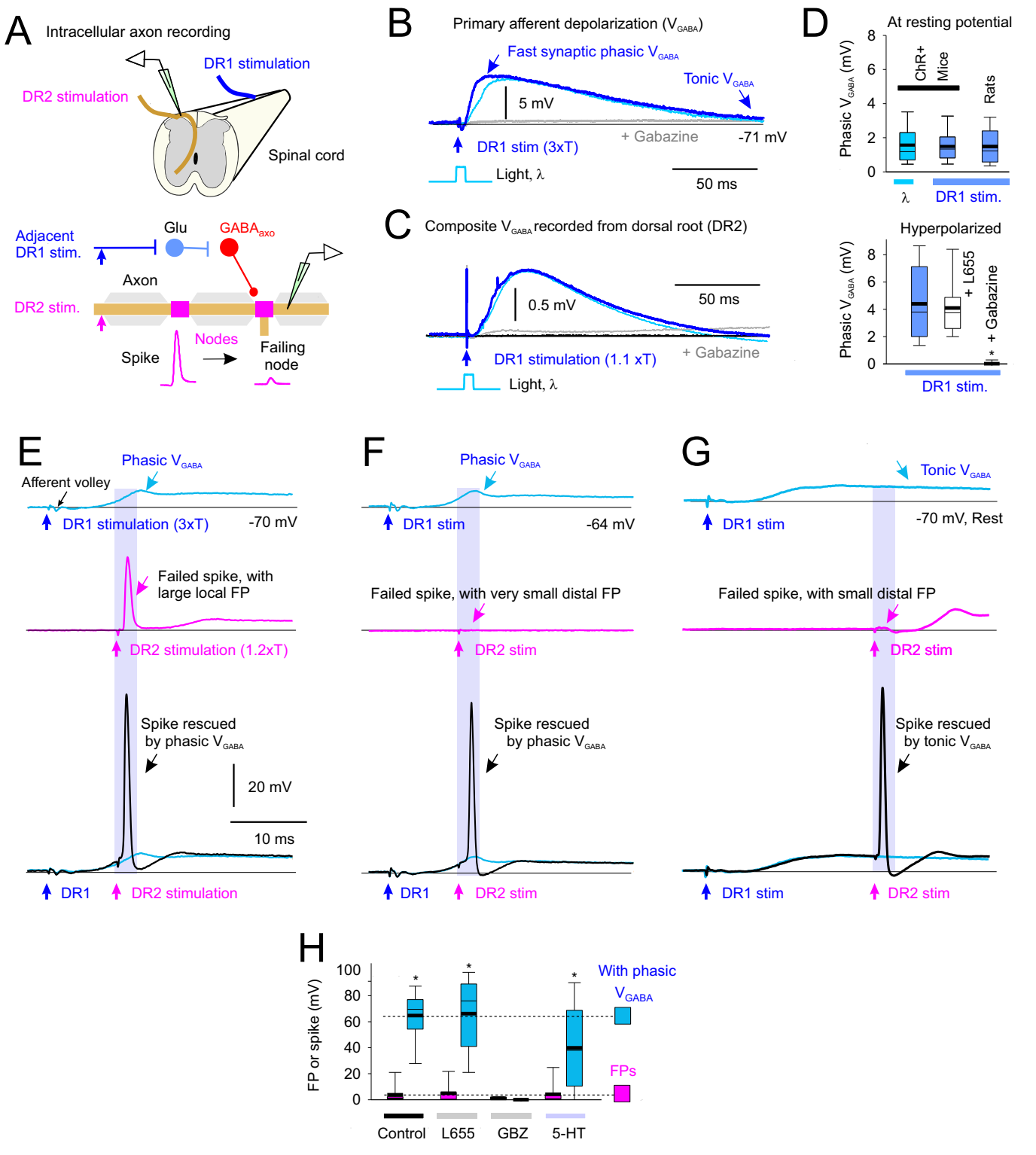

Figure 5

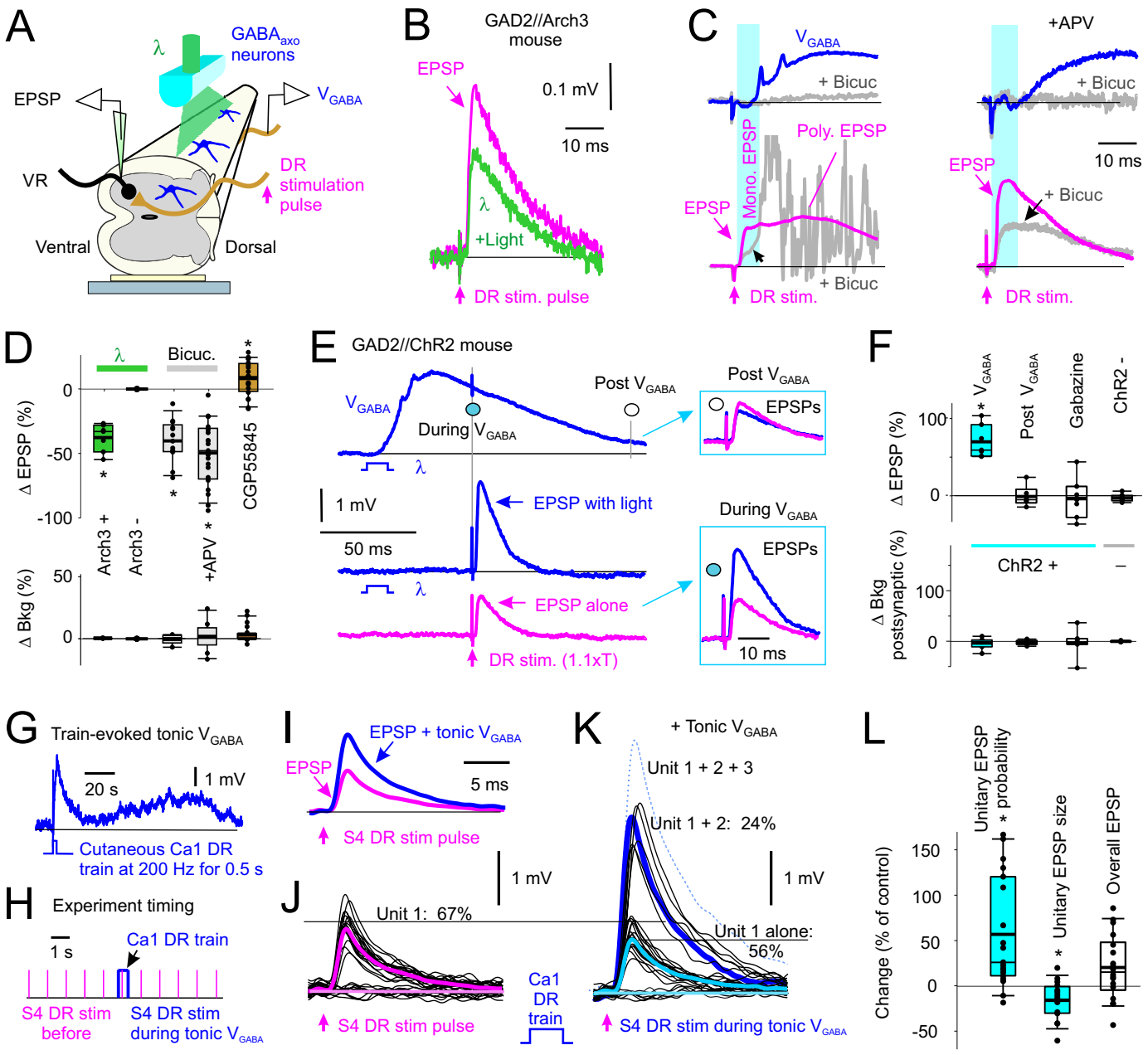

Figure 6

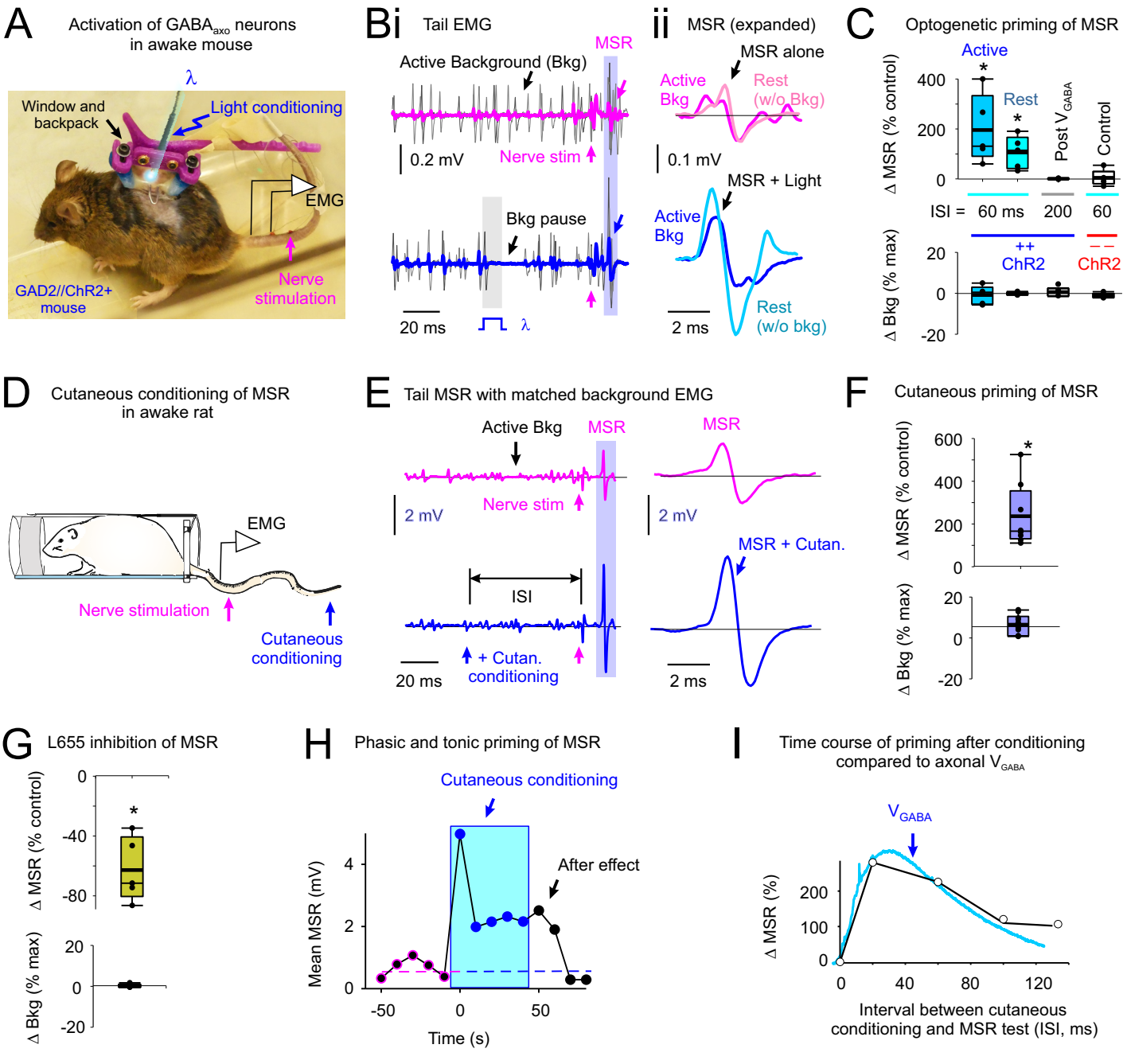

Figure 7

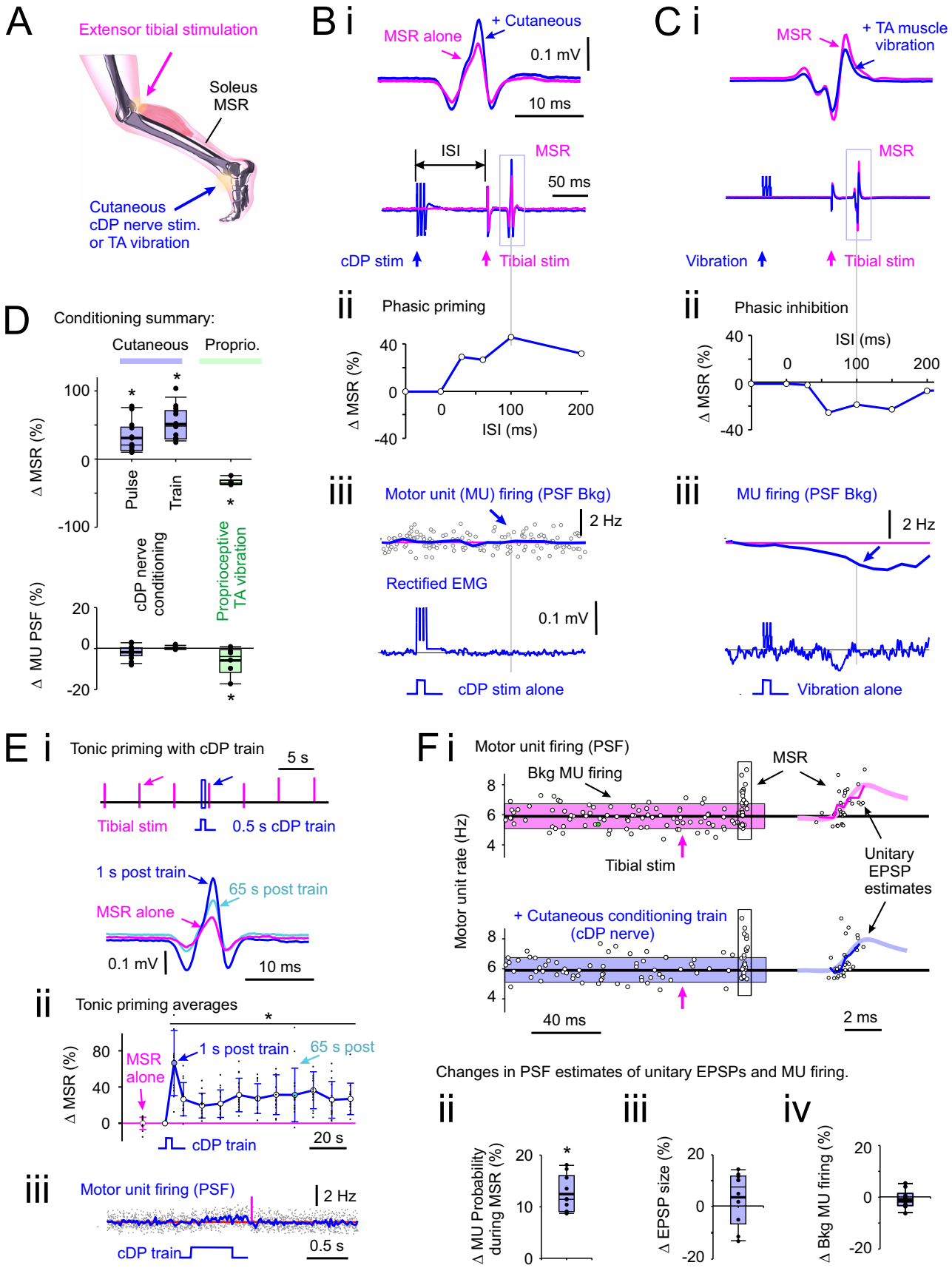

Figure S1

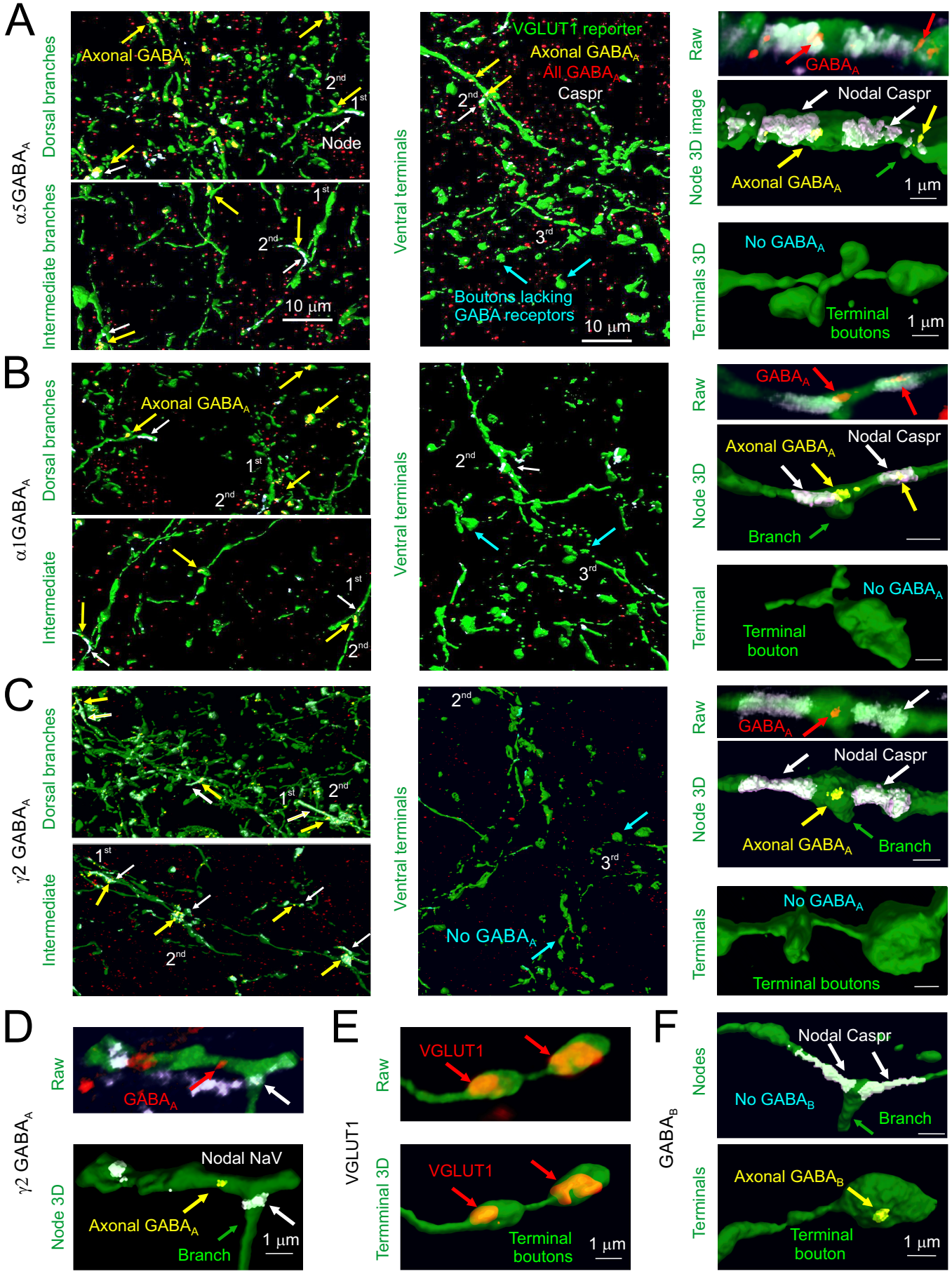

Figure S2

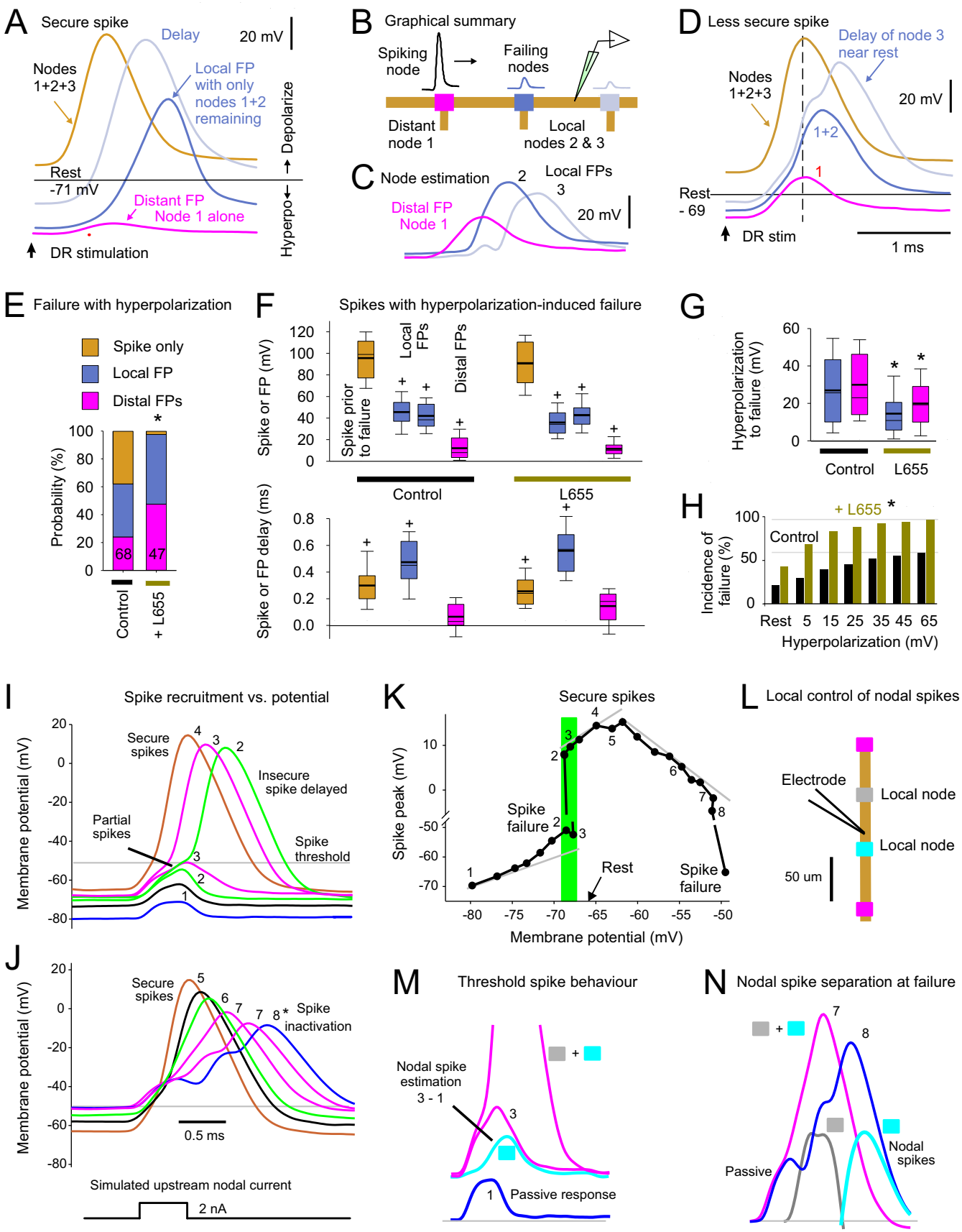

Figure S3

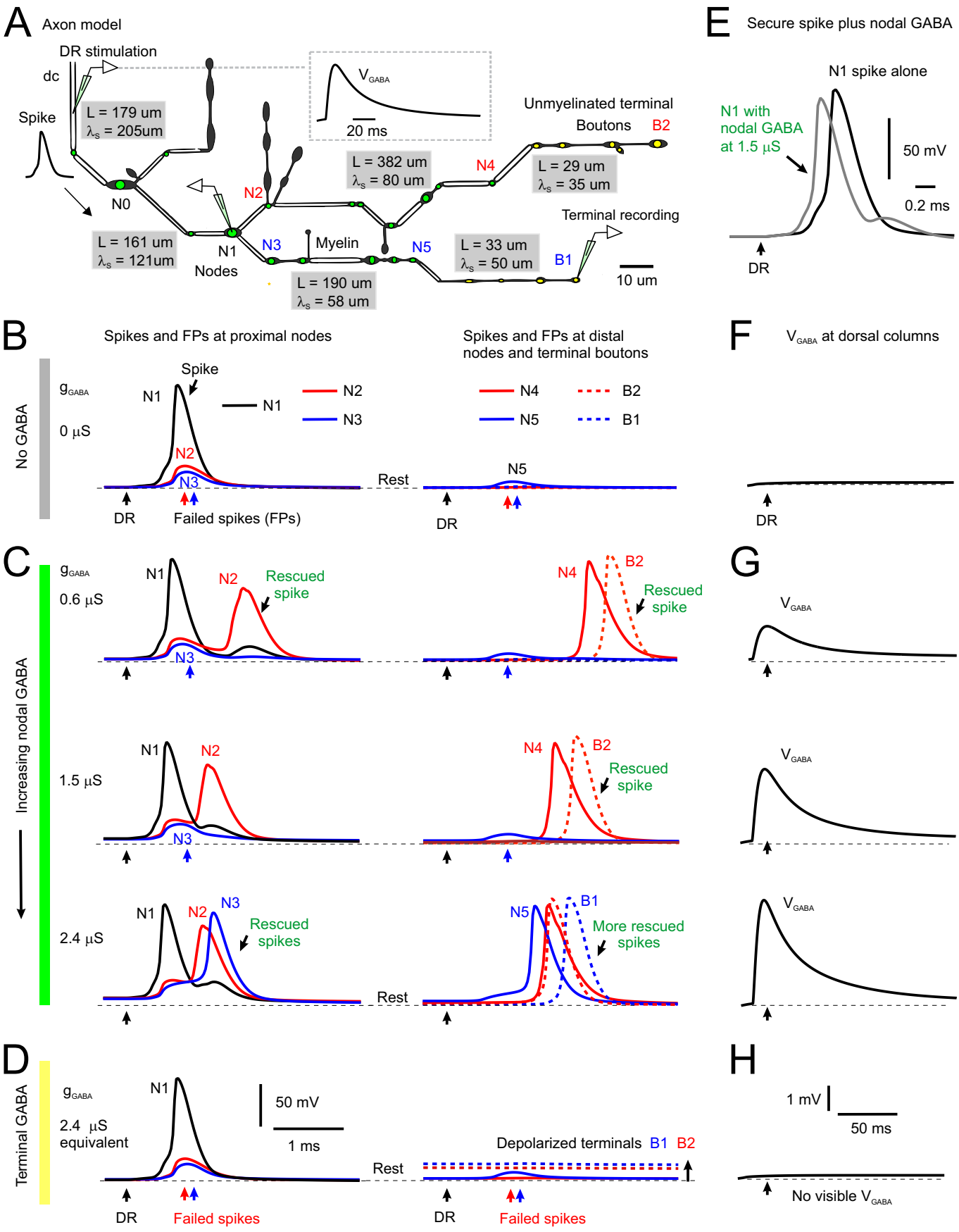

Figure S4

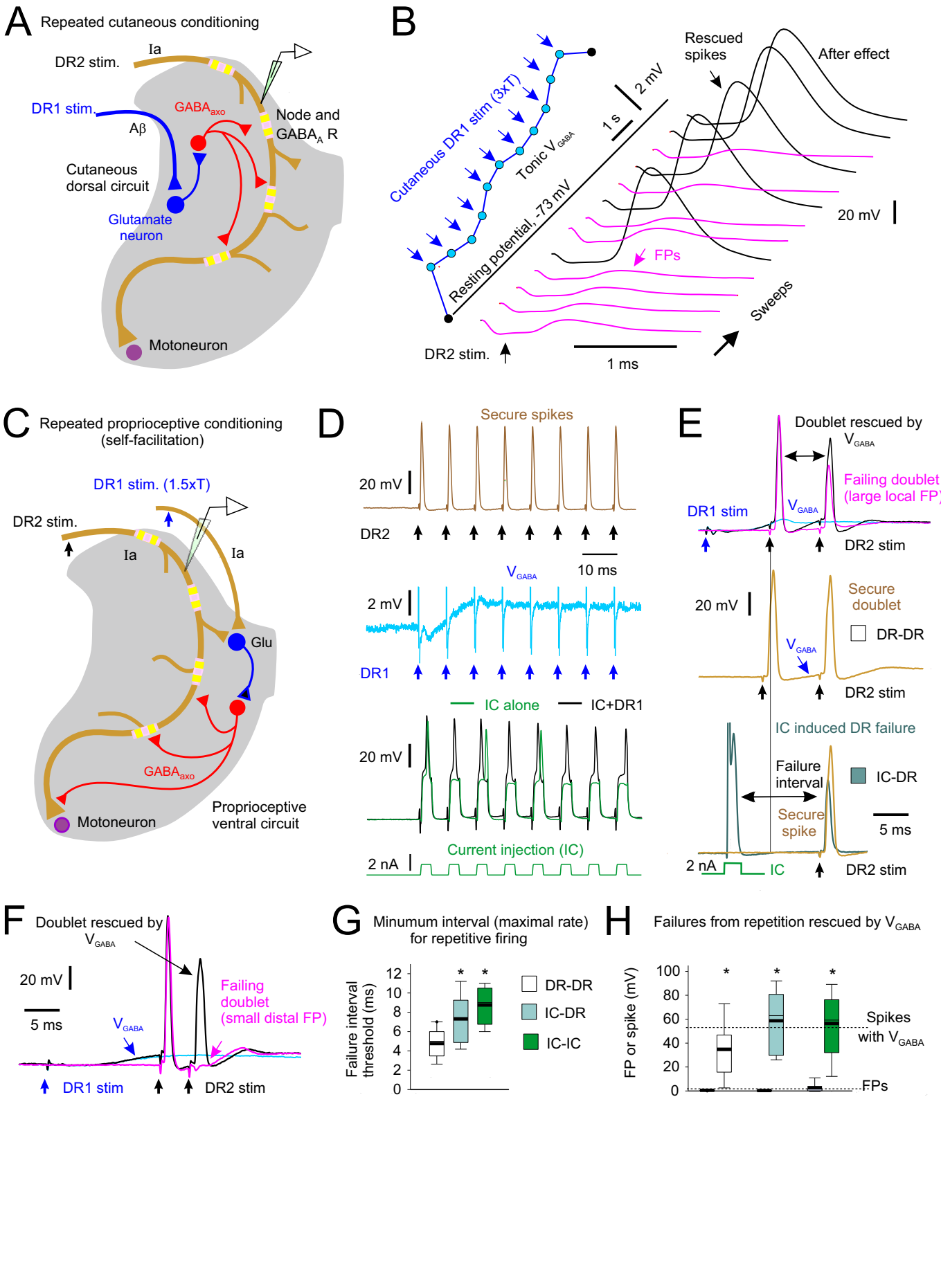

Figure S5

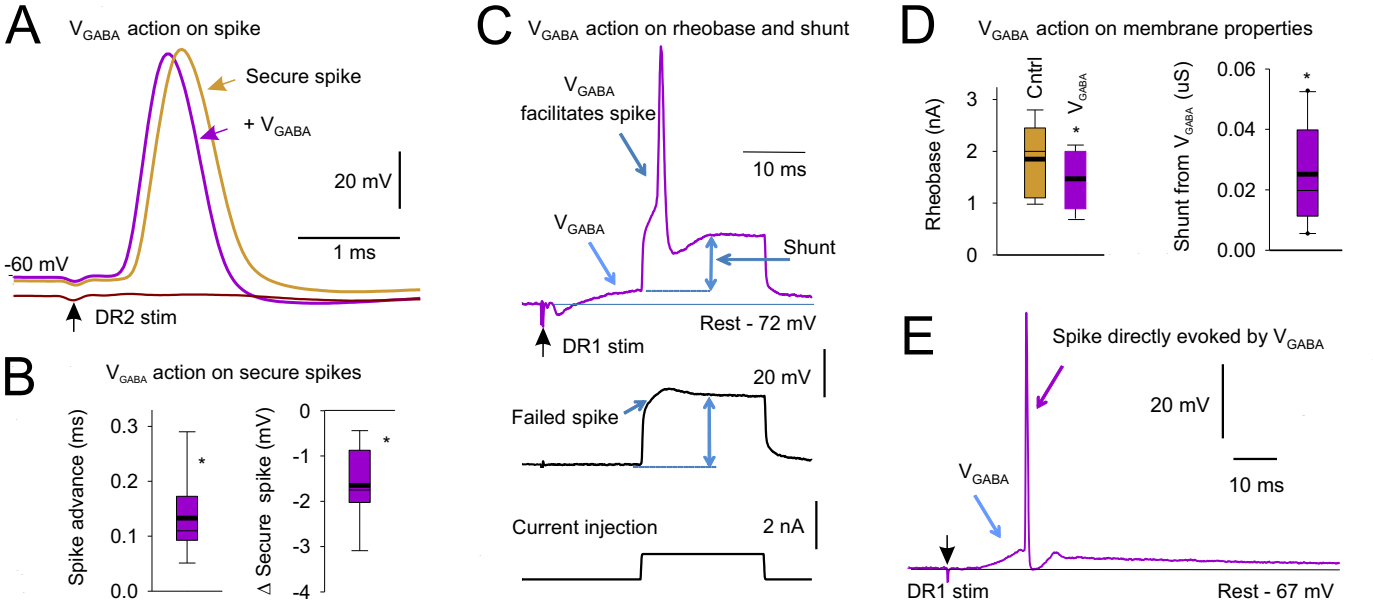

Figure S6

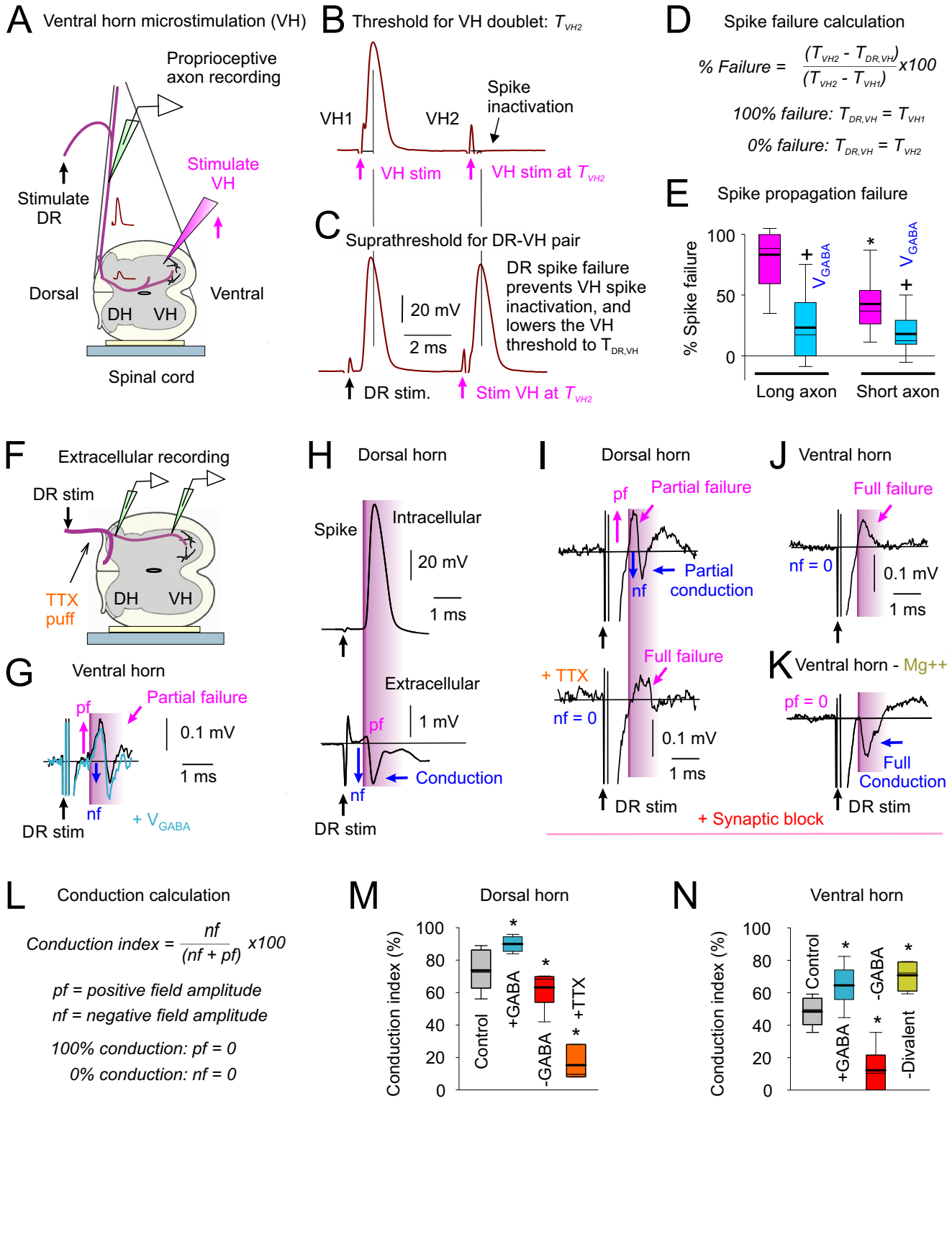

Figure S7